The Dissertation Committee for Qian Wu Certifies that this is the approved version of the following Dissertation:

Advanced Distributed Fiber Optic Sensors for Monitoring Real-Time Cementing Operations and Long Term Zonal Isolation

Committee:

Eric van Oort, Supervisor

Sriramya Duddukuri Nair

Maria Juenger

Christian Claudel

Artur Guzik

Advanced Distributed Fiber Optic Sensors for Monitoring Real-Time Cementing Operations and Long Term Zonal Isolation

by

Qian Wu

Dissertation

Presented to the Faculty of the Graduate School of Engineering

The University of Texas at Austin

in Partial Fulfillment

of the Requirements

for the Degree of

Doctor of Philosophy

The University of Texas at Austin

May, 2019

Dedication

To my father, Weiqiang Wu

To my fiancé, Kewei Ma

In memory of my mother, Meifang Luo

Acknowledgements

I would like to express my special appreciation and thanks to my supervisor, Prof. Eric van Oort offering me the opportunity to pursue my graduate degrees and conduct research at the University of Texas at Austin. Thank you for bringing me to the world of drilling engineering and well construction. Your guidance for my research as well as your advice for the development of my career are invaluable.

I would like extend my gratitude to my committee members: Prof. Maria Juenger, Prof. Christian Claudel, Dr. Sriramya Nair, and Dr. Artur Guzik. Thank you for your support for my PhD study as well as your insightful suggestions and comments on my doctoral dissertation.

I'm extremely thankful and indebted to Dr. Sriramya Nair for her support, invaluable suggestions, and sincere encouragement for my study and research as well as for many aspects of my life.

I place on record my sincere thank you to Dr. Kinzo Kishida, Dr. Artur Guzik from Neubrex Co. Without their support and sharing of their industrial experience and research expertise, this dissertation would not have been possible. Thank you for introducing me to distributed fiber optic sensors.

I'm thankful to Michelle Shuck for her technical assistance with the experimental setups and teaching me a lot of helpful technical skills. I would like to acknowledge the contribution of our undergraduate research assistants: Marjorie Dininger and Hanna Lee, for their help in the experimental work.

I would also like to express my special thanks to Samuel Aldin, Meghana PaiAngle and Metarock Laboratory for their help with the permeability test.

Many thanks to Sriramya Nair, Michelle Shuck, Xiangyu Liu and Katherine Aughenbaugh, my fellow cementing ladies for their help and support in many different ways.

I take this opportunity to express gratitude to everyone in Zonal Isolation lab and my fellow students in Dr. van Oort's research group. I feel lucky to be part of you working hard and having fun together. Special thanks go to Tesse Smitherman, Daryl Nygaard, Glen Baum, and Gary Miscoe for their technical and administrative support.

I would like express my gratitude to Well Construction, Decommissioning and Abandonment (CODA) Consortium and the Rig Automation Performance Improvement in Drilling (RAPID) Consortium at the University of Texas at Austin for sponsoring this research. I would also like to thank Baker Hughes for an enabling gift that allowed for the Zonal Isolation Laboratory at UT-Austin and early support of this research.

Last but not least, I would like to express my deepest thanks to my family and friends who love and support me no matter what happens. I'm always grateful to my mother who loved me with all she could. She is always in my heart and the memory of her will never pass away. I would like to thank my Dad for his endless love and always supporting me to pursue what I want. A lot of thanks to my dear Auntie Xiang for standing out to help me when I was in need. I would also like to thank all my friends who share happiness in the good days and give me a hug in the bad days. Finally, I would like express my appreciation to my dear fiancé for his love, support and encouragement in every aspect of my life.

Abstract

Advanced Distributed Fiber Optic Sensors for Monitoring Real-Time Cementing Operations and Long Term Zonal Isolation

Qian Wu, PhD

The University of Texas at Austin, 2019

Supervisor: Eric van Oort

The main goal of cementing is to provide reliable zonal isolation throughout the life of a well. Subsurface geomechanical changes can cause severe damage to casing strings and cement barriers in oil and gas wells. Inefficient displacement of drilling fluids by spacers and cement slurry can also result in potential contamination of the cement slurry. Such contamination can negatively affect zonal isolation directly by creating paths for hydrocarbon migration or indirectly by weakening the cement annulus, making it susceptible to damage from cyclical pressure/temperature loads.

This dissertation presents a novel real-time *in situ* sensing system for cement and zonal isolation monitoring without the need for wellbore entry for the lifetime of an oil or gas well, using a fiber optic distributed temperature and strain sensing (DTSS) system based on hybrid Brillouin and Rayleigh technique that allows separated strain and temperature measurements using a single optical fiber. In combination with specially designed fiber optic cables coated with the sensitive polymers, the DTSS system also obtains the capability of distributed chemical sensing (DCS). When exposed to well

construction fluids and hydrocarbons, the sensitive polymer coating on the proposed chemical sensing cable swells (or shrinks) which in turn introduces stain changes on the fiber, which can be measured and quantified by using the DTSS system. Multiple applications were investigated and demonstrated in the laboratory experiments. Cement displacement tracking was developed to estimate displacement efficiency by detecting the presence and location of well construction fluids (drilling fluid and spacer fluid) using the proposed sensing cables (DCS) and the exothermic heat release signature from the cement hydration. The cement hydration process was monitored. The capability of the DTSS system to obtain the actual wait-on-cement time and the top of cement, uncemented sections (e.g. voids), as well as the contamination in cement slurry due to incomplete displacement was demonstrated. The DTSS system was also applied to monitor invasion of warmer fluid from another zone, as well as the presence and migration of hydrocarbons in a compromised cement annulus. A technique was developed to monitor the cement-casing bond with the use of a helical wrapping installation of the fiber, which enabled circumferential measurements over the entire cement annulus. The results were used to evaluate the risk of cement debonding. A dual-cable design was employed to differentiate strain changes due to either deformation or due to the presence of hydrocarbons. The DTSS system was successfully used to simultaneously detect casing deformation and presence of hydrocarbons. The proposed system can serve as an early warning system to identify, and possibly prevent, the loss of zonal isolation, by providing detailed information (i.e. location, type, and severity of an event(s)) and guidance that will facilitate any remedial operations, if necessary.

Table of Contents

List of Tables

List of Figures

Chapter 1: Introduction

1.1 MOTIVATION

The main purpose of an oil or gas well cementing operation is to provide zonal isolation over the life of the well, by restricting fluid movement between zones or to the surface, as well as providing structural support for the casing. Zonal isolation is essential for the longevity and productivity of any oil or gas well. Defects in cement annuli such as voids, cracks, and channels or debonding between cement and casing, caused by either a poor cementing operation or due to the thermal/pressure fluctuations in a well, can threaten the integrity of cemented annuli and compromise zonal isolation (Nelson and Guillot, 2006). This can lead to problems such as contamination of water aquifers (see Figure 1.1a), annular pressure buildup, leakage in aging wells (Vignes and Aadnøy, 2010), and the need for extensive/expensive remedial work, which all could negatively affect hydrocarbon production and the productive life of the well. For example, for production wells, the presence of channels in the cement annuli can result in non-productive communication pathways, causing stimulation and completion inefficiency, thus negatively affecting completion effectiveness and well productivity (Kolchanov et al., 2018). For abandoned wells, the failure of cemented layers and plugs can lead to uncontrolled leakage of formation fluids and gas, with vent flows to surface. In some extreme cases, the failure of cemented annuli can even result in well control incidents that could result in loss of life, economic loss, and environmental damage (Carter et al., 2014). One of the most important causes of the Macondo/Deepwater Horizon disaster in 2010 was the failure of the primary production casing cementation, which resulted in the loss of 11 lives, the largest offshore oil spill in the history of the United States, and significant environmental problems in the

Gulf of Mexico (Mueller, 2012). Therefore, assessing and verifying the state of zonal isolation is an important challenge and requirement in the oil and gas industry.

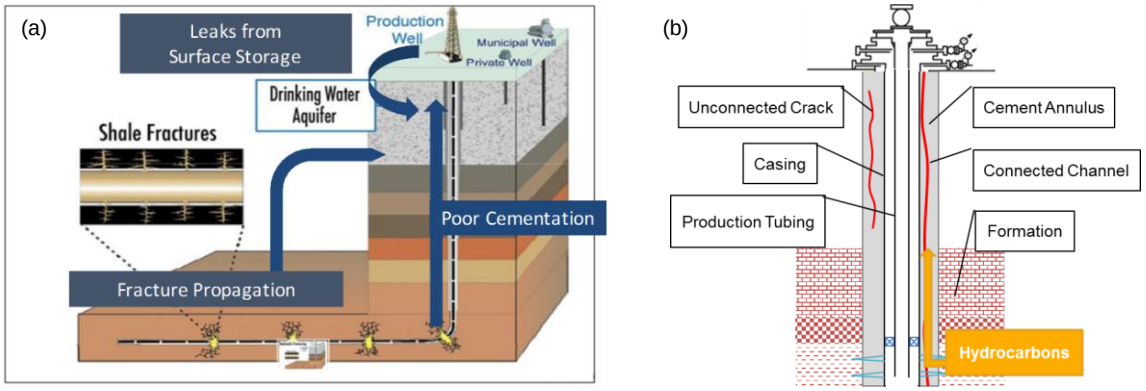

Figure 1.1 – (a) Potential contamination of shallow water aquifers due to poor cementation (Degenhardt, 2011); (b) Unwanted migration of hydrocarbons in cement annulus (Wu et al., 2017).

Several factors can lead to poor zonal isolation. The primary factor that affects zonal isolation occurs during a cementing operation, when incomplete displacement of drilling fluids with cement and / or contamination of cement slurry with drilling fluid can lead to defects such as voids, cracks, and channels in the cement annulus (McLean et al., 1967, Lockyear et al., 1990, Talabani et al., 1993, Al Hammad and Altameimi, 2002). Numerous studies have been conducted to identify the factors that affect cement displacement. These include wellbore quality (Cunningham, 2000), rheological properties of fluids (Miranda et al., 2007), flow rate, casing eccentricity, and pipe movement (Moroni et al., 2009). In the case of directional/horizontal drilling when the casing is not centralized, a cement slurry preferably flows through the wider annular gap while leaving undisplaced drilling fluid in the narrow gap (Nelson and Guillot, 2006). Moreover, contamination of cement, particularly by oil-based and synthetic-based muds (OBM/SBM), negatively

affects the properties of Portland cement. For example, the compressive strength and integrity of the hardened cement sheath can be compromised due to such contamination (Aughenbaugh et al., 2014).

There have been several studies focused on modeling of cement displacement. Other than the 2D displacement representation that is currently used in the field for planning operations (Nelson and Guillot, 2006), 3-D models have been developed to study the intermixing of mud and cement fluids (Chen et al., 2014). More recently, a state-of-the-art cement displacement model has been introduced to better understand the cement displacement process and identify solutions to improve the success of well cementing (Enayatpour and van Oort, 2017). For example, as shown in Figure 1.2, the model simulates the contamination of cement slurry due to the casing eccentricity. However, there is currently no real-time and in-situ sensing technology available to actually track the displacement process and directly verify the results of the aforementioned modeling studies.

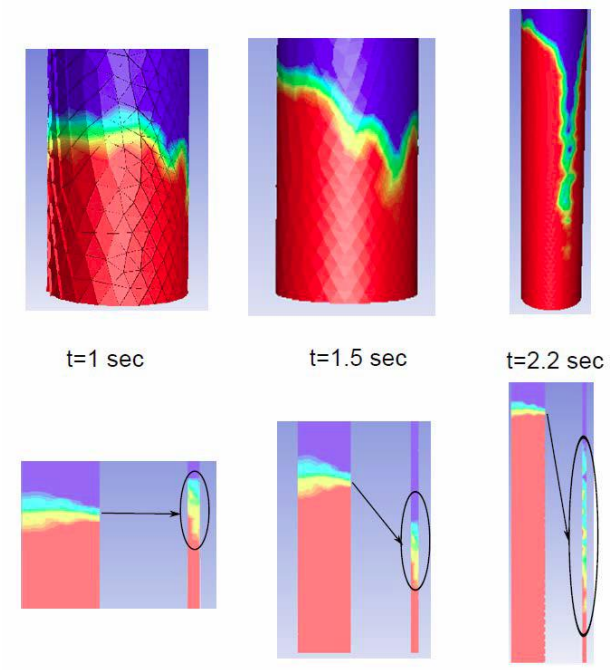

Figure 1.2 – Drilling fluid in blue is being displaced by cement in red and the simulation shows the cross contamination that can occur at the interface due to casing eccentricity as well as poor displacement on the narrow side of the casing annulus (Enayatpour and van Oort, 2017).

Another factor that impacts zonal isolation is the cement-casing bond strength. Any mud filter-cake that has not been removed can prevent bonding between cement and formation (Plank et al., 2014). During or after the cementing process, temperature and/or pressure variations can lead to de-bonding between the casing and cement annulus. To ensure the quality of cementing operation, the cement-casing bond strength should be considered at the beginning when designing a cement recipe. Early studies estimated the cement-casing shear bond strength to be 10% of the cement compressive strength (Evans and Carter, 1962). Other studies found that there is no apparent correlation between the cement compressive strength and shear-bond strength (Parcevaux and Sault, 1984). One of the reasons is that the cement-casing bond strength, or bonding performance, can be

affected by many factors. Some of these are related to cement properties such as fluid loss, free water, and chemical shrinkage tendency. Also, the quality of the cementing job can have an impact on the actual bonding performance. Others include the effects of downhole stress changes, temperature and pressure variations, and the bonding surface conditions, such as the presence of rust or drilling mud on the casing (Nelson and Guillot, 2006). Multiple experimental methods and laboratory setups have been developed in the past to determine the cement bond strength in a laboratory (Evans and Carter, 1962; Parcevaux and Sault, 1984; Jadhav et al., 2017; Khalifeh et al., 2018; Wilson et al., 2018). The use of X-Ray Computed Tomography (CT) and laboratory set-ups for thermal cycling experiments was also proposed to evaluate the quality of cement-casing bond by identifying the magnitude and location of micro-annuli or cracks (Skorpa and Vrålstad, 2016). In some cases, however, laboratory tests might not be able to reconstruct the bonding surface present in real field situations, which results in an inappropriate estimation of the bond strength.

In the field, cement bond logging (acoustic or ultrasonic logging) is frequently used to evaluate the quality of the cement bond (Nelson and Guillot, 2006). However, this requires active wellbore (re-)entry to deploy the logging tools by running drillpipe or wireline after the cementing operations, and it can only provide a "snapshot" of the cement bond in time. Such (re-)entry and well intervention can increase the cost and non-productive time of an oil or gas well, due to the need for suspending any ongoing operations such as hydrocarbon production on actively producing wells. It also carries additional risks associated with potential well control incidents during the well intervention exercise. Limitations exist for accurate measurement and interpretation of the standard cement bond log. For example, contamination of the cement layer could lead to erroneous conclusions,

such as indicating a bad cement bond even though the cement layer has hardened and is impermeable (Batcheller, 2013).

Moreover, even if the bond between the casing and cement annulus is good, many factors in the complicated downhole environment present during drilling, completion, stimulation, and production operations can cause cracking within the cemented annulus. Once these cracks, voids, and other defects are connected, they can become channels that potentially provide pathways for migration and communication of hydrocarbons (oil and/or gas) from different zones, as shown in Figure 1.1b, thus compromising zonal isolation and causing sustained wellhead pressures.

Currently, there is no technique available that can monitor in real-time what happens in the annular space from initial drilling fluid displacement all the way to well abandonment and decommissioning. After reviewing a large number of downhole monitoring techniques, distributed fiber optic sensor technology was chosen for this research because it can provide real-time, long-term, non-destructive/non-interruptive monitoring. Distributed fiber optic sensing (DFOS) technologies have been used in the oil and gas industry since the 1990's (Kamal, 2014). These technologies have been applied to different phases of drilling and production operations, including - but not limited to - borehole seismic surveys, fracture monitoring, flow profiling, well integrity monitoring and well abandonment monitoring (Baldwin, 2014). In a recent study, an advanced DFOS technology, specifically, distributed temperature and strain sensing (DTSS) system based on Brillouin and Rayleigh backscattering, was installed in a test well for CO_2 injection and successfully validated its capability of monitoring wellbore integrity based on the strain measurement (Xue et al., 2014, Xue and Hashimoto, 2016).

This study focuses on the further development of the fiber optic technology to address the evident need for new techniques that allow for continuous, real-time and long-

term monitoring of the cement and casing without interrupting the drilling / completion / stimulation / workover / production / abandonment phases. This can be enabled by novel improvements to the DTSS system and the specific applications focused on the cement evaluation proposed in this research. The fiber optic sensing system (DTSS as mentioned above) is equipped with specially designed sensing cables packaged with hydrocarbon sensitive polymer to achieve distributed temperature, strain and chemical sensing (DTS, DSS, and DCS) in one system. The fiber optic cables are expected to be installed on the outside of a casing string, embedded in the cement annulus, or on the inside of an abandonment plug. DTS and DSS are achieved by a hybrid Brillouin-Rayleigh technique which allows separated temperature and strain measurements in one single optical fiber. DCS is enabled by separating out specific strain changes that only reflect the presence of hydrocarbons. When exposed to hydrocarbons, hydrocarbon-sensitive polymers will swell. Such swelling can introduce strain changes on fiber optic cables coated with these polymers, which can be detected by the DTSS system and differentiated by detailed analysis.

1.2 OBJECTIVES AND SCOPE

The main objective of this dissertation research is to explore the capability of using the fiber optic Distributed Temperature and Strain Sensing (DTSS) system to achieve lifetime monitoring of zonal isolation and cement integrity in oil and gas wells. The scope of the work is illustrated in Figure 1.3. The detailed objectives categorized based on different stages of the well construction and cementing operations are listed as follows:

1. During the fluid displacement stage, the drilling mud is displaced by spacer fluid followed by cement slurry. The first objective of this work is to showcase the use

of the DTSS system in combination with a specially made fiber optic sensing cable to track the cement displacement process and to identify the location of each fluid in real-time to ascertain displacement efficiency.

2. During the Wait-on-Cement (WOC) time while the cement slurry is setting in place, monitoring of the cement hydration process using the DTSS system is proposed to evaluate the quality of the cementing operations.
3. After the cement hardens, the feasibility of using the DTSS system for monitoring the long term integrity of cemented annuli is proposed; specifically for:
    a. detection of unwanted hydrocarbon invasion in the cement annulus or cement plug using a hydrocarbon sensitive cable;
    b. detection of casing deformation and its effect on zonal isolation;
    c. evaluation of the cement-casing bond and predictability of potential bond failure.

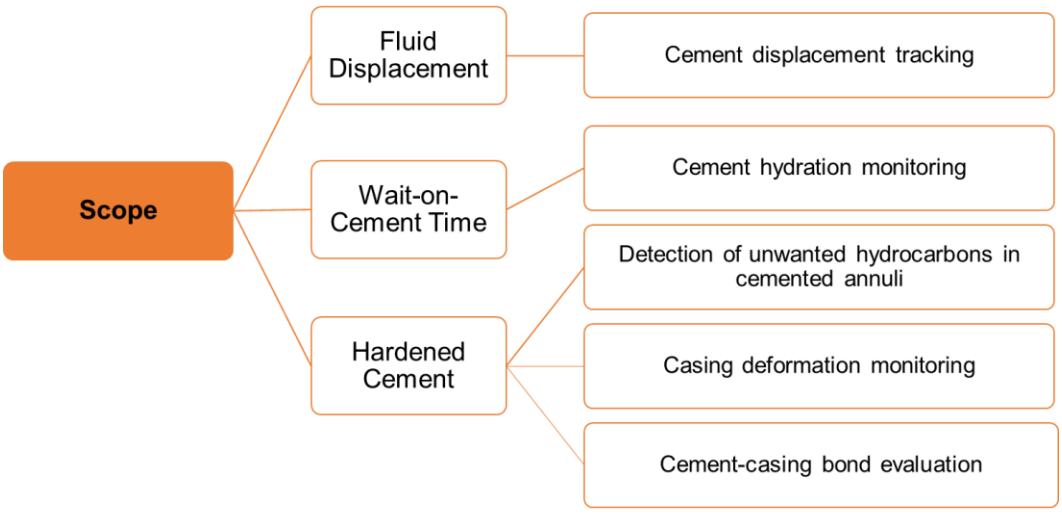

Figure 1.3 – A summary of the scope of this dissertation research.

1.3 DISSERTATION ORGANIZATION

The contents of this dissertation are divided into several chapters. Chapter 1 covers the introduction including the motivation and the objectives of this study as well as the organization of this dissertation. Chapter 2 is a literature review on the current status of distributed fiber optic sensing technologies, their applications in oil and gas industry, and factors impacting zonal isolation. Chapter 3 provides a detailed description of the fiber optic sensing cables, the materials and laboratory test set-ups, and the experimental methods used to demonstrate the proposed new applications using the DTSS system. Chapters 4, 5, and 6 cover the results from the experiments. In Chapter 4, the capability of using the DTSS system in combination with a specifically designed fiber for cement displacement tracking in real-time is demonstrated. Chapter 5 presents the results and discussions on cement hydration monitoring by analyzing the temperature and strain measurements using the DTSS while the cement slurry is setting in place. Chapter 6 focuses on using the DTSS system and the embedded fiber optic sensing cables to conduct long-time or even lifetime monitoring of the zonal isolation as well as the integrity of cement and casing. The first part of this chapter discusses unwanted hydrocarbon detection in the cement annulus due to compromised zonal isolation. The mechanism of using the proposed fiber optic system for distributed chemical sensing (DCS) was illustrated. The selective sensing capability was explored and verified in the experiments. The second part integrates the casing deformation detection into the sensing system. The third part presents the use of the DTSS system as a new evaluation tool for the cement-casing bond. At the end, Chapter 7 summarizes all the objectives, experiments, and results presented in this dissertation, and gives suggestions for future work, especially for actual field application of the system.

Chapter 2: Background

This chapter provides a background for the dissertation. Section 2.1 presents a literature review on the current status of the applications of distributed fiber optic sensors in the oil and gas industry, and a summary regarding the placement and deployment of these sensors. Both fully distributed and quasi distributed fiber optic sensing technologies are reviewed in this chapter. The fully distributed fiber optic sensing technologies are discussed based on individual measurement parameters such as temperature (DTS), acoustic (DAS), strain (DSS), and chemical (DCS) sensing. The quasi-distributed fiber optic sensing section focuses on the fiber Bragg grating system. In section 2.2, distributed temperature and strain sensing (DTSS) is introduced in detail. The DTSS system has been used in this study in order to leverage its multi-parameter (such as strain, temperature and chemical changes) sensing capabilities. In Section 2.3, to emphasize the need for a DTSS system, a brief overview of the factors impacting zonal isolation due to well cementing and subsurface geomechanical loads is provided.

2.1 Distributed Fiber Optic sensors and Their Applications in Oil and Gas

Distributed fiber optic sensing (DFOS) technology was first introduced to the oil and gas industry in 1990's (Kamal, 2014). Since then, more than 4000 wells world-wide have been equipped with fiber optic sensors (see Figure 2.1). Compared to other sensing technologies, DFOS has unrivaled advantages for downhole sensing. In a DFOS system, there is no need for downhole electronics since a light wave is used for both sensing and data communication, and thus it is immune to electromagnetic interference (EMI) (Udd and Spillman, 2011). DFOS technology provides real time monitoring capability and reliable measurement in harsh environments (e.g. high temperature). Also, since it is a

distributed sensing technique, it can cover the entire length of the well with one optical fiber, without the need for complex integration of numerous traditional point sensors. With permanent installation of the fiber optic cable in the well, DFOS can achieve lifetime monitoring without the need for wellbore re-entry. Multiple sensing parameters are available including temperature, strain, pressure, and acoustic. Based on the sensing mechanism, there are two major types of fiber optic sensing: fully distributed and quasi-distributed, which will be described in the following sections.

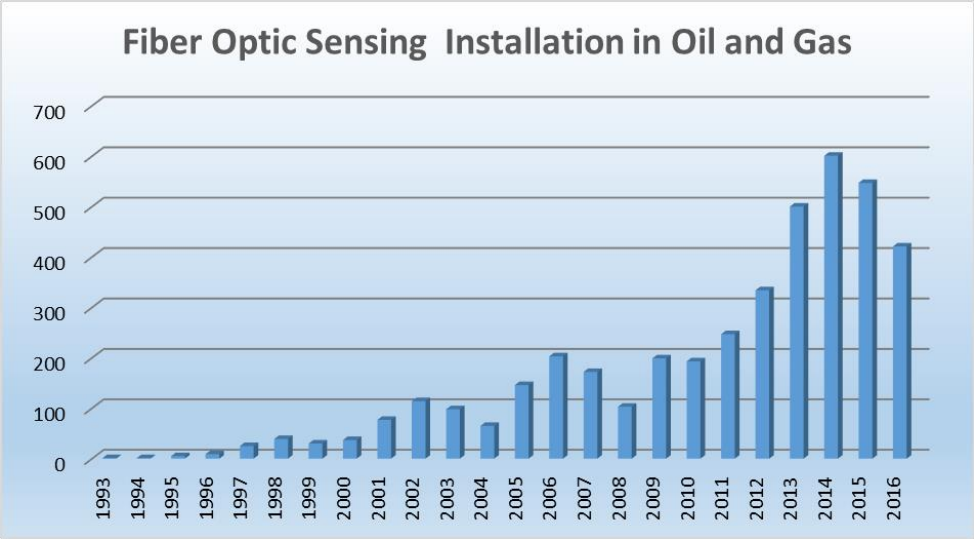

Figure 2.1 – Yearly fiber optic sensing installation plot reproduced based on SEAFOM fiber optic sensing deployment survey data (SEAFOM, 2018).

2.1.1 Fully Distributed Fiber Optic Sensing

The fully distributed fiber optic sensing is based on optical backscattering of light. As shown in Figure 2.2, when light transmits into an optical fiber, the light is scattered by tiny imperfections or density variations in the fiber glass core. Such backscattered light

carries valuable information for sensing, wherein every point along the optical fiber becomes a sensing element, and thus distributed sensing can be achieved. Three light backscattering phenomena, i.e. Raman, Brillouin and Rayleigh backscattering, are shown in Figure 2.2. The location where an event occurs (e.g. where there is a change in temperature and/or strain) can be determined from the amount of time the backscattered light takes to return to the detection unit. Thus, the presence, location, and intensity (or severity) of such an event can be quantified using the DFOS technology, providing more detailed information for decision-making. The most widely applied DFOS techniques in the oil and gas industry are Distributed Temperature Sensing (DTS) and Distributed Acoustic Sensing (DAS). In recent years, emerging DFOS technologies such as Distributed Strain Sensing (DSS), Distributed Chemical Sensing (DCS) and Distributed Temperature and Strain Sensing (DTSS) have been studied and introduced to the industry.

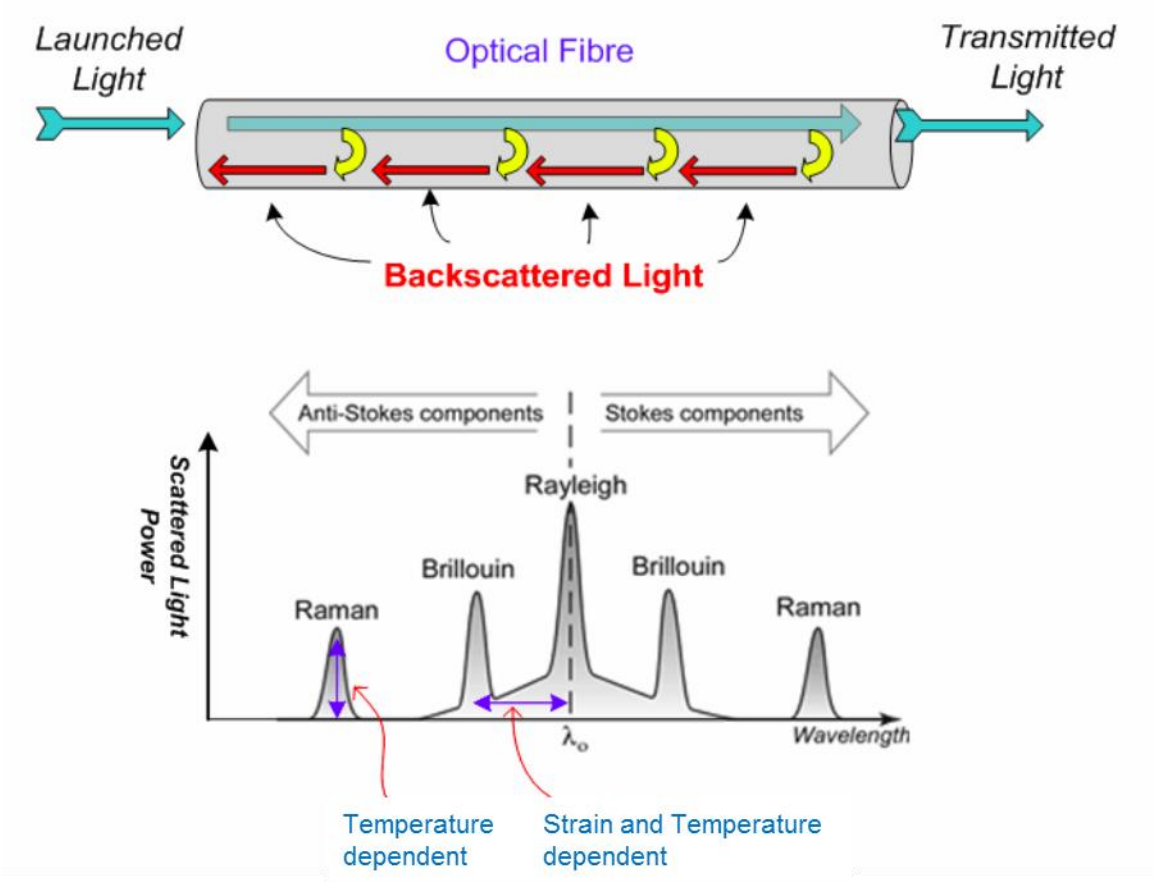

Figure 2.2 – Raman, Brillouin, and Rayleigh backscattering (Soga et al., 2008).

Distributed Temperature Sensing (DTS)

The most commonly used DTS system is based on Raman inelastic scattering using a multi-mode optical fiber (Hartog, 2017). Both multi-mode and single-mode optical fibers can be used for fiber optic sensing. An illustration of the difference between these two is provided in Figure 2.3. Multi-mode optical fiber has a larger glass core in diameter (50 or 62.5 microns) in comparison to a single-mode optical fiber (9 microns). Each potential path for light propagation in the optical fiber is known as a mode of the fiber. The larger glass

core of the multi-mode fiber allows for the propagation of multiple light modes (see Figure 2.3) and also simplifies connections (e.g. ease of splicing). In contrast, with extremely small glass core size, a single-mode optical fiber only transmits light in one mode that is paralleled to the length of the fiber as shown in Figure 2.3 and requires more precise alignment for connections (Crisp, 2005). Single-mode optical fibers exhibit superior performance over longer distances compared to multi-mode fibers due to their lower attenuation, which equates to less reduction or loss in optical power while the light wave travels along the optical fiber (Mathur, 2018). However, for Raman-based DTS, multi-mode optical fibers are normally used since it requires more optical power for data acquisition.

As illustrated in Figure 2.2, Raman scattering is only sensitive to temperature; a temperature change on the optical fiber introduces a change in the intensity of the Raman scattering light (Rajan and Prusty, 2016). By establishing a correlation between the Raman scattered light intensity and temperature, the downhole temperature can be obtained accurately. Another type of DTS is based on Brillouin scattering using a single-mode optical fiber. It is referred to as Brillouin Distributed Temperature Sensing (B-DTS). Brillouin backscattering, which is also inelastic scattering, occurs when light interacts with acoustic phonons caused by thermal excitation or strain as the light travels in a transparent medium such as an optical fiber (Bao and Chen, 2011). The Stokes light generated by the Brillouin backscattering exhibits a center frequency shift with respect to the incident light, which is called the Brillouin frequency shift. Since Brillouin scattering is sensitive to both temperature and strain (see Figure 2.2), to avoid the effect of strain on Brillouin center frequency shift in temperature measurement, B-DTS requires strain-free installation of optical fiber such as the use of Fiber in Metal Tube (FIMT) by placing the optical fibers in stainless steel tubing. Note that in some cases when there is significant strain applied on

the optical fiber, the temperature measurement can still be negatively affected even using FIMT, which leads to errors in temperature reading.

Raman-based DTS has been studied and deployed in the field for many applications including gas lift monitoring and optimization (Sanchez et al., 2005; Weaver et al., 2005), production monitoring and gas breakthrough detection (Brown et al., 2007; Fryer et al., 2005), injection profiling (Brown et al., 2004; Rahman et al., 2011), fracture stimulation diagnostics (Huckabee, 2009), acid stimulation monitoring (Clanton et al., 2006), well integrity monitoring such as tubing and casing detection (Julian, 2007) and pipeline leak detection (Walker and Carr, 2003). Brillouin-based DTS has been used for pipeline leak detection (Mishra et al., 2017)

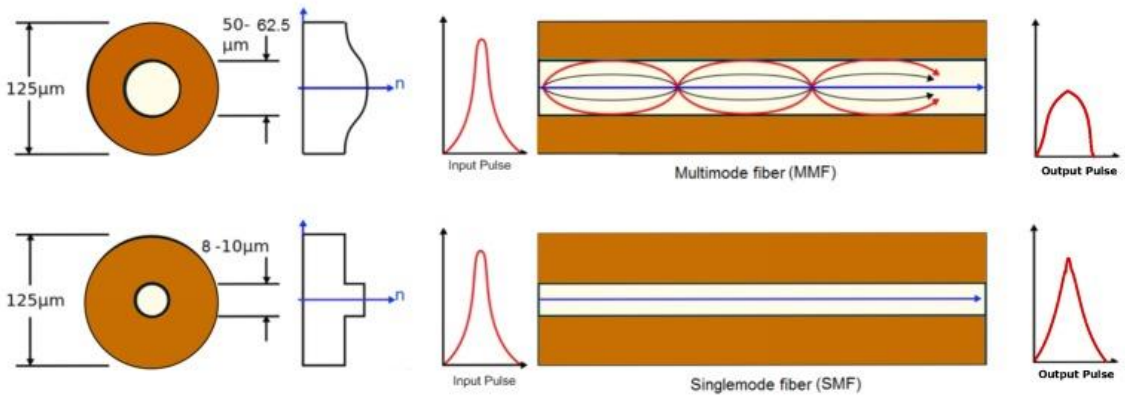

Figure 2.3 – Difference between single-mode and multi-mode optical fiber (Miah and Potter, 2017).

Distributed Acoustic Sensing (DAS)

DAS is based on Rayleigh elastic scattering. In elastic scattering, the frequency (wavelength) of the scattered light remains same as the incident light while the direction of

the light propagation changes. In DAS, small sections along the optical fiber act as an interferometer. When the pressure pulse of an acoustic wave strikes the optical fiber, the changes in intensity or phase of the Rayleigh scattered light caused by localized changes of the fiber segment length are measured (M. Molenaar et al., 2012). The data analysis and interpretation of DAS can be more complex compared to the Raman or Brillouin based DFOS due to the large quantities of acoustic data produced. For example, DTS can send a reading every 4 seconds along the optical fiber while the DAS can send 10,000 times as much data every second (Rassenfoss, 2012). The major applications of DAS in the oil and gas industry are related to production and inflow monitoring (In 't Panhuis et al., 2014; van der Horst et al., 2014), injection monitoring (Carpenter, 2016; Johannessen et al., 2012), hydraulic fracture diagnostics (Denney, 2012; MacPhail et al., 2012; M. M. Molenaar et al., 2012), sand production detection (Mullens et al., 2010), vertical seismic profile (VSP) (Koelman et al., 2012) and microseismic (Webster et al., 2013), as well as leak detection for pipelines (Siebenaler et al., 2015; Thodi et al., 2014) and abandoned wells (Boone et al., 2014).

Distributed Strain Sensing (DSS)

Over the past decade (2008-2018), various studies have focused on strain measurements using DFOS for downhole applications (Earles et al., 2011, van der Horst, 2015, Krietsch et al., 2018). One type of DSS exploits Fiber Bragg Gratings, which will be introduced later in the quasi-distributed fiber optic sensing section. The other commonly used technique for DSS is based on Brillouin scattering. Under downhole conditions, changes in temperature and strain can occur simultaneously. As mentioned in previous section, Brillouin scattering is sensitive to both temperature and strain variations. To obtain

a strain measurement, the effect of temperature on the Brillouin center frequency shift is eliminated using various methods. One commonly used method for temperature compensation is to add another strain-free optical fiber to measure temperature in order to subtract the Brillouin frequency shift due to temperature (Bao et al., 1994). Several studies also proposed the use of a multi-core optical fiber (Mizuno et al., 2015; Zhao et al., 2017) or two special modes of a multi-mode optical fiber (Weng et al., 2015; Xu et al., 2016) to differentiate between the Brillouin center frequency changes due to temperature and strain. Integrating a Raman-based DTS using an additional multi-mode optical fiber (for temperature measurement only) into a Brillouin-based system was another method that has been investigated and developed (Alahbabi et al., 2005). The newest method, deployed in this study, applies hybrid Brillouin and Rayleigh technique to separate temperature and strain measurements using only one single-mode fiber. It falls under the category of DTSS (Kishida et al., 2012), which is illustrated in Section 2.2.1. The majority of current applications of DSS (Brillouin-based) are focused on well integrity such as monitoring of casing mechanical deformation (Li et al., 2004).

Distributed Chemical Sensing (DCS)

The idea of distributed chemical sensing using fiber optic sensors was first introduced in the late 1980s (Kersey and Dandridge, 1990). One way to enable DCS is the use of specific coating on the fiber optic sensing cable. When exposed to a chemical of interest, the special coating tends to swell. This swelling can be converted into strain variation that is transferred to the optical fiber by a packing mechanism. Thus, the changes in strain due to the presence of a chemical are measurable by using a DSS system. Such a fiber optic sensing cable coated with hydrocarbon sensitive polymers has been studied and

applied to hydrocarbon leakage detection in the Civil Engineering field for pipelines, tanks, and other storage facilities since the early 2000's as shown Figure 2.4 (see e.g. Buerck et al., 2004; Carrillo et al., 2002; López et al., 2002; MacLean et al., 2003). However, this type of cable design has not been used in oil and gas wells for monitoring of the cement displacement process or to detect the presence of unwanted hydrocarbons in the cement annulus.

In some cases, instead of applying a coating on the optical fiber, the cladding of an optical fiber is modified to achieve specific chemical sensing. Cladding is a low-refractive-index layer coated on the high-refractive-index glass core of the optical fiber to confine the light to the core by total internal reflection (c.f. Figure 2.5). For example, for fluorescence-based corrosion monitoring using DFOS, an optical fiber was modified to include a fluorescent dye in the cladding (Sinchenko et al., 2008). In another example, the cladding of the optical fiber was modified with phenol red (dye used as pH indicator) for pH monitoring (Potyrailo and Hieftje, 1998).

The current use of DCS in the oil and gas industry is limited to corrosion detection (Buerck et al., 2004) and hydrocarbon leakage of pipelines (Buerck et al., 2004; López et al., 2002; MacLean et al., 2003).

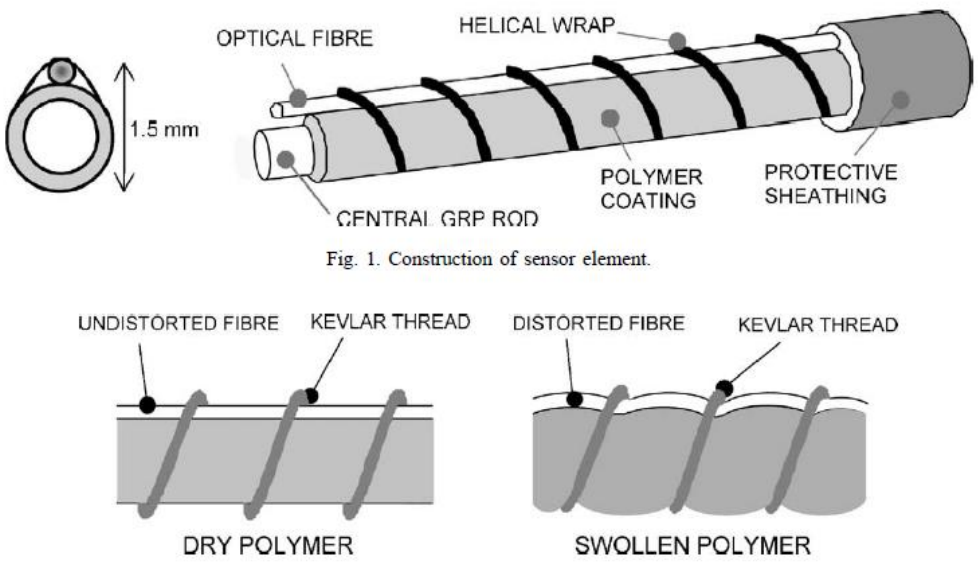

Figure 2.4 – A prototype fiber optic sensing cable proposed for hydrocarbon fuel spill (MacLean et al., 2003).

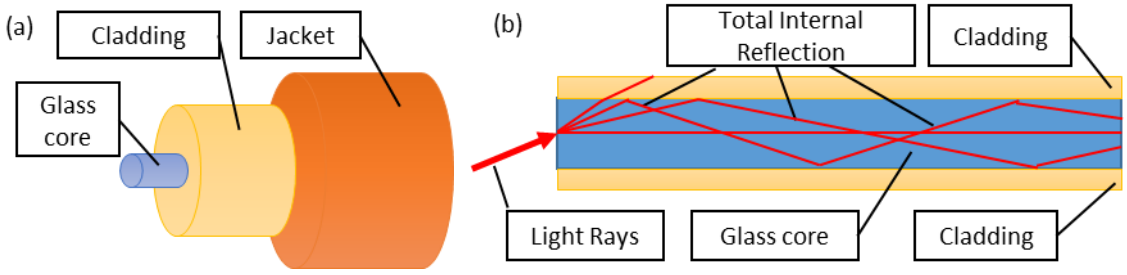

Figure 2.5 – (a) Schematic of a typical fiber optic cable; (b) total internal inflection of the light travels in the optical fiber.

2.1.2 Quasi-Distributed Fiber Optic Sensing

The most commonly used quasi-distributed fiber optic sensing method, using Fiber Brag Grating (FBG), relies on tracking the reflected light from the grating written on the optical fiber. This is another well-known fiber optic sensing technology that has been successfully used in the oil and gas industry (Kamal, 2014). The reason why FBG is considered as a quasi-distributed fiber optic sensor is that not every point along the optical fiber can be a sensing element in FBG system. Instead, each grating along the fiber represents an individual sensor, as shown in Figure 2.6. A special optical fiber has to be drawn and carved with gratings at specific intervals along the length of the fiber using standing wave, point-by-point writing, holography or phase mask (Fang et al., 2012). The location of FBG sensors along the optical fiber is pre-determined and the number of gratings in a single fiber is limited. The reflected light at each grating (FBG1 and FBG2, c.f. Figure 2.6) has a different wavelength. As illustrated in Figure 2.6, the reflected light wavelength from FBG1 is λ_1 and that from FBG2 is λ_2. When an event (temperature or strain change) occurs at the location of FBG1, the wavelength of reflected light at FBG1 shifts by $\Delta\lambda$ while there is no change in the wavelength of reflected light at FBG2. In this way, the location of such an event can be determined.

In oil and gas industry, the FBG system has been applied for compaction monitoring (Pearce et al., 2009a) , structural integrity monitoring (e.g. flexible riser, offshore platform, pipeline, etc.) (Morikawa et al., 2010; Nie et al., 2018; Ren et al., 2005), reservoir monitoring (Bostick, 2003), flow monitoring (Earles et al., 2011), and cement curing monitoring (Pearce et al., 2009b).

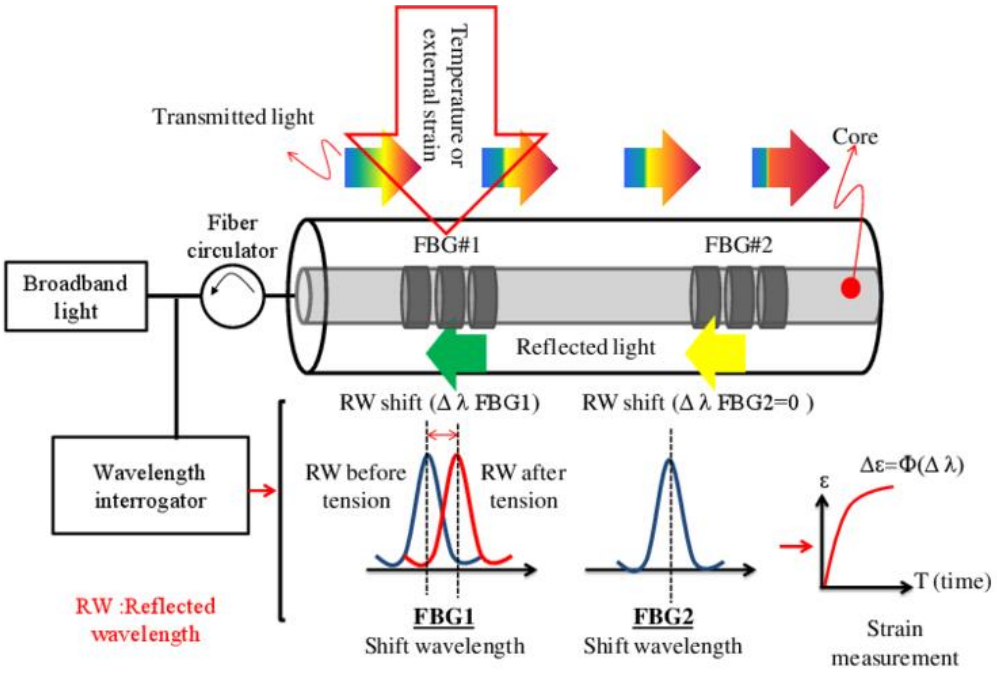

Figure 2.6 – Fiber Bragg Grating Mechanism (Malekzadeh et al., 2014).

The above-mentioned distributed fiber optic sensing technologies and their basic mechanisms are summarized below in Table 2.1.

Table 2.1 – Summary of distributed fiber optic sensing technologies.

Type of DFOS	Mechanism
Distributed Temperature Sensing (DTS)	Raman scattering light intensity changes due to temperature variations
	Brillouin center frequency shift due to temperature variations without the effect of strain
Distributed Acoustic Sensing (DAS)	Intensity or phase of Rayleigh scattering light changes due to acoustic wave generated by an event
Distributed Strain Sensing (DSS)	Brillouin center frequency shift due to strain changes on the optical fiber without the effect of temperature
Distributed Chemical Sensing (DCS)	Different DCS techniques have different mechanisms. For example, loss (intensity reduction) of Rayleigh scattering light due to micro-bending.
Fiber Bragg Grating (FBG)	Each grating reflects light with a different wavelength. The temperature or strain changes causes wavelength shift at certain gratings and thus can be located.

The most common uses for distributed fiber optic sensing technologies in the oil and gas industry are summarized in the Table 2.2. Although DFOS is extensively used in the oil and gas industry for various applications, studies based on evaluation of cement and zonal isolation monitoring using DFOS are relatively limited. A few of the reported studies include the use of slickline DTS to evaluate cementing operations and determine the location of the TOC (Diarra et al., 2014), the use of DAS to detect leaks in abandoned wells

(Boone et al., 2014), and the use of FBG as temperature sensors for cement curing monitoring (Pearce et al., 2009b).

Table 2.2 – A list highlighting the usage of distributed fiber optic sensing technologies for various applications in the oil and gas industry.

Production Optimization • Production and inflow monitoring • Gas breakthrough detection • Gas lift monitoring and optimization	**Well Integrity** • Sand production detection • Casing and tubing leak detection • Leak detection in abandoned well
Stimulation Monitoring • Acid stimulation monitoring • Hydraulic fracture diagnostics	**Seismic** • Microseismic • Vertical seismic profile (vsp)
Injection Management • Injection profiling	**Downstream** • Pipeline leak detection

2.1.3 Placement and Deployment of Distributed Fiber Optic Sensors

There are a variety of methods to deploy DFOS in an oil or gas well. The temporary deployment method is similar to other retrievable or through-tubing well logging tools that are conveyed by wireline or coiled tubing. A permanent installation can be conducted behind the casing or outside the tubing to provide continuous or on-demand interrogation without well intervention. The selection of installation methods depends on the specific

applications. For example, the deployment of the fiber optic cables cemented behind casing is required for fracture diagnostics (Sierra et al., 2008). Most of the fiber optic cables have been installed axially along the length of the casing or tubing. It is possible to install multiple fiber optic cables on the tubing/casing axially at different angles to increase sensing area. The other type of installation method, the helical installation, which covers the annular space of the casing or tubing, has been explored and developed for the FBG system (Rambow et al., 2010). Although the helical installation can be more costly than the straight axial installation, it can provide a 360 degree image of the casing and annular space, which has a significantly larger sensing area and thus provides more information. The helical installation can be applied for critical zones with specific needs for annular monitoring. In any of these cases, the fiber optic cable installation plan needs to be carefully designed and pre-determined to prevent any damage to the cables from well completion operations such as perforations by using clamping and centralization system (see Figure 2.7). The quality of the deployment can also affect the analysis and interpretation of the sensing results. For example, poor installation and thermal coupling of the fiber optic cable embedded in the cement annulus can lead to noisy DTS measurements (Sierra et al., 2008).

In terms of the cable selection, it depends on the requirements of the application, the type of sensing techniques used and the downhole environment. In most cases, there will be more than one optical fiber inside the fiber optic cable installed although theoretically one optical fiber is sufficient for measurement using the DTSS system. These additional optical fibers can serve to obtain more accurate measurement (e.g. temperature compensation as mentioned before) and/or as backup in case one of them fails. They can also be used for different sensing purposes such as one optical fiber for DTS and the other one for DAS in an integrated system. The fiber optic sensing cable is usually protected by multiple layers as shown in Figure 2.8a. Pressure control at the wellhead is required to

prevent any leak through the fiber optic cables (Figure 2.8b). Figure 2.9 presents various components of the crossover and wellhead outlet with required pressure rating. In summary, placement and deployment of the DFOS, which require professional knowledge and experience, are important parts to achieve high quality of the measurement data and thus accurate interpretation and analysis of the data.

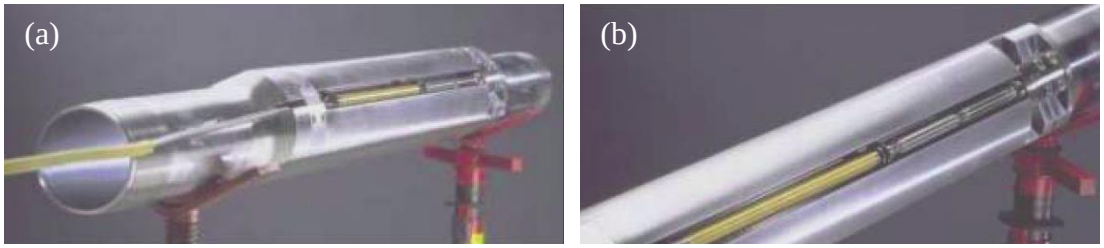

Figure 2.7 – (a) An example of fiber optic cable installation using a gauge carrier, which was run with the completion string; (b) the fiber optic cable was mounted on the gauge carrier (Weaver et al., 2005).

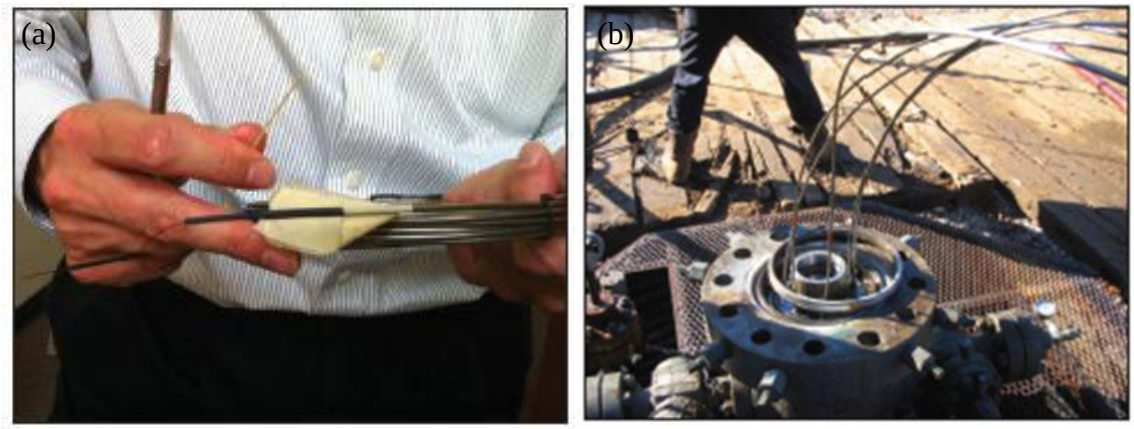

Figure 2.8 – (a) An example of fiber optic sensing cable used in downhole applications; (b) An example of fiber optic sensing cable installed at the wellhead (Rassenfoss, 2012).

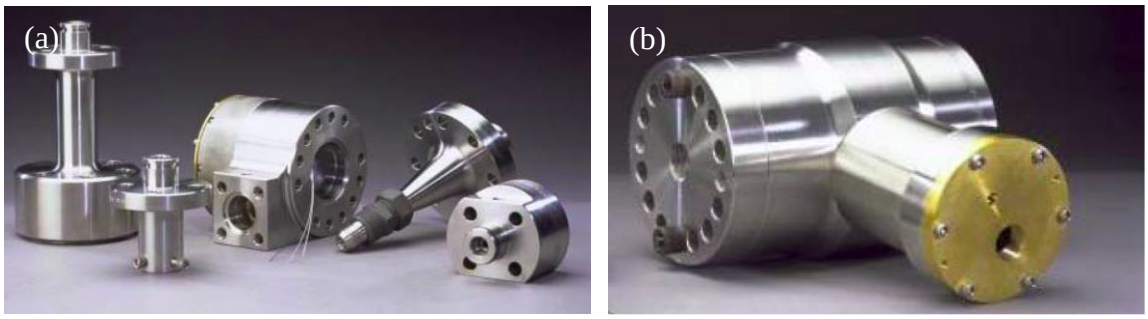

Figure 2.9 – (a) An example of assembled wellhead outlet with specific pressure rating for the fiber optic sensing cable; (b) components of this well head outlet and crossover assembly (Weaver et al., 2005).

2.2 DISTRIBUTED TEMPERATURE AND STRAIN SENSING (DTSS)

To maximize the capability of DFOS, in many cases, multiple sensing techniques are integrated into one system to achieve multi-parameter sensing. For example, a system integrated with DTS and DAS was evaluated in the field to improve fracture diagnostics (Sookprasong et al., 2014; Ugueto et al., 2014). In this dissertation, DTS and DSS are both concurrently achieved by using a hybrid Brillouin and Rayleigh technique.

2.2.1 Hybrid Brillouin and Rayleigh technique

The distributed fiber optic sensing system used in this study (referred to in the following as "the DTSS system") is based on hybrid Brillouin-Rayleigh monitoring, which offers the capability to measure temperature and strain using one single-mode fiber over long distances (up to 25 km), with high accuracy and spatial resolution on the order of centimeters (10^{-2}m) (Kishida et al., 2012). The system is built on Pulse-Pre-Pump Brillouin Optical Time-Domain Analysis (PPP-BOTDA) and Tunable Wavelength Coherent Optical

Time Domain Reflectometry (TW-COTDR) techniques. These techniques are briefly introduced in the following paragraphs.

PPP-BOTDA is based on stimulated Brillouin backscattering which can be achieved by using two laser sources in a closed-loop, double-ended optical fiber. Two light waves, one a pulse and the other a continuous wave, are generated by the two lasers and are counter-propagating along the optical fiber. When the frequency offset between the two matches the Brillouin frequency shift, a significant amplification occurs on the light wave at lower frequency as it propagates and is detected by the receiver for frequency analysis (Horiguchi and Tateda, 1989). As shown in Figure 2.10, strain and/or temperature variations along the optical fiber can cause Brillouin frequency shifts, which are detected by the BOTDA. The conventional BOTDA system can only achieve spatial resolution down to 1 m (Horiguchi et al., 1994). PPP-BOTDA enables the breakthrough increase in spatial resolution to 2 cm (Kishida et al., 2005). In a single-mode optical fiber, this Brillouin frequency shift ($\Delta\nu_B$), is proportional to the variation in strain ($\Delta\varepsilon$) (Horiguchi, Kurashima, and Tateda 1989), and the variation in temperature (ΔT) (Kurashima, Horiguchi, and Tateda 1990) along the fiber. The relationship between them can be represented by the following equation:

$$\Delta\nu_B = C_{11}\,\Delta\varepsilon + C_{12}\,\Delta T \quad \text{Eq. 2.1}$$

where C_{11} is the strain-frequency coefficient and C_{12} is the temperature-frequency coefficient for the Brillouin frequency shift (Kishida et al., 2012).

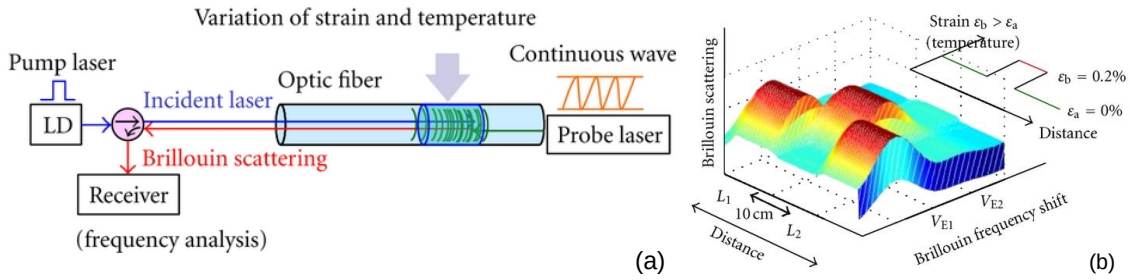

Figure 2.10 – (a) Principle of BOTDA; (b) A strain on the optical fiber causes a shift in the center frequency (Zhang and Wu, 2012).

The TW-COTDR technique is based on Rayleigh backscattering, which occurs due to small variations in the refractive index of the glass core of the fiber when light travels through it (Froggatt and Moore 1998). However, it is considerably different from the Rayleigh technique that has been used in the oil and gas industry for seismic surveys (Mateeva et al., 2012) and production inflow profiling (van der Horst et al., 2014). The latter technique, known as Distributed Acoustic Sensing (DAS), either utilizes changes in intensity or, more recently, changes in phase of Rayleigh scattered light due to an acoustic wave (Shatalin et al., 1998, Juarez et al., 2005). Almost all of the DAS applications are based on the use of a single laser wavelength (Liehr et al., 2018). The TW-COTDR technique uses a tunable wavelength laser ranging between 1530 nm and 1560 nm. Since the Rayleigh backscattering is elastic scattering, the frequency of Rayleigh scattered light does not shift with presence of environmental changes such as temperature and/or strain like the center frequency of Brillouin backscattering. Instead, TW-COTDR is more similar to the technique used for Fiber Bragg Grating (FBG) without the need for gratings written on the optical fiber. Density fluctuations in the optical fiber causing random fluctuations of the power spectrum are utilized as natural ‘gratings’ (Kishida et al., 2014). In FBG, as illustrated in Section 2.1.2, each grating reflects a specific wavelength. The reflected

wavelength of a grating shifts with the presence of temperature and/or strain changes at that grating. The location and magnitude of such temperature and/strain change can be obtained by analyzing the reflected wavelength shifts. In TW-COTDR, similarly, the power spectrum also shifts with the presence of temperature and/or strain changes. The initial power spectrum is recorded as a reference with a certain incident light frequency. When the temperature or strain changes occur, the laser is tuned to a new incident light frequency to restore the previous power spectrum. The difference of the incident light frequency before and after the temperature or/and strain changes is proportional to these changes. Such frequency shift of the incident light can be determined by comparing the power spectrum between the measured state and the reference state via cross-correlation. The relationship among the frequency shift ($\Delta\nu_R$) for TW-COTDR, strain variations ($\Delta\varepsilon$), and temperature variations (ΔT) can be represented by the following equation:

$$\Delta\nu_R = C_{21}\,\Delta\varepsilon + C_{22}\,\Delta T \quad \text{Eq. 2.2}$$

where C_{21} is the strain coefficient and C_{22} is the temperature coefficient for the TW-COTDR incident light frequency shift. Parameters C_{11}, C_{12}, C_{21} and C_{22} in Eq. 2.1 and 2.2 can be obtained from calibration experiments (Kishida et al., 2012), allowing the two equations to be used in tandem to solve for the two unknowns, strain change $\Delta\varepsilon$ and temperature change ΔT. Since the optical fiber is not modified, it can be used for other purposes, such as communication, while serving at the same time as a distributed strain/temperature sensor. Unlike the spatial resolution of FBG, which is limited by the spacing of the gratings, the spatial resolution of TW-COTDR can be adjusted, based on the requirements of the intended application(s). The DTSS system allows one to use a spatial resolution of 2, 5, 10 or 20 cm (Kishida et al., 2012), covering distances of up to 25 km. In addition, TW-COTDR only requires access to a single-end of the optical fiber.

In oil and gas wells (and most other engineering applications for that matter), it is possible that both strain and temperature vary at the same time at any given location. In order to solve the problem of such strain-temperature cross-sensitivity, a number of methods have been proposed. These include using a strained fiber with another strain-free fiber for temperature measurement (Kwon et al., 2003), adding Raman-based distributed temperature sensing (DTS) for temperature compensation (Alahbabi et al., 2005), applying the amplitude measurement method (Parker et al., 1998), using polarization-maintaining fibers (Zou et al., 2009), or using dispersion-shifted fibers (Lee et al., 2001). Most of these methods require additional optical fibers or specific types of optical fibers. However, the DTSS system based on the hybrid Brillouin-Rayleigh technique can obtain a separated temperature and strain measurements using only one single-mode optical fiber by simultaneously solving Eq. 2.1 and Eq. 2.2. This presents a significant technical advantage of the DTSS system.

An additional advantage of the DTSS system is that it delivers a fully distributed sensing system, where every point along the optical fiber can be used as a sensor. Any single-mode optical fiber without any special modifications can be used. The DTSS system does not require gratings to be written on the optical fiber like the Fiber Bragg Grating (FBG) system (Bao and Chen, 2012). By comparison, with the DTSS system, the location of temperature and/or strain variations can be precisely determined by measuring the time of flight of the light from the location where the scattered signal gets modulated (Bao and Chen, 2012). PPP-BOTDA can provide fast and robust measurements while TW-COTDR has the same sensitivity as a conventional FBG system (Delepine-Lesoille et al., 2013) and is especially well suited to detect small temperature and/or strain changes.

In this study, the closed-loop (or double-ended) configuration, which requires connecting two ends of the optical fiber to the measurement device, was deployed in order

to achieve 2-cm special resolution using PPP-BOTDA technology for laboratory-scale experiments. The closed-loop configuration allows downsizing the specimens and reducing the costs for laboratory demonstrations but is not necessary for actual field applications. Instead, the single-ended configuration, which only requires connecting one end of the optical fiber to the measurement device, is most commonly applied in the field considering higher challenges of installation and risk of loss of functionality due to breaks in the optical fiber for closed-loop configuration. Such single-ended Brillouin-based technique can achieve a best spatial resolution of 10 cm (Bao and Chen, 2012), which is also sufficient in field application when it is compared with the 2-cm spatial resolution of closed-loop configuration.

2.3 FACTORS IMPACTING ZONAL ISOLATION

Several factors such as poor cementing operation, significant thermal/pressure fluctuations in a well, and/or continual formation and pressure changes can significantly impact zonal isolation (Nelson and Guillot, 2006). This section will focus on highlighting some of these factors that related to the research in this dissertation.

2.3.1 Well Cementing

After a cement slurry is placed in an annulus, drilling operations have to be suspended until cement slurry solidifies, hardens, and develops sufficient compressive strength. This period is known as waiting-on-cement (WOC) time, which can range from a few hours to several days depending on the slurry design, required compressive strength of the hardened cement, and downhole conditions. The WOC period will be longer at the

top of the cement (TOC) column, where the temperatures are lower than the bottom hole circulating temperatures (BHCTs) (Nelson and Guillot, 2006). Insufficient WOC time can result in poor quality of cement. In addition, even under almost ideal conditions, a cement slurry may get contaminated with drilling fluid during displacement. Existing literature shows that SBM contamination in cement slurries due to insufficient fluid displacement negatively affects compressive strength of hardened cement slurries (Aughenbaugh et al., 2014). WOC time may also be affected by contamination. The actual required WOC time may therefore be significantly different from the estimated one, resulting in cement that gains insufficient strength, which can compromise zonal isolation. Previous studies have identified possible methods to improve cement displacement efficiency, such as using rotation and reciprocation of the casing string (Lee and Dorge, 1983) or using magnetorheological cement formulations (Nair et al., 2015).

Cement hydration involves complex chemical reactions that are exothermic, releasing heat as the cement slurry cures into hardened cement and develops compressive strength. The heat evolution of cement hydration follows a specific pattern, which can be used to characterize the cement hydration kinetics. A typical heat of cement hydration curve with five distinct stages is shown in Figure 2.11. Stage I is marked by a rapid evolution of heat due to initial dissolution of ions. This stage ends within a few minutes after cement comes in contact with water and is usually difficult to capture. Stage II is the induction or transition period, where continued dissolution of ions and precipitation of hydration products occurs, but the heat evolution slows down significantly compared to stage I. Stage III indicates the acceleration in growth of hydration products and the onset of stage III is an indicator for initial set (Bentz and Ferraris, 2010) or end of the transition period (Sabins and Sutton, 1986). The end of stage III is denoted as final set. Initial and final set can be measured using the Vicat needle test (ASTM-C191, 2013). In stage III the

cement slurry starts to change from a viscous fluid to a solid-like material with a measurable compressive strength (Sabins et al., 1982). Beyond this in stages IV and V, cement hydration products continue to form, compressive strength continues to increase, but the rate of heat evolution begins to slow down because of the continuous reduction in available space and ions. Although heat evolution can be monitored and recorded accurately in a laboratory using an isothermal calorimeter, it is difficult to obtain such information in an actual well.

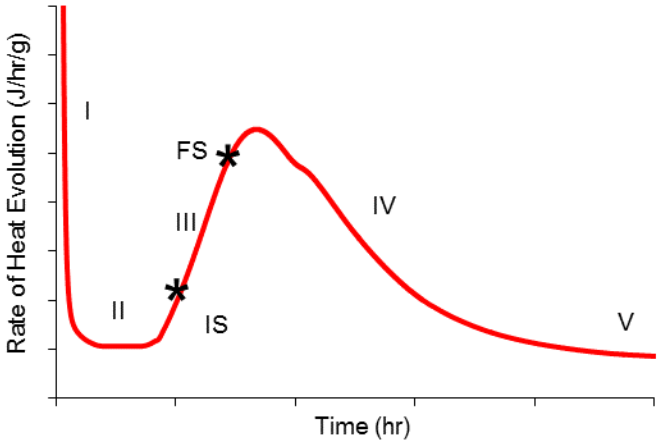

Figure 2.11 – Typical heat of hydration curve for cement slurry showing the five different stages. Note: IS stands for initial set and FS for final set.

2.3.2 Subsurface Geomechanical Changes

Subsurface geomechanical changes, e.g. changes in formation stress, temperature and pore pressure, can also threaten the integrity of the cement annulus while at the same time causing damage to casing strings (Cernocky and Scholibo, 1995). The deformation of

casing usually results from geomechanical loads associated with reservoir compaction, subsidence, and fault (re-)activation. Loads associated with these phenomena can cause severe damage to casing and production strings, negatively affecting production, and even threaten or shorten the life of the well. To mitigate casing damage due to reservoir compaction and subsidence, previous studies have focused mainly on improvement of well design based on complex geomechanical modeling and analysis (see e.g. Fredrick et al., 1998, Fredrich et al., 2000, Bruno, 2001). Monitoring for geomechanically-induced damage on casing, other than from passive observations of severe production problems or compromised barriers on abandoned wells, has received considerably less attention, with very few options available for such monitoring. Several studies proposed and developed strain measurements using distributed fiber optic sensors to monitor casing deformation due to compaction in the early 2000s (Li et al., 2004, Childers et al., 2007). One of these studies introduced a casing imager using the FBG system. The combination of FBG and helical wrapping was successfully demonstrated for monitoring casing deformation in multiple experimental tests and field trials (Pearce et al., 2009, Rambow et al., 2010) as shown in Figure 2.12.

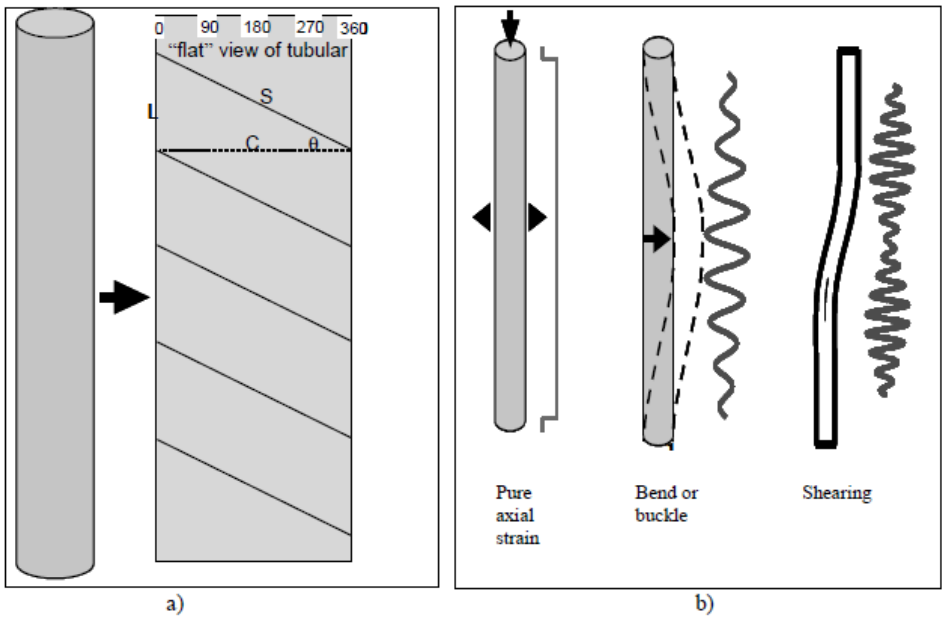

Figure 2.12 – (a) schematic of helical installation of fiber optic cable; (b) characteristics of FBG signals generated under different casing deformation modes (Childers et al., 2007).

Chapter 3: Materials and Experimental Methods[1]

Chapter 3 introduces the fiber optic sensing cable designed for temperature, strain and chemical sensing as well as the materials and experimental methods used for the laboratory demonstration. In Section 3.1, the designs for different types of fiber optic cables used in this study and the calibration methods to obtain the strain and temperature coefficients of the fiber are illustrated in detail. Section 3.2 presents the materials including the test fluids, the polymers studied for improving fiber optic sensing cables, and the materials to build experimental setups. Section 3.3 provides a full description of the experimental setups and methods to investigate the capability of the DTSS system for cement displacement tracking, cement hydration monitoring, unwanted hydrocarbon detection in the cement annulus, casing deformation, as well as cement-casing evaluation. It also presents the permeability test method used to determine the effect of cement-embedded fiber optic cables on the cement hydraulic properties. It also includes the test method to evaluate the sensitivity of different polymers that can be potentially used to enable chemical sensing.

3.1 Fiber Optic Sensing Cable

3.1.1 Types of Fiber Optic Cables

A single-mode (SM) optical fiber was used to collect data. The optical fiber was spliced to patch cables with FC/APC connectors. The patch cables were then connected to the pump and probe laser connectors of the DTSS system. Although the Rayleigh (TW-COTDR) sub-system requires only single-end access, both ends of the optical fiber were

[1] Parts of this chapter was published in Journal of Petroleum Science and Engineering:
Wu, Q., Nair, S., Shuck, M., et al., 2017. Advanced distributed fiber optic sensors for monitoring real-time cementing operations and long term zonal isolation. J. Pet. Sci. Eng. 158, 479–493. doi:10.1016/j.petrol.2017.08.072. Wu is the primary contributor (first author) of this paper.

connected to the DTSS system to form a closed-loop required for measurement by the Brillouin (PPP-BOTDA) sub-system to achieve 2-cm spatial resolution for laboratory-scale experiments in this study.

In some experiments, the optical fiber was used as is, and in other cases, the optical fiber was packaged with sensing materials and reinforcement. There are three major types of fiber optic cables used in this research. The first type of cable (shown in following figures in green color) is a typical single-mode optical fiber, referred to as 'the green cable' in the following sections. The first type of cable was used to demonstration the application of the DTSS system for cement hydration monitoring, casing deformation monitoring, and cement-casing bond evaluation.

The second type of cable (shown in Figure 3.1 in purple color), referred to as 'the purple cable' or 'p1 cable' in the following sections, includes a single-mode optical fiber, hydrocarbon sensitive polymer, a steel rod, and Kevlar thread. The steel rod with 0.64-cm (1/4-in) outer diameter (OD) was used to provide reinforcement for the cable. The reinforcement rod was coated with a thin layer of a hydrocarbon sensitive polymer. Such polymer will swell when exposed to certain types of hydrocarbons. The optical fiber was attached to the coated reinforcement rod longitudinally using a Kevlar thread. While helically wrapping the Kevlar thread, a weight was attached to the thread to ensure a uniform initial strain on the optical fiber. At both ends, the Kevlar thread was attached to the reinforcing rod using epoxy. The taut Kevlar thread ensures that any swelling in the hydrocarbon sensitive polymer can be converted into strain on the optical fiber. The modified version of the purple cable (named 'p2 cable') includes a steel braid was placed over the hydrocarbon sensitive polymer (Figure 3.1), before wrapping the cable with Kevlar thread (Figure 3.2), to provide additional protection for the fiber in the downhole environment. Note that the configuration of the lab-made purple cables represents a "proof-

of-concept" that will require further improvement and optimization before being employed in field practice. This particular configuration, however, does not pose any limitations on the system as long as the strain induced by a swelling polymer can be effectively transferred to the fiber using a suitable mechanism.

The third type of cable (shown in Figure 3.3 in black color), referred to as 'the black cable', previously used for strain sensing for concrete or steel structures (Neubrex Co., Ltd., 2007). It was designed for either surface attachment or embedding installation. In a preliminary study, the black cable was also found to have a similar response to that of the lab-made prototype purple cables (p1 and p2 cables). The coating of the sensor cable can selectively identify different fluids and detect their presence from the strain response caused by induced swelling or shrinkage. The black cable can be equipped with steel braids for additional protection and abrasion resistance. The steel braids can also provide additional confinement to enhance the response of the black cable to hydrocarbons. As shown in the Figure 3.3, it consists of two single-mode (SM) optical fibers in the center, two stainless steel wires (0.3 mm in diameter) on both sides for reinforcement, and a black-colored polyolefin elastomer used as a sensing polymer and a protective sheath. The cross-section of the cable has a dimension of 3.8 x 2.0 mm. The cable was designed to be used in the temperature ranging from -20 to 80 °C. The black cable was primarily used for cement displacement tracking and hydrocarbon detection.

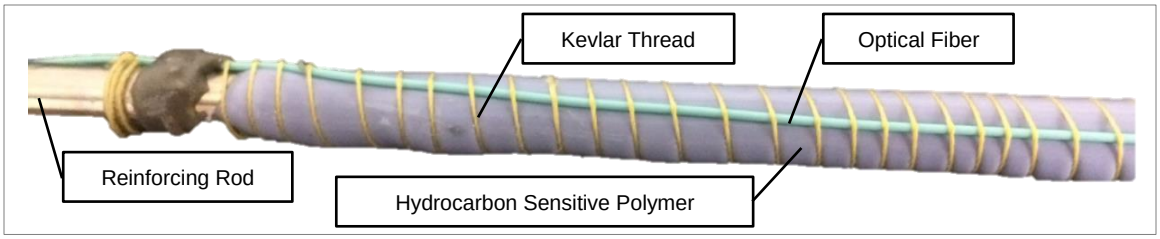

Figure 3.1 – Picture of p1 cable, which consists of an optical fiber and a hydrocarbon sensitive polymer held by Kevlar thread.

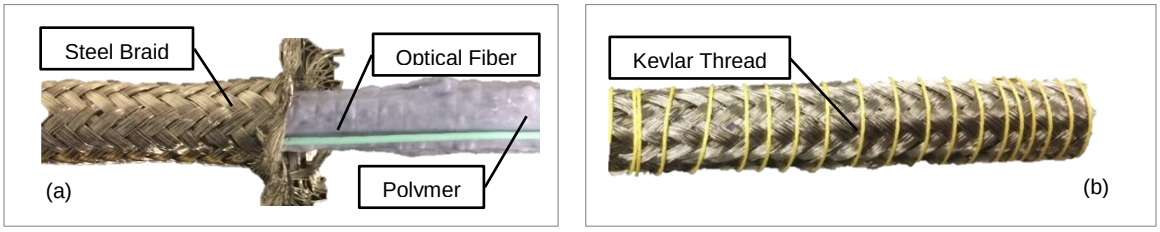

Figure 3.2 – Picture of p2 cable, which consists of an additional steel braid.

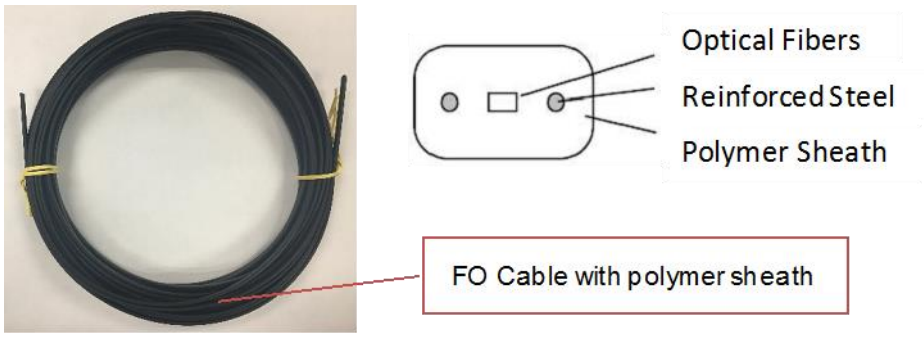

Figure 3.3 – Picture of the black cable.

3.1.2 Calibration Methods for the Fiber Optic Cables

The default values of the strain coefficients (C_{11} and C_{21}) and temperature coefficients (C_{21} and C_{22}) in the DTSS system are for the bare optical fiber. Different

coating on the bare fiber, used to protect the fragile glass fiber in real-world applications, can influence the sensing properties of the fiber. Thus, the strain and temperature coefficients (C_{11}, C_{12}, C_{21}, and C_{22}) in Eq. 2.1 and Eq. 2.2 in Chapter 2 had to be determined for each type of optical fiber used. These coefficients were obtained using calibration methods described in a previous study (Kishida et al., 2012). To obtain the strain coefficients (C_{11} and C_{21}), an experimental setup was assembled as shown in Figure 3.4. The calibration was conducted at constant room temperature (23 °C) to eliminate the effect of temperature on Brillouin center frequency shifts and Rayleigh incident light frequency shifts. Both ends of the optical fiber were connected to the DTSS system. Along the length of the optical fiber, one point was attached to a fixed block and another point was fixed on an adjustable clamp using epoxy resin. By rotating the threaded rod on the clamp, the optical fiber was subjected to various levels of axial strain. At each step, the displacement was measured using a dial strain gauge (Figure 3.4) to calculate the applied strain on the optical fiber. For strain ranging from 50 to 300 με, the step size was 50 με for each step; for strain ranging from 300 to 1550 με the step size was 250 με and finally, for strain ranging from 1550 to 5050 με, the step size was 500 με. At every step, Brillouin center frequency shifts and Rayleigh incident light frequency shifts were measured and recorded using the DTSS system.

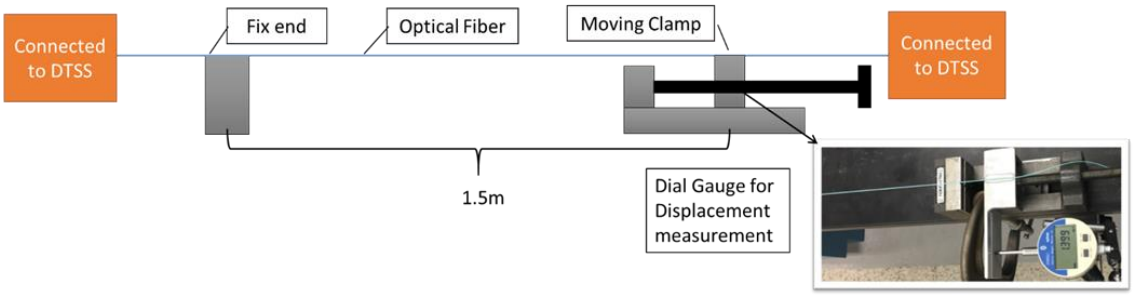

Figure 3.4 – Schematic of the experimental setup used for measuring the strain coefficients (see Eqs 2.1 and 2.2) of the optical fiber by elongating the optical fiber in small increments.

To obtain the temperature coefficients (C_{12} and C_{22}), a free section of the optical fiber was placed inside a water bath and the response was measured using the DTSS system as shown in Figure 3.5. The temperature was increased at 5 °C intervals from 20 °C to 75 °C and then decreased back to 20 °C, also at 5 °C intervals. At every increment/decrement, the temperature was kept constant for half an hour before Brillouin center frequency shifts and Rayleigh incident light frequency shifts were measured.

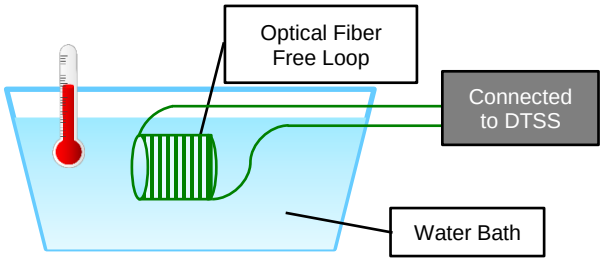

Figure 3.5 – Schematic of the experimental setup used for measuring the temperature coefficients (see Eqs. 2.1 and 2.2) of the optical fiber.

3.1.3 Coefficients from the Calibration of Fiber Optic Cables

For each type of the fiber optic cables, two sets of calibration tests were run to measure the strain and temperature coefficients. For the green cable, both sets of the calibration tests were in complete agreement with each other and the average results from the two sets are shown in Figure 3.6. In Figure 3.6a, the Brillouin center frequency difference measured as a function of applied strain is shown along the top horizontal axis and the frequency difference measured due to change in temperature is shown along the bottom horizontal axis. Similar information is shown in Figure 3.6b for the Rayleigh (incident light) frequency difference. The slopes of the trend lines in these plots represent the corresponding coefficient values, which are listed in Table 3.1. These strain and temperature coefficient values were used to convert the measured Brillouin/Rayleigh frequency shifts of the green cable for all the experiments conducted in this study. Unless otherwise stated, the temperature and strain measurement results for all applications (i.e. cement hydration monitoring) in this study were obtained by simultaneously solving Eq. 2.1 and Eq. 2.2 in Chapter 2. In some cases, when assessing temperature changes with minimal strain changes (or when assessing strain changes with minimal temperature changes), either the Brillouin or the Rayleigh technique was used by itself depending on the situations. For small temperature or strain changes only, the Brillouin frequency difference was neglected and Rayleigh technique, which is more accurate with higher spatial resolution, was used exclusively. For relatively large temperature or strain changes only, the Brillouin technique was chosen over the Rayleigh one since its measurement time was shorter. These particular instances are pointed out in the following relevant sections.

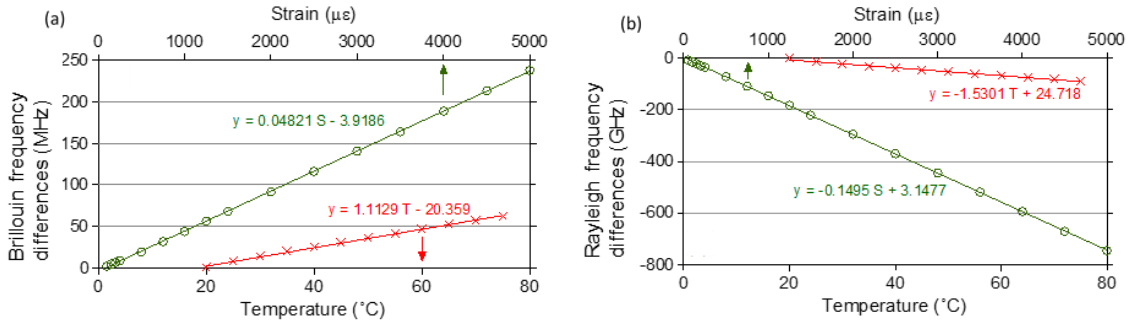

Figure 3.6 – Plots showing frequency difference v.s. applied strain (green circles) or external temperature (red crosses) for (a) Brillouin center frequency shift and (b) Rayleigh incident light frequency shift. Note: In the trend line equations, T represents temperature and S represents strain.

Similarly, such calibration tests were conducted for the black cable. The strain and temperature coefficients (C_{11}, C_{12}, C_{21}, and C_{22} in Eqs 2.1 and 2.2) for Brillouin and Rayleigh frequency changes for all types of cable are summarized in Table 3.1. Since the purple cable is, in fact, made out of the green cable with sensing packing material and reinforcement, the same coefficients as the green cable were used in this study.

Table 3.1 – PPP-BOTDA and TW-COTDR strain and temperature coefficients (C_{11}, C_{12}, C_{21}, and C_{22}) for all types of cables used in this study.

	Black cable		Green/ Purple Cable	
	PPP-BOTDA	TW-COTDR	PPP-BOTDA	TW-COTDR
Strain	C_{11} = 0.0409 MHz/με	C_{12} =-0.1271 GHz/με	C_{11} = 0.0482 MHz/με	C_{12} = -0.1495 GHz/με
Temperature	C_{12} = 1.7792 MHz/^{0}C	C_{22} = -3.1111 GHz/^{0}C	C_{12} = 1.1129MHz/^{0}C	C_{22} = -1.5301 GHz/^{0}C

3.2 MATERIALS

3.2.1 Test Fluids

In this study, all the neat cement slurries were prepared by mixing the Class H cement based on API 10-A classification (API-10A, 2011) and 38.5% tap water by weight of cement (bwoc) (water/cement ratio of 0.38) according to API Standard specification (API RP 10B-2, 2013). The synthetic-based mud (SBM) selected for this study is commonly used in the Gulf of Mexico. It has a water/oil ratio of 70/30 and a density of 9.7 ppg. The SBM was obtained from a drilling fluid supplier.

To study the effect of synthetic-based mud (SBM) on cement hydration monitoring using the DTSS, 5-15% (by volume) of the cement slurry was replaced with the SBM. The SBM was mixed into the cement slurry for 1 minute using a paddle-type stirrer attached to a drill press operating at 480 rpm. To study the cement dilution effect (i.e., less cement) on cement hydration monitoring, tests were also conducted by replacing the same volume of cement with silica sand as an inert filler. Silica sand particles with a particle size below 100 μm can act as nucleation sites that affect the hydration kinetics (Wang et al., 2013). To use the silica sand as an inert filler with only a dilution effect, the silica sand was passed through a #30 sieve and the fraction retained on a #60 sieve was used. This yielded particles in the 250-600 μm size range.

To study the effectiveness of the fiber optic sensing cables in detecting hydrocarbons, kerosene that met ASTM 1-K specification (ASTM D3699-13be1, 2013) was used to represent a reservoir hydrocarbon fluid. The major components of kerosene are branched and straight chain alkanes and cycloalkanes (naphthenes), characteristic of a light volatile crude oil.

In addition, since the fiber optic sensing cable is expected to be installed on the casing before a cementing job, it will be exposed to well construction fluids such as drilling fluids and spacer fluids upon installation and during cement displacement. This makes it possible to be used to track the cement displacement process. To understand the sensitivity of the cables to well construction fluids, other than the SBM mentioned above, the cables were tested with a spacer fluid. The spacer fluid used in this study was specifically designed for cleaning the wellbore after drilling with SBM. It was a water-based fluid with a few chemicals added to change the surface wettability of the rock, in order to ensure good bonding of the rock and casing with cement. The components and mixing procedure of the spacer fluid used in this study were obtained from a service company. The spacer fluids were prepared in the laboratory. The cables were also tested with other downhole fluids which they can potentially expose to, including brine, mineral oil, and crude oil, to evaluate their sensitivity to these fluids. The mineral oil was also obtained from a major drilling fluid supplier. The crude oil used for testing was a sweet crude oil with a specific gravity value ranging from 0.7 to 1.03, which was obtained from Oklahoma, USA. The artificial seawater was prepared to represent a brine in the laboratory following the recipe presented in Table 3.2.

Table 3.2 – Recipe of artificial seawater brine used in the experiments (Wu et al., 2016a).

Components	NaCl	Na_2SO_4	KCl	$NaHCO_3$
Weight (g/L)	25	4	2	1.5

3.2.2 Other Test Materials

An aluminum beam was used for cantilever beam test described in Section 3.3.2, and a polyurethane rod was used for testing helical wrapping installation. Their material properties are listed in Table 3.3.

Table 3.3 – Material properties of specimens used in the study.

Aluminum beam	Polyurethane rod
Modulus of Elasticity, E: 68.9 GPa	Hardness: 60A Durometer Modulus of Elasticity, E: 5.76 MPa Poison Ratio, ν: 0.5

To improve the fiber optic cable design and explore the sensitivity to different fluids, samples of sensitive polymers were tested in the lab. According to existing literature, various types of polymers, especially elastomers, can be used as hydrocarbon sensitive polymers in the fiber optic cables (see e.g. Carrillo et al., 2002, MacLean et al., 2003). This makes it possible to tailor the cable to the unique requirements for specific applications with a variation of types and chemistries of fluids tested, temperature ranges, and material hardness requirements, etc. In this study, five different types of elastomers (2.54-cm long and 0.16-cm diameter), i.e. silicone rubber, EPDM, natural rubber, soft silicone rubber, and neoprene, were tested to evaluate their sensitivity to hydrocarbons (kerosene) as well as various well construction fluids. The specifications for the elastomers tested are given in Table 3.4.

Table 3.4 – Elastomer specifications.

Elastomer Name	ASTM specifications	Temperature Range	Durometer Hardness
Soft silicone	ASTM D2000	-50 °C to 205 °C	50A (Soft)
Natural rubber	N/A	-24 °C to 121 °C	40A (Medium Soft)
Neoprene	ASTM D2000	-1°C to 100 °C	50A (Soft)
Silicone	ASTM D2000	-50 °C to 205 °C	70A (Medium)
EPDM	ASTM D2000	-4 °C to 100 °C	70A (Medium)

3.3 Experimental Setups and Methods

3.3.1 Rectangular Cement Sample Test

Monitoring Cement Hydration

In this study, either the green cable or the purple cable described in Section 3.2 was embedded inside a cement sample. Both the strain and temperature profiles were measured during the cement hydration process using the DTSS system. Thermocouples were also placed inside the cement samples in order to validate the temperature values measured by the DTSS. A Data Acquisition/Data Logger Switch Unit was used to record the data from the thermocouples. For this experiment, a single optical fiber and a thermocouple are required for monitoring cement hydration. The other set of sensors (another optical fiber and thermocouple) was used as a backup and for comparison to ensure good repeatability of measured data. It should be noted that while the thermocouple is a point sensor, the optical fiber is a distributed sensor providing data all along the entire length of the sample. Both the DTSS system and the data acquisition unit were started at the same time and

recorded for 48 hours. Various experiments were conducted to monitor the cement hydration process under different downhole situations, as detailed below.

Effect of External Temperature on Cement Hydration

To evaluate the effect of reservoir temperature on cement hydration, cement slurry was poured into a 25.5 cm x 8.5 cm x 4.5 cm box (internal dimensions) made out of insulation foam board (R-3 Insulating Sheathing). As shown in Figure 3.7b, two optical fibers were placed 2 cm apart at the center of the box. Before attaching the fibers to the end of the box using epoxy resin, 350 g weights were hung on the fiber outside the box to ensure uniform initial strain on both fibers (Figure 3.7a). Two thermocouples were placed close to the optical fiber in order to measure the temperature at the same height. A water bath with a heating function was used to simulate the downhole temperature environment at elevated temperatures but at atmospheric pressure. The water bath temperature was monitored using an additional thermocouple for reference. The temperature of the water bath was pre-set to either 24 °C (~75 °F), 49 °C (~120 °F) or 77 °C (~170 °F) and was maintained for 5 hours before conducting the experiment. Cement slurry was mixed and poured into the box before placing it in the water bath.

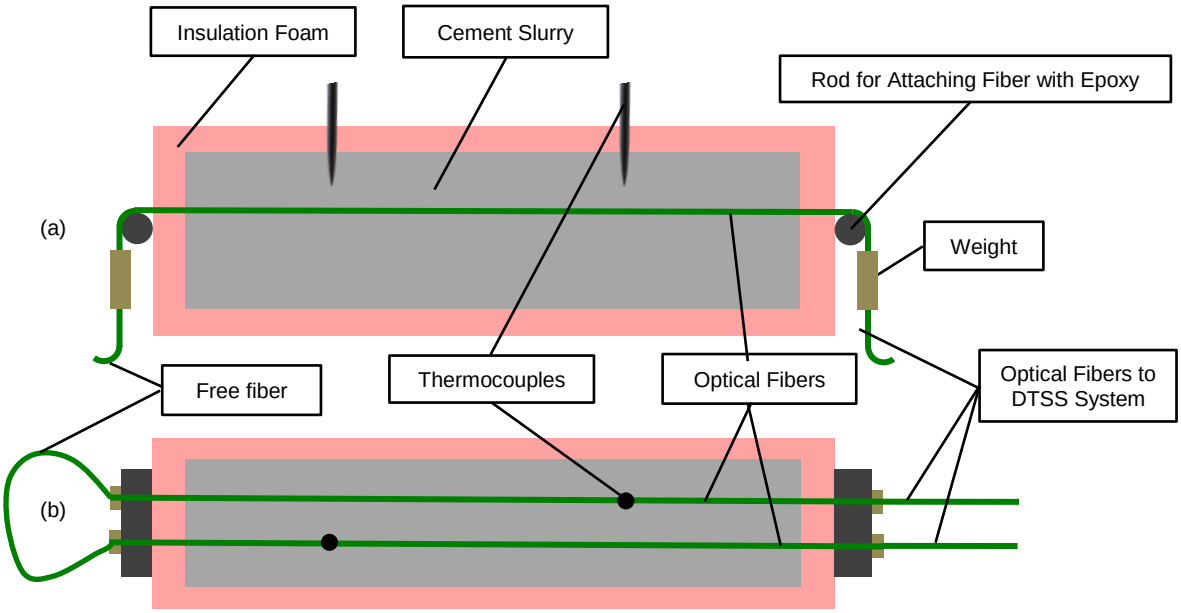

Figure 3.7 – Schematic showing (a) vertical and (b) horizontal cross sections of the setup used for monitoring cement hydration.

Effect of Contamination with SBM

The effect of cement contamination with SBM or silica sand was evaluated using the experimental setup shown in Figure 3.7. The foam box equipped with optical fibers and thermocouples was placed in an insulted chamber to maintain a uniform environment with similar thermal boundary conditions (i.e. similar heat loss) for all samples. An additional thermocouple was placed inside and outside the insulated chamber to monitor the temperatures. Contamination levels of 5%, 10%, and 15% SBM by volume of cement slurry were used, and the results were compared with the neat cement slurry sample. The same percentages (5%, 10%, and 15%) of silica sand as an inert filler were used as replacement in cement slurry to evaluate the dilution effect.

Presence of Uncemented Sections (or Voids)

The following two experiments were conducted at a constant temperature of 23 °C. The goal of the first experiment was to evaluate the capability of the DTSS system to determine the TOC via temperature monitoring. To achieve this goal, the purple cable was installed at the center of the box (with inner dimension of 2.5 cm × 2.5 cm × 50 cm) made out of the foam board as mentioned before. As shown in Figure 3.8, half the box was filled with cement slurry (25 cm) and the other half (25 cm) was left empty.

In the second experiment, the goal was to simulate a situation in which improper displacement of cement slurry resulted in voids in the cemented annulus. The purple cable was placed in the center of the box (with inner dimension of 2.5 cm × 2.5 cm × 50 cm) and cement slurry was poured into sections 1, 3, and 5 as shown in Figure 3.9. The remaining sections 2 and 4 were left empty.

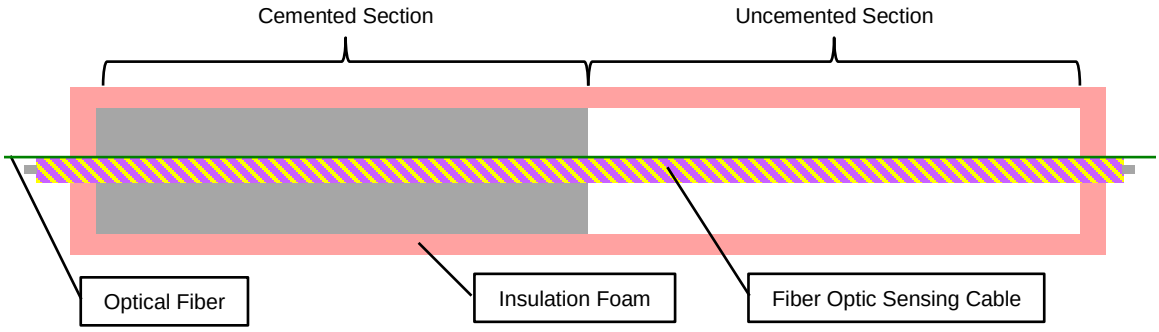

Figure 3.8 – Schematic showing the vertical cross section of the box with the purple cable used to determine top of cement. Half the length of this box was filled with cement slurry.

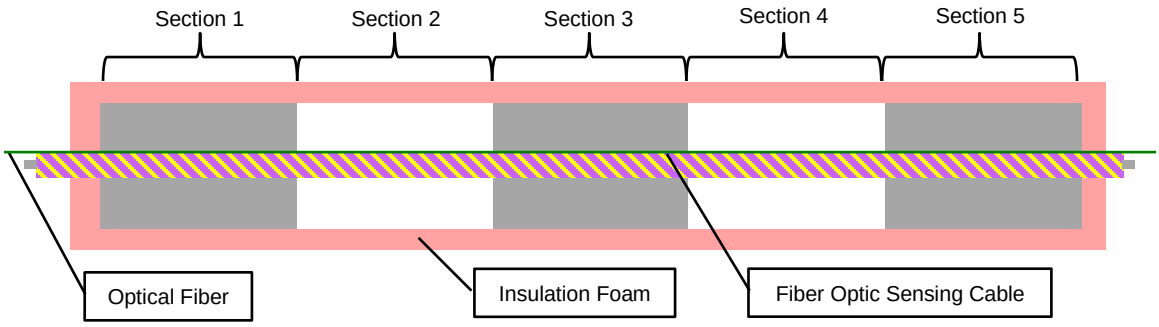

Figure 3.9 – Schematic showing the vertical cross section of box with the purple cable. Sections 1, 3 and 5 were filled with cement slurry and the other sections were left empty to simulate voids.

Sensitivity of Fiber Optic Cable to Different Fluids

All experiments involved hydrocarbons in this study were conducted at a constant temperature of 23 °C in the fume hood to reduce human exposure to hazardous fumes. To evaluate the sensing capabilities of both the green and black cables, each type of cable was placed in a 5 cm × 12.5 cm × 61 cm container and completely submerged in various fluids including kerosene, brine, mineral oil, synthetic oil, drilling fluid (synthetic-based mud) and spacer fluid for 18 hours and the response was monitored using the DTSS system. A new cable was tested in each fluid.

Detecting Hydrocarbons in Cement Annulus

The cement samples with the purple cable embedded were prepared to mimic the compromised cement annulus with uncemented section (Figure 3.8), voids (Figure 3.9), and a channel (Figure 3.10) and presence of hydration. To simulate a channel inside the cement annulus, fiber optic cable was embedded in a 2.5 cm × 2.5 cm × 50 cm cement sample and a 0.6-cm channel was created as a pathway, exposing the cable to any migrating

fluids. All cement samples were cured for 24 hours before any experiments were conducted and placed in a 5 cm × 12.5 cm × 61 cm container one at a time, and the top of the container was sealed using plastic wrap. Small holes were provided at each end for the optical fiber. The samples were fully submerged in kerosene for a specified period of time and the response was monitored using the DTSS system. Since there was no change in temperature during the test, all the strain values reported were calculated using measured Rayleigh frequency difference. Rayleigh scattering was chosen over Brillouin scattering in this case due to its oders of magniture higher sensitivity when detecting small strain changes.

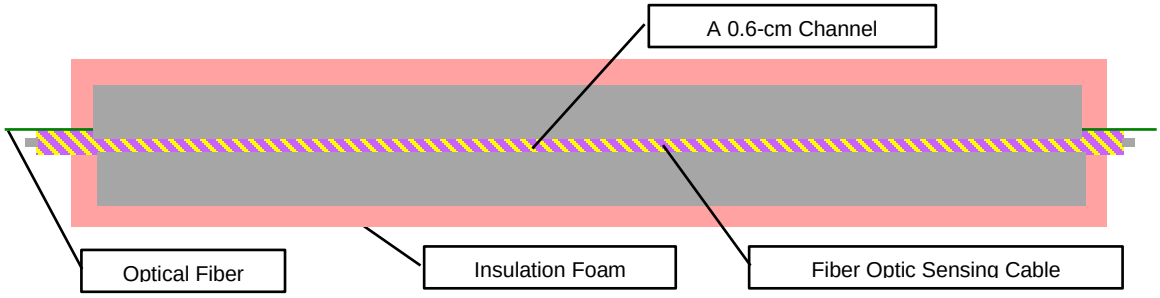

Figure 3.10 – Schematic showing the vertical cross section of box with the purple cable. A 0.6-cm channel was created above the cable in the cement sample.

Cement Displacement Tracking

To demonstrate the idea of cement displacement tracking using the DTSS system and the black cable described in Section 3.2, several experiments were conducted in the laboratory. The first experiment was to evaluate the sensitivity of the cable when the same cable was exposed to different fluids (SBM, spacer fluid, and cement) sequentially. The cable was attached to a thermal insulated box with the inner dimension of 2.5 cm x 2.5 cm x 50 cm as shown in Figure 3.11.

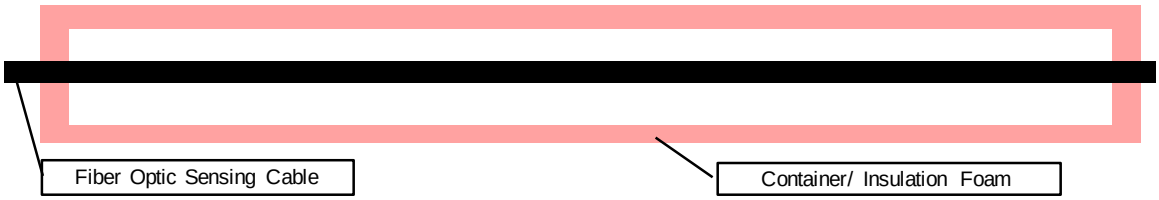

Figure 3.11 – An insulated box used for testing various fluids.

In the second experiment, to demonstrate the idea of cement displacement tracking, the cable was attached to an thermal insulated box with the dimension of 5 cm x 2.5 cm x 95 cm as shown in Figure 3.12. The box was divided into three sections. The first section with the length of 40 cm was filled with SBM. The second section filled with spacer fluid is 20 cm in length. The rest of the box (35 cm) was filled with cement slurry.

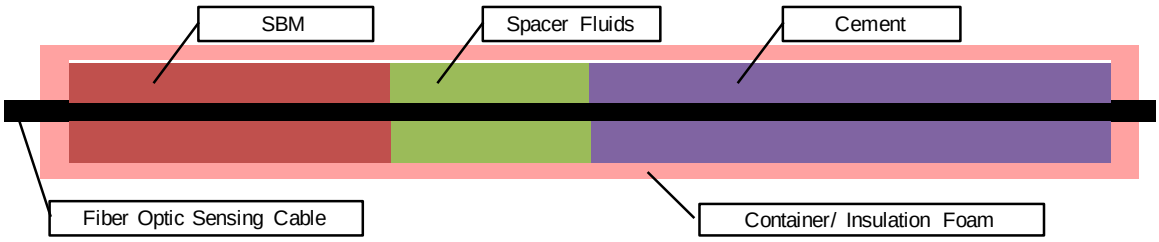

Figure 3.12 – An insulated box with three sections for testing all three fluids at once.

3.3.2 Cantilever Beam Test

To demonstrate the capability of monitoring casing deformation and detecting hydrocarbon leakage, a dual-cable installation design was applied on a 58.4 cm x 2.54 cm x 0.318 cm (23 in. x 1 in. x 1/8 in.) aluminum beam for cantilever beam test (Figure 3.13). One end of the beam was fixed while multiple standard weights of 50 g were clamped at

the other end of the beam to apply a load. The two cables were installed right next to each other. In this test, the green cable described in Section 3.2, used for deformation monitoring and referred as the DEF cable, was attached on the beam with initial strain using epoxy. The black cable described in Section 3.2, used for hydrocarbon detection and referred as the HC cable, was wrapped with a layer of steel braids. Only the bottom side of the steel braids was epoxied to the beam, while the HC cable inside remained strain-free. The top side allowed for exposure of the HC cable to hydrocarbons through the braids. The test was conducted at constant room temperature.

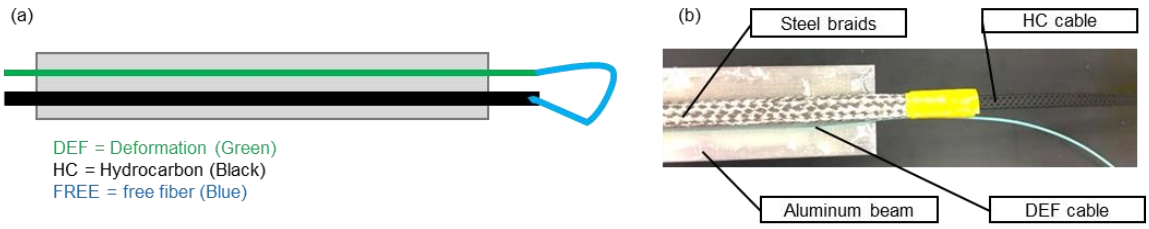

Figure 3.13 – a) Illustration of dual-cable installation; b) close-up of the test specimen with fiber-optic cables installed.

The strain of the cantilever beam (Figure 3.14) can be calculated using the following two equations:

$$\varepsilon = \frac{Mc}{IE} \quad \text{..... Eq. 3.1}$$

$$I = \frac{bh^3}{12} \quad \text{..... Eq. 3.2}$$

where ε is the strain, M is the moment (force x length), c is the distance from the center of the beam to the point where the strain is being measured (e.g. h /2), E is the modulus of elasticity, I is the moment of inertia, b is the width, and h is the thickness of the beam.

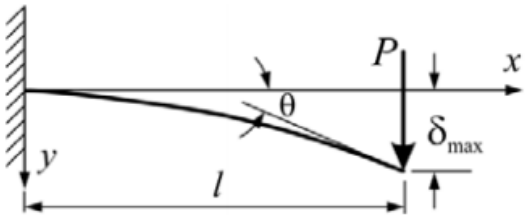

Figure 3.14 – Geometry of the cantilever beam test where P is the force applied at the end of the beam, and $\boldsymbol{\delta_{max}}$ is the maximum deflection (Sathyamoorthy, 1997).

3.3.3 Polyurethane Rod Tests

A polyurethane rod was used as a model representative of a casing string, being small enough to be handled within the limited capability of the load frame in the laboratory. Similar to the cantilever beam test described in Section 3.3.2, the green cable and the black cable described in Section 3.2 were mainly used for deformation monitoring and hydrocarbon detection accordingly and thus referred as the DEF cable and the HC cable in this test as well. The DEF cable and the HC cables were attached to the rod of 5.08 cm (2 in.) in diameter and 30.5 cm (12 in.) in height (Figure 3.15a) using epoxy. These cables were installed helically with a winding angle of 20°, as shown in Figure 3.15b. The DEF cable was attached under tension provided by a small hanging weight, which increased the sensitivity of the measurement and ensured that the cable was stretched out uniformly and able to respond to external loads. In order to ensure contact between the hydrocarbons and the HC cable, care was taken not to apply any epoxy on the cable's top surface. A load frame was used to apply an axial load to the rod (Figure 3.15c), and a Linear Variable Differential Transformer (LVDT) was used to measure its axial displacement.

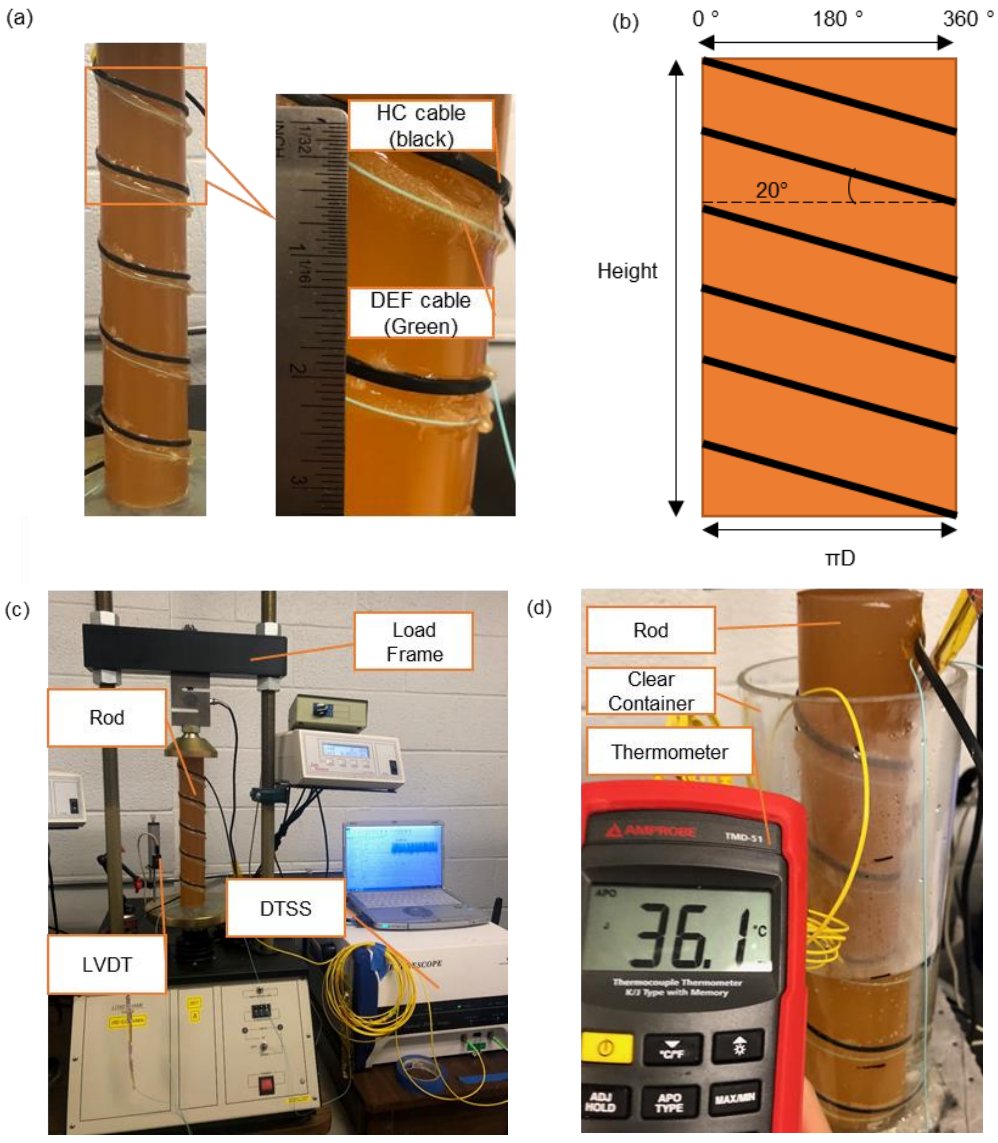

Figure 3.15 – a) The HC and DEF cables installed helically on the polyurethane rod; b) illustration for helical wrapping of optical fibers on the surface area of the rod, with a wrapping angle of 20°; experimental set-ups for c) deformation test, and d) fluid migration test.

Deformation Detection

The axial strain of the polyurethane rod was obtained by three different methods, as summarized in Table 3.5. The first method is based on the load applied to the rod and its material properties, described by Eq. 3.3. The second method uses the displacement of the rod measured by the LVDT as described by Eq. 3.4. The third method is based on strain measured by the DTSS and fiber optic cable attached to the rod, as given by Eq. 3.5 (Childers et al., 2007).

Table 3.5 – The axial strain on the rod was calculated based on (1) the load applied, (2) the measurement of displacement, and (3) the strain measured on the optical fiber (named as 'FO strain').

Based on load	**Based on displacement**	**Based on FO strain**
$\varepsilon = \frac{P}{AE}$ …… Eq. 3.3	$\varepsilon = \frac{\Delta L}{L}$ ……Eq. 3.4	$\varepsilon_f = -1 + \sqrt{sin(\theta)^2(1-\varepsilon_a)^2 + \cos(\theta)^2(1+\nu\varepsilon_a)^2}$ ……Eq. 3.5
ε is the axial strain P is the axial load A is the cross-sectional area E is the modulus of elasticity	ε is the axial strain L is the rod height ΔL is the displacement of the rod under the axial load	ε_f is the strain measured by the optical fiber ε_a is the rod axial strain θ is the helical wrapping angle ν is the Poison ratio

Fluid Migration Detection

To simulate the upward migration of a warmer formation fluid from a lower zone due to compromised zonal isolation, a known quantity of 36°C water was poured into a clear container containing the helically wrapped polyurethane rod as shown in Figure 3.15d. The external temperature (room temperature) was maintained at 25°C. A measurement was taken with the DTSS system and additional amount of the 36°C water was added to mimic upward migration of formation fluid. This was repeated for a total of four times and the results are shown as 25% full, 50% full, 75% full and 100% full of 36°C water in the annulus between the clear container and the polyurethane rod.

Hydrocarbon Detection

One-quarter of the height of the polyurethane rod was submerged in kerosene. The DTSS system monitored and recorded strain changes on the HC cable for 12 hours. This experiment was used to simulate the invasion of hydrocarbon into the cement sheath due to the presence of channels in cemented annuli or because of cement plug failure.

Cement Job Monitoring

The polyurethane rod was placed at the center of a PVC pipe of 7.6 cm (3 in.) in diameter and 28 cm (11 in.) in height, thereby creating an annular space. Freshly prepared cement slurry was poured into this annulus and the cement hydration process was then monitored by the HC cable wrapped helically on the rod and the DTSS system for 48 hours. Two thermocouples were placed in the annulus as references for comparison with the temperature measurement obtained by the DTSS system.

3.3.4 Cement-Casing Bond Test

To demonstrate the capability of fiber optic sensors to evaluate the cement-casing bond in the laboratory, a small-scale well model based on a previously reported pipe bond test (Liu et al., 2017) was built for testing. The green cable describe in Section 3.2 was helically wrapped on a 3.8-cm (1.5-in.) diameter steel pipe at a winding angle of 10° as shown in Figure 3.16a. The steel pipe was placed into a 7.6-cm (3-in.) diameter PVC pipe to create an annulus of 1.9 cm in width and filled with cement slurry. After pouring the cement slurry, the DTSS system was used to continuously monitor the temperature and strain changes for 50 hours, allowing observation of the exothermic cement hydration reactions as described in the Chapter 2. Two thermocouples were placed into the cement annulus to measure temperature changes for reference. After the cement slurry hardened, the entire set-up was placed in a load frame (Figure 3.16b). The steel pipe (casing) was subsequently subjected to incremental axial loads until debonding between casing and cement annulus occurred. A strain measurement was taken using the DTSS system at every load step.

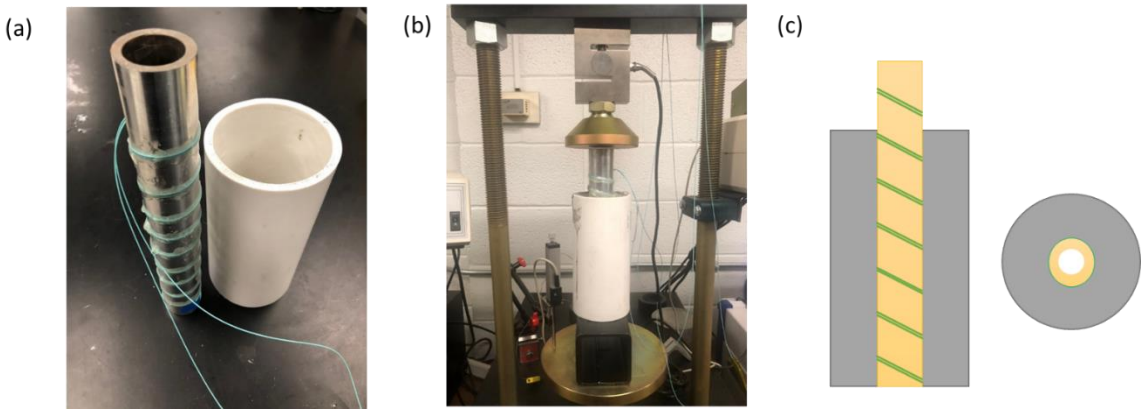

Figure 3.16 – a) Steel pipe with helically installed fiber optic cable on a steel pipe (representing casing) and a PVC pipe (representing a wellbore or outer casing); b) load frame used for applying loads on the casing; c) a simple schematic of the well model.

3.3.5 Permeability Test

When it comes to embedding a fiber optic cable in the cement annulus, one of the common concerns is whether the cable itself will create a conduit or a potential leak path for fluid and gas migration. Since fiber optic sensing technologies were first introduced to the oil and gas industry in the 1990s (Kamal, 2014), a large numbers of fiber optic sensing cables have already been installed outside of casing strings and embedded in the cement annulus for Distributed Temperature Sensing (DTS) and Distributed Acoustic Sensing (DAS). Studies that have focused on the hydraulic implications of embedding cables in the cement annulus, however, are very limited. In this study, a gas permeability test was used to evaluate the effect of embedded cables on cement hydraulic integrity.

The permeability test setup used was originally designed to accurately measure nano-Darcy permeability of rock samples at a controlled temperature, based on an API standard (API RP 40, 1998). Three types of cement cylinder samples of 2.54 cm (1 in.) in

diameter and 10.2 cm (4 in.) in length were prepared with Class H cement and the API standard mixing procedure (API RP 10B-2, 2013). The three types of samples included: 1) plain cement; 2) plain cement with an embedded mesh cable; 3) plain cement with an embedded braided cable (c.f. Figure 3.17). The dimension of mesh cable is 0.2 cm x 0.7 cm x 10.2 cm and the dimension of the braided cable is 0.2 cm x 0.5 cm x 10.2 cm. Each sample was cured in a cylindrical mold at room temperature of 25 °C for 24 hours and then submerged in a saturated lime water solution for 90 days prior to testing. A high-precision rock saw was used for cutting the sample ends to preserve the integrity of the samples and to limit any damage that might jeopardize an accurate measurement of permeability. The prepared cement cylinders were cut into smaller cylinders that were 1.27 cm in length. The dimensions of each sample were measured and recorded. The temperature-controlled environment in which the permeability tests were performed was set at 50 °C. Each sample was carefully loaded into the pressure cell with flexible radial sleeves to create a gas-tight seal on the cylindrical walls of the sample. A radial confining stress was applied to the sample by adding hydraulic pressure in the annular space between the flexible sleeves and the cell. Nitrogen gas was injected across sample until saturation occurred, while maintaining horizontal effective stress (HES) of 500 psi (pressure differential between confining and gas pore pressure) by slowly adjusting the confining pressure. After the sample was saturated, a steady flow of nitrogen gas was injected through the sample. Permeability was measured after allowing the sample to stabilize and reach a steady state, which was typically reached after 2-3 hours.

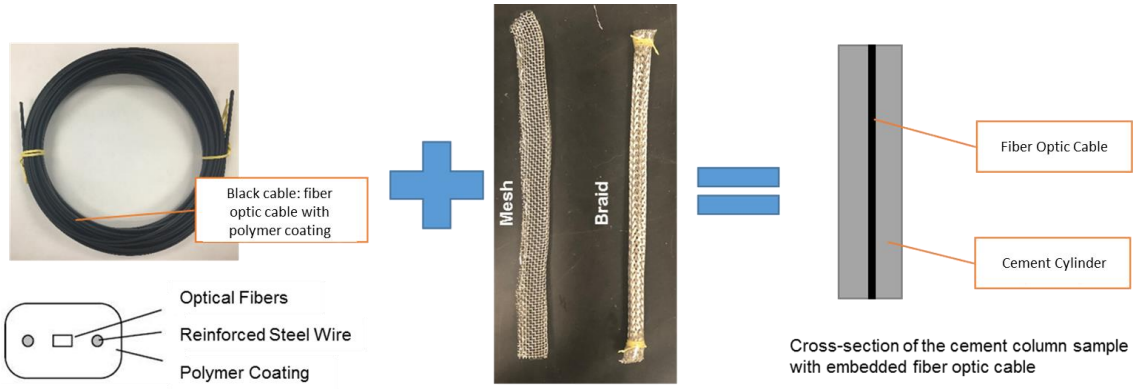

Figure 3.17 – Fiber optic cables were wrapped with either a steel mesh or a steel braid to ensure that the fiber was protected in the annular space, e.g. when the casing is lowered into the borehole and installed at depth.

3.3.6 Sensitivity of Different Polymers Test

To study the sensitivity of different polymers to various well construction fluids, the elastomer samples described in Section 3.1.2 were placed in glass jars. Each jar was filled with 25 ml of fluid such as kerosene, SBM, and spacer fluid. The weight of the samples was measured before and after submersion in fluid at every 2 minutes for the first 10 minutes. The weight measurement was then taken every 10 minutes for another 50 minutes. After an hour of measurement, the measurement was taken every 30 minutes until the weight of samples reached an equilibrium. The test was repeated at least twice to obtain the average values.

Chapter 4: Cement Displacement Tracking

To date, there is no available sensing technology to track the cement displacement process in time. The concept of using a fiber optic sensor for such tracking is also completely novel. During cement displacement, the fiber optic cables installed on the casing will be exposed to well construction fluids such as drilling mud, spacer fluids and cement slurry. The distributed chemical sensing capability can be added to the DTSS system by using a specially designed fiber optic cable where the coating exhibits a different response to each of the fluids. Such system can be applied to detect the type and location of each fluid during the displacement process by analyzing the temperature and strain measurements from the DTSS system. This enables estimation of displacement efficiency and identification of any abnormal situations.

This chapter first presents the results of fiber optic sensing cables tested *individually* in well construction fluids and other commonly seen downhole fluids in Section 4.1. In Section 4.2, the results and detailed illustrations were provided for the idea of cement displacement tracking by exposing the fiber to the fluids *one after the other*. Section 4.3 presents the discussion on the sensing capability of several polymers that can be used as the sensitive coatings on the fiber optic sensing cables and suggestions on selection of polymer type to tailor the response from the cables.

4.1 SENSITIVITY OF FIBER OPTIC CABLES TO DIFFERENT FLUIDS

4.1.1 Well Construction Fluids

Cable in Synthetic Oil and Synthetic-based Drilling Mud

One of the well construction fluids that the fiber optic sensing cable is expected to be exposed to is drilling mud. There are three major types of drilling muds: water-based mud (WBM), oil-based mud (OBM), and synthetic-based mud (SBM). SBM is widely used for drilling operations in offshore well and its primary component is synthetic oil, which constitutes the continuous phase of the mud. Figure 4.1 shows the test result for the sensitivity of the purple cable to synthetic oil, while the sensitivity to SBM is shown in Figure 4.2. Since the experiments were conducted under constant temperature (and thus no temperature changes), there was no need to use hybrid Brillouin and Rayleigh technique to separate temperature and strain measurement. The Brillouin technique was chosen because of its faster measurement speed compared to that of the Rayleigh technique for all the results presented in Section 4.1. The details of the experimental setup can be found in Section 3.1.1. In both the synthetic oil and the SBM derived from it, the swelling in the hydrocarbon sensitive polymer (see Figure 4.1a-b, Figure 4.2a-b) was observed visually and detected by the DTSS system (shown in Figure 4.1c and Figure 4.2c). The maximum strain on the optical fiber caused by the presence of synthetic oil is 180 με and by the presence of SBM is 200 με. The cable is sensitive to synthetic oil and SBM, which enables tracking of the location of SBM in the downhole during well construction.

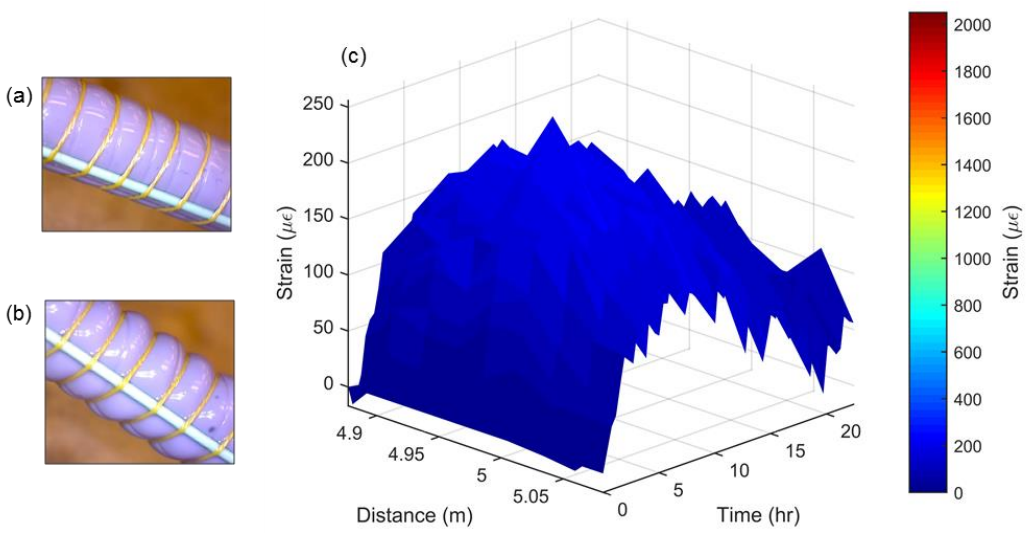

Figure 4.1 – Fiber optic sensing cable ('the purple cable') (a) before and (b) after being submerged in ***synthetic oil***. (c) The swelling observed in the hydrocarbon sensitive polymer is converted into strain on the fiber, which is shown in the 3D plot. These strain values were measured using Brillouin frequency shift.

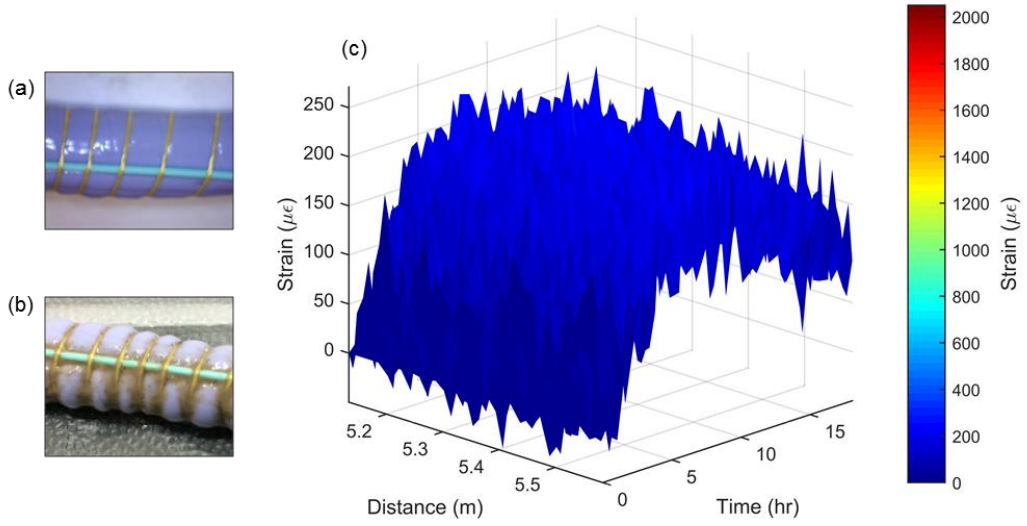

Figure 4.2 – Fiber optic sensing cable ('the purple cable') (a) before and (b) after being submerged in ***SBM***. (c) The swelling observed in the hydrocarbon sensitive polymer is converted into strain on the fiber, which is shown in the 3D plot. These strain values were measured using Brillouin frequency shift.

Cable in Mineral Oil

Following the first result, another fiber optic cable was tested in mineral oil. Mineral-OBM is another common type of non-aqueous well construction fluid, and mineral oil is the continuous phase in these fluids. After the cable was submerged in mineral oil for 18 hours, there was no detectable difference in the images taken before (Figure 4.3a) and after (Figure 4.3b). Strain values shown in the 3D plot (see Figure 4.3c) validated the visual observation that little to no swelling was observed in the hydrocarbon sensitive polymer in the presence of mineral oil. The strain values fluctuated between +/- 50 με, which can be considered to be negligible. Clearly, the purple cable does not response to mineral oil. The results presented the selective sensitivity of the cable to the type of drilling muds.

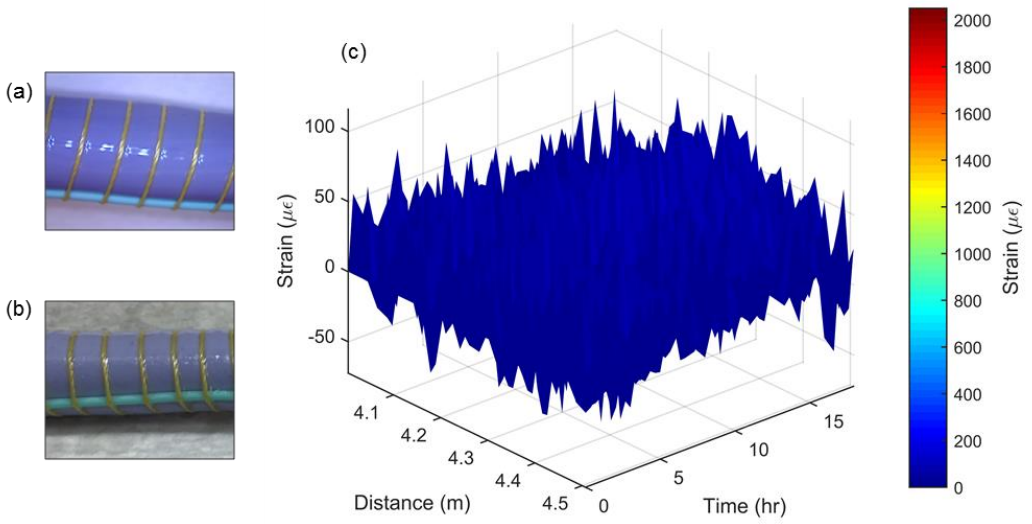

Figure 4.3 – Fiber optic sensing cable (‘the purple cable’) (a) before and (b) after being submerged in ***mineral oil***. (c) Strain values obtained from Brillouin frequency shift shown in the 3D plot confirm the visual observation that little to no swelling was observed in the hydrocarbon sensitive polymer in the presence of mineral oil.

Cable in Spacer Fluid

Another common well construction fluid, the spacer fluid, was tested, although the fiber optic sensing cable is expected to only expose to it for a short amount of time in the actual application. The spacer fluid is used to displace the SBM to clean the hole and change the wettability of the rock surface before cementing to ensure a good cement bond. When the cable was submerged in spacer fluid, there was no visual change in the hydrocarbon sensitive polymer (Figure 4.4a-b). However, the strain values shown in Figure 4.4c decreased over time, which indicates that the spacer fluid caused a small amount of shrinkage in the polymer. Although this shrinkage was not significant as the values are relatively low, it was still detected by the DTSS system and thus make it possible to track the displacement process for the spacer fluids.

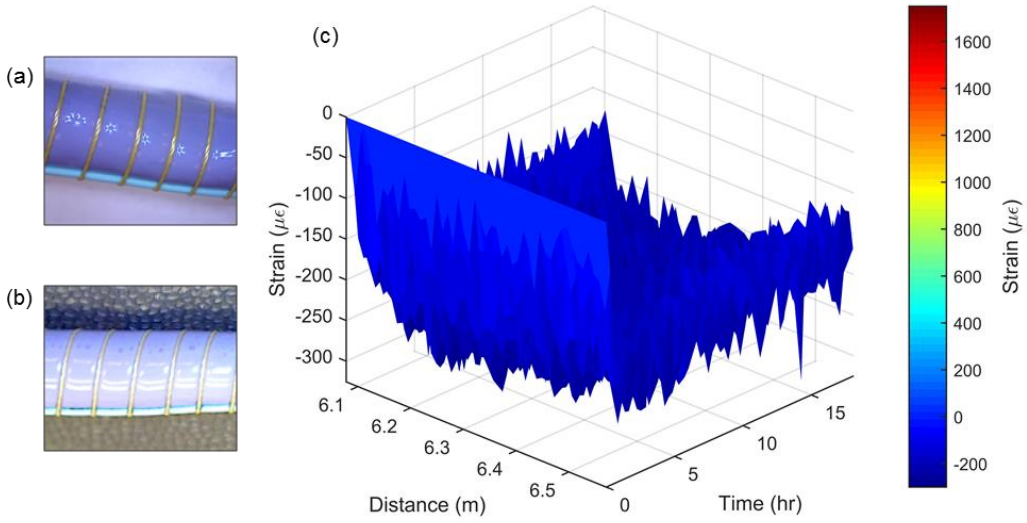

Figure 4.4 – Fiber optic sensing cable (‘the purple cable’) (a) before and (b) after being submerged in ***spacer fluid***. (c) The negative strain values shown in the 3D plot indicate that the hydrocarbon sensitive polymer actually shrinks in the presence of spacer fluid. These strain values were measured using Brillouin frequency shift.

4.1.2 Other Test Fluids

The selective response characteristics of the sensitive polymer on the purple cable was further tested with other potential fluids such as brine and hydrocarbons. As described in Section 3.2.1, artificial seawater was used to represent a brine and kerosene was used as a representative for a hydrocarbon.

Cable in Brine

In most wells, brine could be present as either pore fluid in the surrounding reservoir, or could be used as a well construction fluid (e.g. base fluid for water-based mud). After submerging the cable (Figure 4.5a) in brine for 18 hours, no swelling was visually observed in the hydrocarbon sensitive polymer (Figure 4.5b). The conclusion that the strain was indeed minimal can be drawn from the strain measurements obtained from the DTSS system (Figure 4.5c). Strain values fluctuated between +/- 50 με, which can be considered near the accuracy limit for Brillouin for the given spatial resolution and measurement conditions. It can be seen in Figure 4.6 that the strain obtained from Rayleigh technique is far smoother. This is because Rayleigh technique, TW-COTDR, is more precise and is orders of magnitude more sensitive when detecting small changes in strain. Thus, Rayleigh technique should be used preferentially instead of Brillouin technique when the change is expected to be small. Based on the findings, it can be concluded that the cable system is not sensitive to brine.

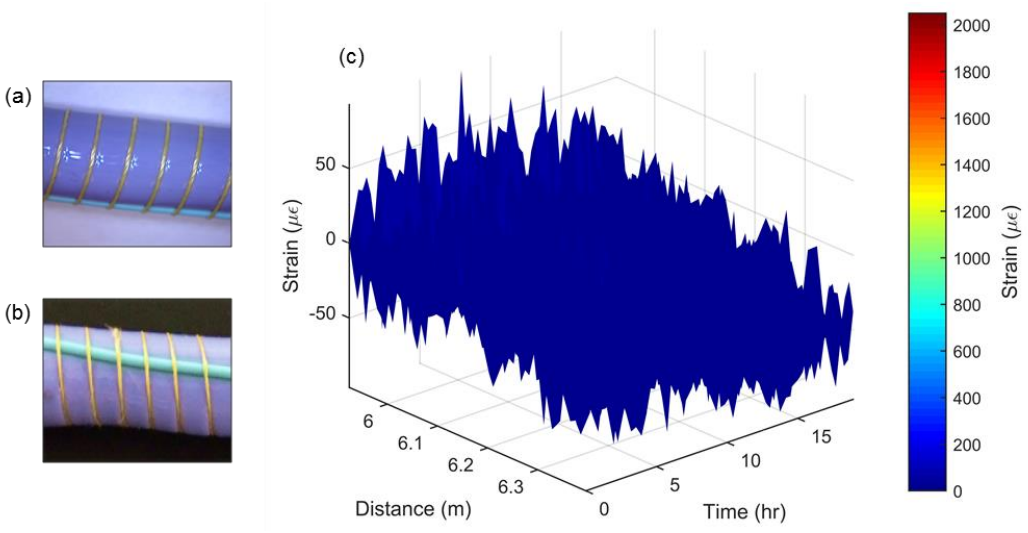

Figure 4.5 – Fiber optic sensing cable ('the purple cable') (a) before and (b) after being submerged in ***brine***. (c) Strain values obtained from Brillouin frequency shift shown in the 3D plot confirm the visual observation that little to no swelling was observed in the hydrocarbon sensitive polymer in brine.

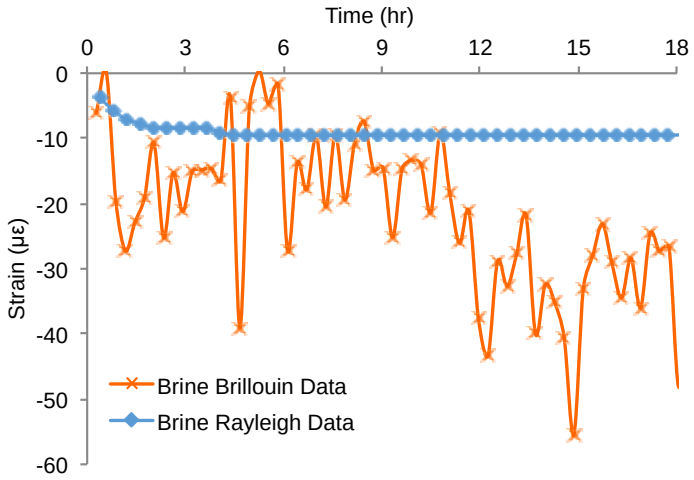

Figure 4.6 – Comparison of data obtained from both Brillouin and Rayleigh techniques for the cable that was completely submerged in ***brine***. Note the smoothness of the Rayleigh data compared to the Brillouin data.

Cable in Kerosene

The purple cable was tested in kerosene to evaluate its sensitivity to hydrocarbons. Figure 4.7 shows a section of the fiber optic sensing cable before (Figure 4.7a) and after (Figure 4.7b) being submerged in kerosene. It was observed that the presence of kerosene led to significant swelling of the hydrocarbon sensitive polymer. This swelling was transferred into strain variations on the optical fiber through the Kevlar thread packaging of the purple cable. Such changes in the strain on the optical fiber were recorded by the DTSS system (Figure 4.7c). Along the entire submerged length of the fiber optic sensing cable, the changes in strain measurement recorded were relatively uniform. Along the time axis, the strain increased sharply in the first hour and reached a maximum value of 1500 με in approximately three hours. After three hours, the strain fluctuated between 1200 με to 1600 με, and remained at a relatively high level when compared with the initial state (at time = 0 hr), which is approximately 10 times larger than that caused by SBM (cf. Figure 4.2). This clearly demonstrates the measurable effect that hydrocarbons have on the submerged polymer sample, shown as strain values in Figure 4.7c. Because of the significant difference in strain values between synthetic oil or SBM and kerosene, the effect of synthetic-based oil or drilling mud on the cable can be differentiated and filtered in the analysis based on the range of strain values.

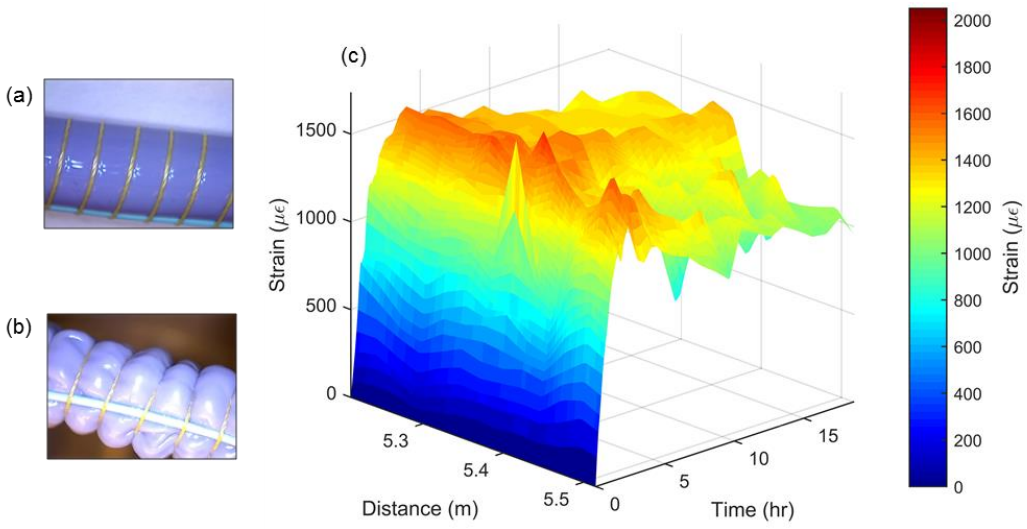

Figure 4.7 – Fiber optic sensing cable ('the purple cable') (a) before and (b) after being submerged in ***kerosene***. (c) 3D plot showing the strain generated on the fiber due to the swelling of the hydrocarbon sensitive polymer in the presence of kerosene. The strain values were calculated based on the Brillouin frequency shift values measured using the DTSS system.

In Figure 4.8, it can be seen that there is a good correlation between the strain values obtained using both Rayleigh and Brillouin frequency shifts. The results above prove that the fiber optic sensing cable (purple cable) is capable of detecting the presence of kerosene, which in this case was used as a model system for hydrocarbons in general.

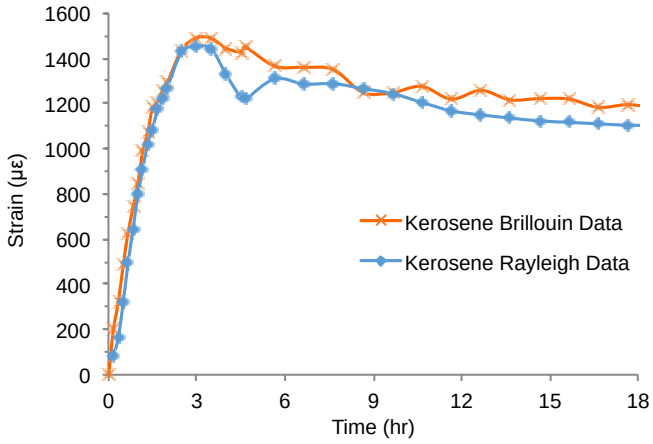

Figure 4.8 – Comparison of data obtained from both Brillouin scattering and Rayleigh scattering for the purple cable that was completely submerged in ***kerosene***.

Summary of Test Results for the Purple Cable

Figure 4.9 summarizes the results presented in the previous sections. As can be seen, the purple cable is selectively sensitive to well construction fluids such as spacer fluids and SBM while it is minimally affected in its strain response by other fluids such as brines and mineral oil. The results supported the idea to track the cement displacement process in real time using the DTSS system, which was illustrated and validated in the laboratory experiments in the following Section 4.3. In addition, the cable has significantly higher strain response to kerosene compared to any of the other fluids. This shows that the proposed cable has selective sensitivity to certain hydrocarbons. These positive and encouraging results were further investigated to develop the application of the DTSS system for distributed chemical sensing (DCS), which was applied for hydrocarbon detection in the cement annulus (see Chapter 6).

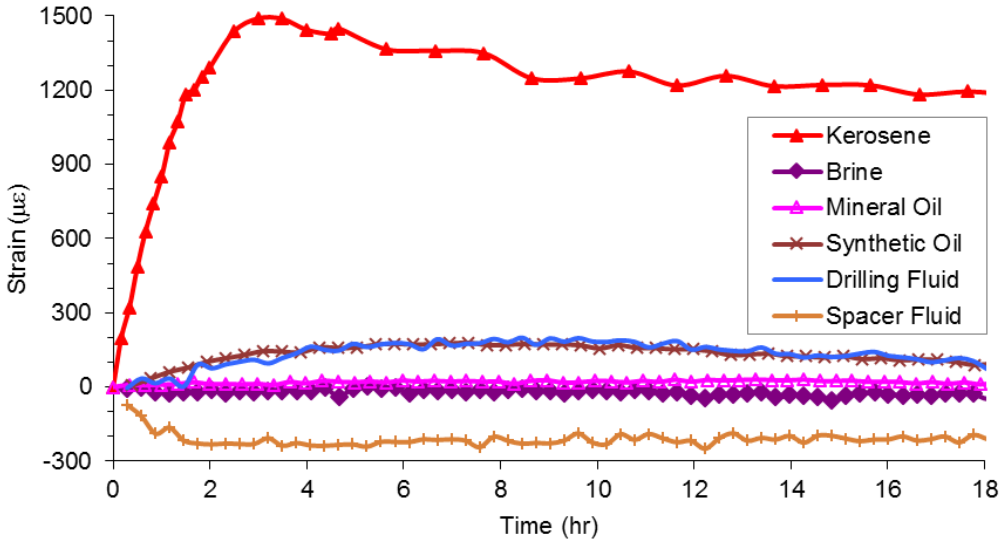

Figure 4.9 – Summary plot showing the response of the fiber optic sensing cable ('the purple cable') in the presence of various fluids. Note: Drilling Fluid refers to SBM. These strain values were measured using Brillouin frequency shift.

Summary of Test Results for the Black Cable

Similar to the tests conducted with the lab-made purple cable, a commercially available 'black' cable was tested in various fluids as described in Section 3.2.1. Figure 4.10 summarizes the response of the black cable in the presence of kerosene and various downhole fluids including SBM, spacer fluid, mineral oil, and crude oil. During the 24-hour measurement, the measured strain values had a similar trend to the results of the purple cable (Figure 4.8). When submerged in kerosene, the strain increased by 100 με in the first 2 hours. There was a significant increase in strain to 500 με after 2 hours and the strain continued to increase up to 1100 με. For SBM, the strain increased to 150 με over a span of 9 hours and then increased at a faster rate to 500 με. For crude oil, an approximately 100 με increase in strain was recorded. The strain on the cable only increased to 50 με when it

was exposed to mineral oil. For spacer fluid, the strain on the cable decreased to -50 με. In other words, the strain changes on the black cable can in principle be correlated to the type of downhole fluid, provided such correlation can be done in a timely fashion. By analyzing the strain measurement, this technique can be used to identify the presence and type of the fluid in the annulus, and thus paving a path for tracking well construction fluid, which is demonstrated in the following Section 4.2.

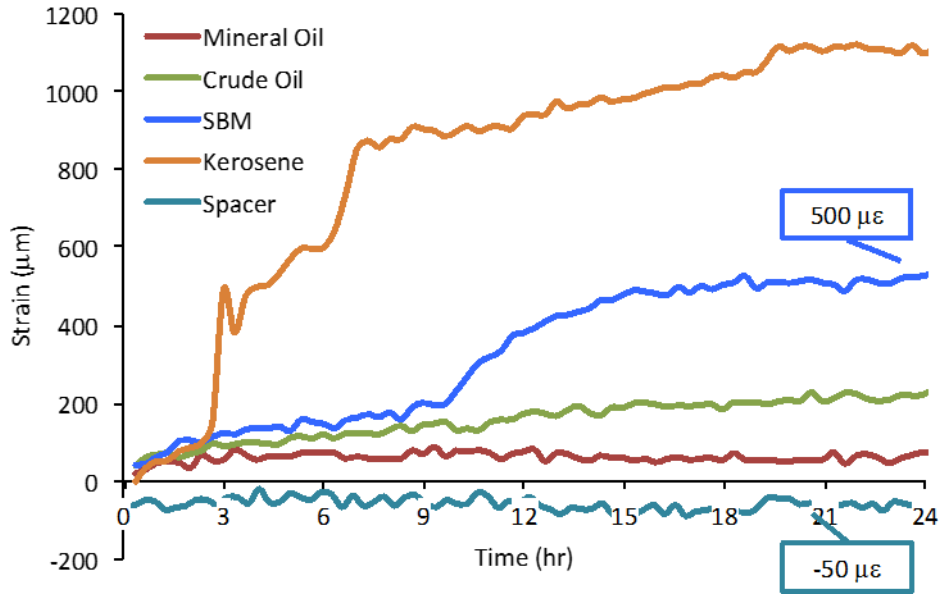

Figure 4.10 – Summary plot showing response of the black cable in various fluids.

4.2 Cement Displacement Tracking

4.2.1 Tracking the Cement Displacement Process

A black fiber optic sensing cable was exposed to SBM, spacer fluid and cement slurry sequentially and the resulting changes in strain and temperature are shown in Figure 4.11, where the regions shown in red are an indicator for peak values. In the presence of

SBM and spacer fluid, as expected, there were no detectable changes in temperature (Figure 4.11a), however significant change in temperature was detected after the fiber was exposed to cement slurry. For the plot showing changes in strain (Figure 4.11b), the peak values occurred when the cable was submerged in SBM. There is a clear change in color (strain values) when the SBM was replaced with spacer fluid. Thus, by analyzing the signatures in both the temperature and strain plots together, all three fluids can be clearly differentiated.

To compare the temperature and strain responses for the sample, Figure 4.12 presents the *average* values over a 20-cm section of the box verses time. When the black cable was submerged in SBM (for the first 21 hours), as expected few changes in temperature were recorded. For the strain measurement, 100 με was detected in the first 9 hours. After 9 hours, similar to the response in Figure 4.10, the strain value increased to 600 με. In the second stage, after SBM was replaced with spacer fluid, strain decreased to around 400 με in average with negligible changes detected in temperature. This shows that the cable can be used to successfully identify spacer fluid even after it was submerged in SBM for 21 hours. In the third stage when the spacer fluid was removed and replaced with cement slurry, the temperature changes due to the cement hydration were successfully recorded. As shown in Figure 4.12, the temperature starts to increase at 29 hours (5 hours after placing cement), reaches a peak value at 35 hours, and decreases until 41 hours. After removing the cable from spacer fluid, the strain on the cable decreased and reached a relatively stable value around 300 με.

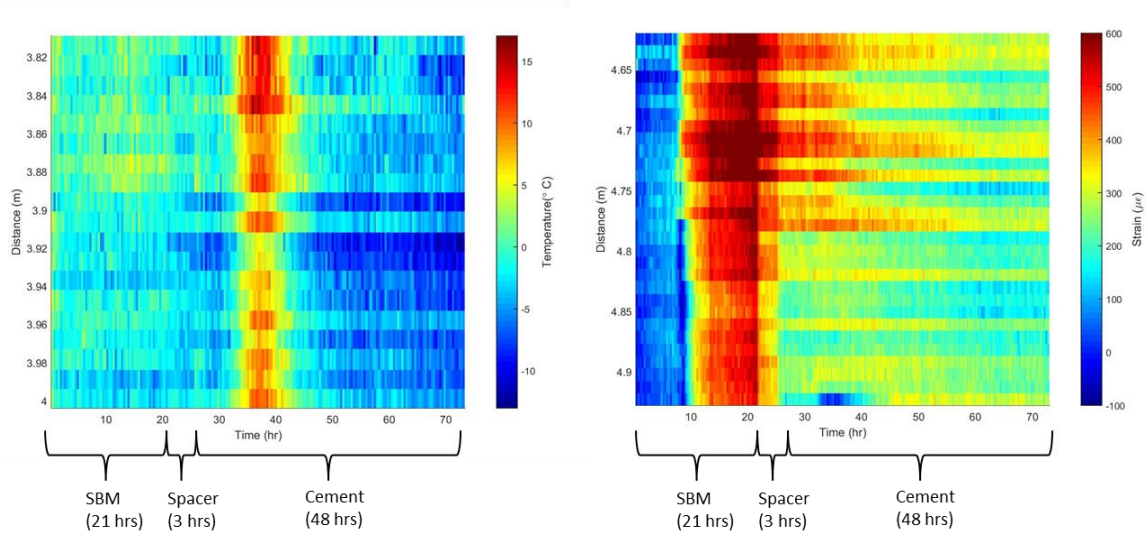

Figure 4.11 – Results from placing the cable in SBM, spacer and cement ***sequentially***; a) temperature change vs. time, b) strain vs. time. Note that the temperature values are temperature changes with respect to the initial temperature (30°C) after mixing.

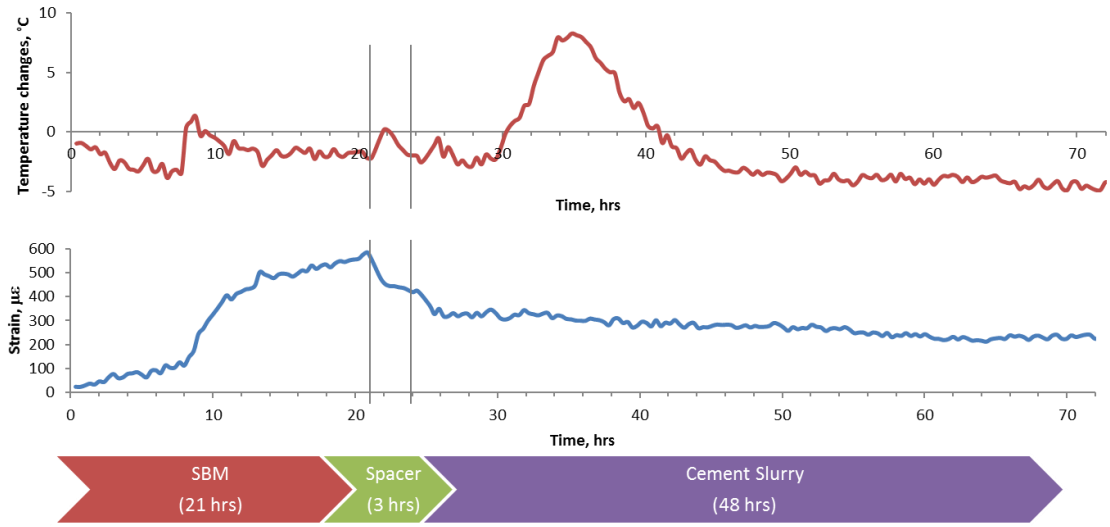

Figure 4.12 – Average temperature and strain v.s. time. Note that the temperature values are temperature changes with respect to the initial temperature (30°C) after mixing.

After displacing SBM with cement slurry in the annulus, wellbore activities are suspended to allow the cement to solidify, harden, and develop minimum compressive strength. The amount of time required to achieve minimum strength is wait-on-cement (WOC) time. Disturbing the cement slurry before it has set can negatively affect the long-term strength development (Nelson and Guillot, 2006). Downhole temperature and pressure variations can also affect the actual WOC. By tracking the cement hydration process in real-time, the WOC time can be obtained in-situ thus increasing the success of the cementing operation. WOC time can actually be characterized by the DTSS system by observing the declining temperature after the cement slurry is placed, as shown in Figure 4.11, and correlating the temperature signature in time with the time at which minimum strength is obtained. Minimum WOC time can be guaranteed in this way, whereas unnecessary excessive WOC time, i.e. extra time that is spent waiting on cement to set because of uncertainty in cement set time under downhole conditions, can be avoided. Overall, this experiment demonstrates the capability of the proposed system to track the cement displacement process by monitoring the temperature and strain changes on the cable. Note that in actual field practice, the exposure times to SBM and spacer fluid may be significantly shorter than those used in the laboratory experiments. The experiments described here should be seen as a clear feasibility study and proof of concept of the ability to carry out real-time displacement tracking, with a viable system for field application still to be further researched and developed.

4.2.2 Detecting the location of each fluid

Figure 4.13 shows the strain and temperature variations when the cable was placed in a box filled with the fluids in three sections for 48 hours. Since cement hydration is an

exothermic reaction, the released heat causes an increase in temperature. From the temperature profile, the section with cement slurry can be clearly identified while few changes in temperature were detected in the other two sections containing SBM and spacer fluid. From the strain profile, the response varies due to the presence of different fluids. The section with highest strain response corresponds to the section containing SBM. The location where the strain values become negative is an indicator for the presence of spacer fluids. Considering both temperature and strain measurements, the three sections of fluids (SBM, spacer fluid, cement) were successfully identified. This experiment demonstrates that the location of fluids in the annulus can be identified *in situ* and used to determine critical cementing and zonal isolation parameters such as the top of cement (TOC). Note that this can be conducted *in situ* and in real time with a direct measurement of the exothermic behavior of the setting cement, without the need for wellbore re-entry with e.g. cement bond logging tools.

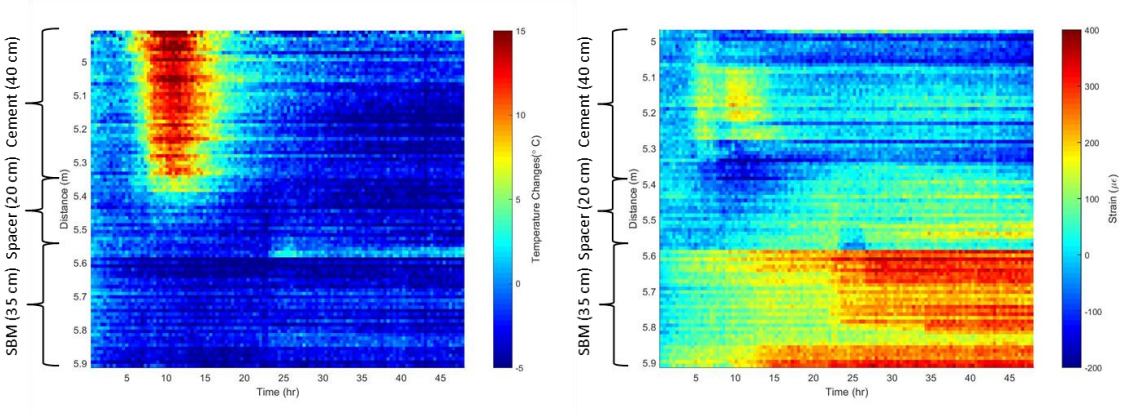

Figure 4.13 – Results from placing the black cable in all three fluids ***side by side***; a) temperature changes vs. time; b) strain vs. time. Note that the temperature values are temperature changes with respect to the initial temperature (30°C) after mixing.

4.3 SENSITIVITY OF DIFFERENT POLYMERS

As shown in Figure 4.10 of the previous section, in the presence of SBM, the black cable took a few hours to obtain significantly high values of strain. To modify and accelerate the response time of the cable, the type of elastomer and the packaging mechanism were studied to select the best combination. The very first step was to identify various types of suitable elastomers and evaluate their sensitivity to hydrocarbons and well construction fluids. Therefore, different elastomers (neoprene, natural rubber, soft silicone, EPDM, and silicone) were submerged in various fluids (kerosene, SBM, spacer) for at least one hour or until the measured weight of the samples elastomer reached an equilibrium and the maximum (Figure 4.14). In general, all five types of elastomers showed little response when submerged in spacer fluids. The natural rubber showed the highest percentage of weight increase (254%) when submerging in kerosene, followed by soft silicone (83%), silicone (46%), EPDM (76%), and neoprene (9%). When submerged in SBM, natural rubber also had the highest response increase at 124%. The silicone and soft silicone had a similar percentage of weight increase at 19% and 20%, respectively. EPDM showed a higher response at 33% while neoprene only increased by 2.5%. Since neoprene showed only a minor response to the fluids of interest, it was considered to be less desirable for this study. Other than neoprene, the other elastomers appear to have the potential to be used as the fluid-sensitive component coated on the fiber optic cable. In addition, the tested elastomers showed selective swelling response to different hydrocarbons and well construction fluids, which suggests that different sensing polymer may have to be used on the fiber optic sensing cable when monitoring cementing job involved certain well construction fluids and/or opposite particular hydrocarbon reservoirs.

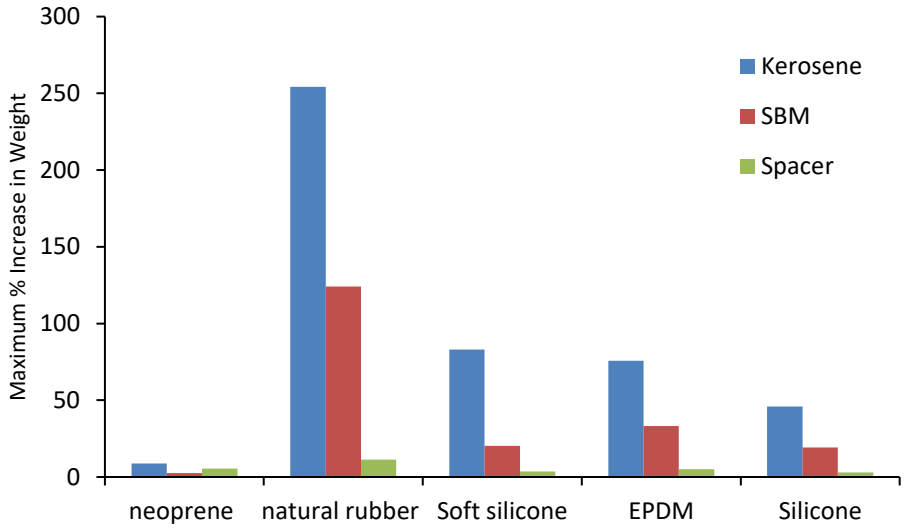

Figure 4.14 – Results of five elastomers in fluids.

As already mentioned, another important factor to consider is the response time of each elastomer. As shown in Figure 4.15, except for neoprene, all four elastomers respond to SBM in a very short period of time. Natural rubber responds to SBM with 18% increase in weight while the other three show about 10% increase in weight in the first 10 minutes. By 1 hour, a significant increase in weight was observed for natural rubber (37%), silicone (18%), soft silicone (20%), and EPDM (32%). These results are encouraging and provide guidance on the selection of sensitive polymers. Note that elastomers such as silicone and EPDM in fact consist of a large "family" of different materials, providing a large variety of potential candidates for selection.

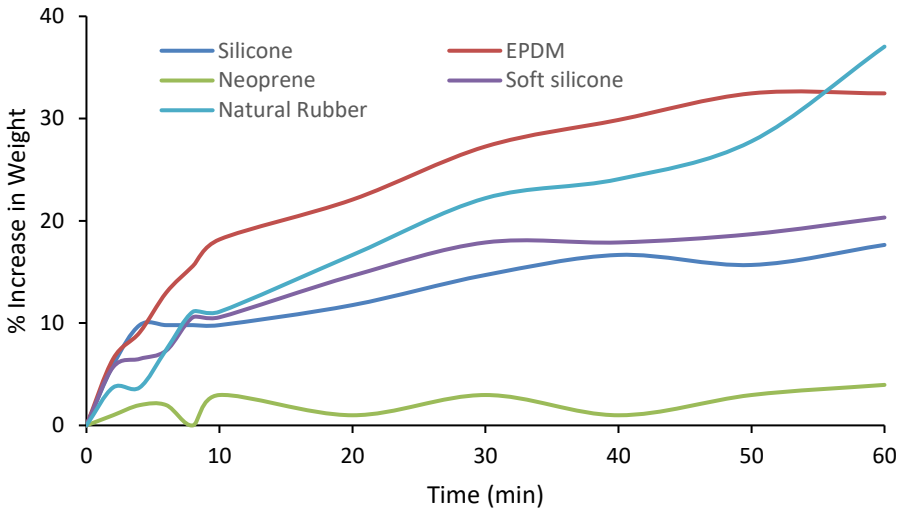

Figure 4.15 – The response time of five elastomers in presence of SBM.

To tailor the cable to specific well conditions, the operational temperature range and desirable hardness of the elastomers as shown in Table 3.4 should also be considered. For example, natural rubber yields the strongest response to the testing fluids compared to other elastomers tested. However, it also exhibits the lowest hardness (durometer 40 A) among the five tested elastomers as shown in Table 3.4. This could potentially render it vulnerable to damage in challenging downhole environments. In addition, since the DTSS system measures the strain applied on the optical fiber (and not change in weight), the packaging mechanism can also significantly affect the efficiency of converting the swelling of the elastomer to the strain that can be detected, which requires further study.

Chapter 5: Cement Hydration Monitoring[2]

Sections 5.1 to 5.4 illustrate the experimental results for demonstrating the capability of the DTSS system to monitor cement hydration process, detect contamination of cement slurry by drilling muds, evaluate the effect of external temperature changes on cement hydration, as well as identify the top of cement (TOC) and defects like voids in the cement annulus, based on the rectangular cement sample test introduced in Section 3.3.1. Section 5.5 presents the results from the polyurethane rod test described in Section 3.3.3 to showcase the advantage of increasing cement job monitoring area using helical installation method for the fiber optic cable.

5.1 Cement Hydration Monitoring using the DTSS System

Figure 5.1a shows temperature profile along a targeted section of the optical fiber ('the green cable') during hydration of neat cement slurry in an insulated chamber. Details of the experimental setup can be found in Figure 3. 7 of Section 3.3.1. Two thermocouples were used to verify the data obtained from the DTSS system. The average values from the thermocouples and the targeted fiber section are shown in Figure 5.1b and curves of the data obtained from for both measurements are nearly identical. This shows that quantitative values obtained from the DTSS system during cement hydration are reliable.

In Figure 5.1b, along with the average temperature changes obtained from the thermocouple and the DTSS system, the temperature changes calculated solely from Brillouin (PPP-BOTDA) and Rayleigh (TW-COTDR) techniques are also shown. If temperature changes were calculated solely from the sensing data of Brillouin or Rayleigh

[2] Parts of this chapter was published in: Wu, Q., Nair, S., Shuck, M., et al., 2017. Advanced distributed fiber optic sensors for monitoring real-time cementing operations and long term zonal isolation. J. Pet. Sci. Eng. 158, 479–493. doi:10.1016/j.petrol.2017.08.072. Wu designed and conducted the experiments, analyzed the data and wrote the paper. Other authors advised the research and edited the paper.

technique without any consideration for the strain-temperature cross-sensitivity, they would be significantly higher than the actual values. However, the qualitative trends would be the same. Thus, the DTSS system is preferred in instances when accurate quantitative information is required, but Brillouin and Rayleigh techniques can be used individually in cases where qualitative information suffices or cases when only changes in strain or temperature exist.

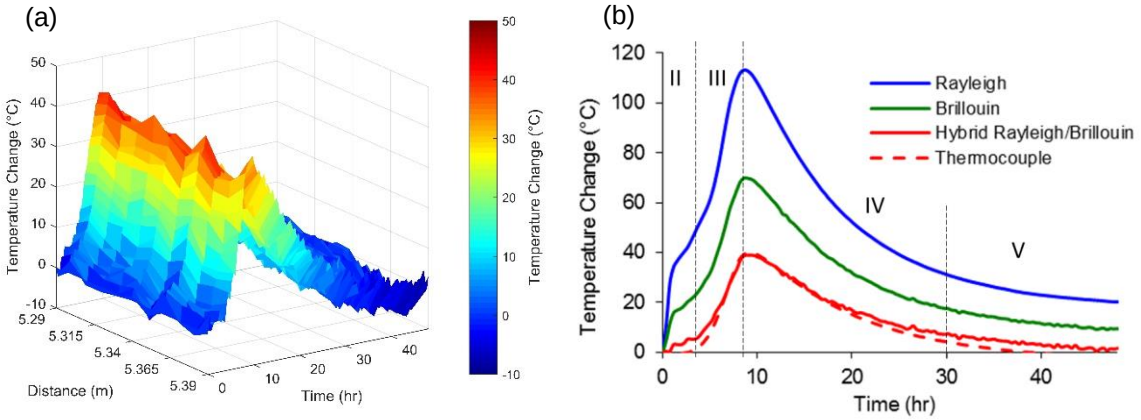

Figure 5.1 – (a) 3D plot showing temperature changes as a function of distance along a section of the cement-embedded fiber optic sensor (‘the green cable’) over a period of 48 hours, measured during hydration of neat cement slurry at room temperature in an insulated chamber. (b) 2D line plot showing average temperature changes obtained from the thermocouple and the DTSS as well as the temperature values calculated solely from Brillouin or Rayleigh technique. On the plot various stages of cement hydration have been identified.

The values shown in Figure 5.1 are temperature differences with respect to the initial recorded temperature of 28 °C at the time when the cement slurry was placed in the chamber and the test was started. The resulting curves exhibit a profile that is similar to data typically obtained using an isothermal calorimetry (c.f. Figure 2.11). In Figure 5.1b,

the end of the induction period (or stage II) can be clearly seen. The onset of the acceleration phase (stage III) occurred approximately around 5 hours, which is an indicator of initial set. The initial set point corresponds to a viscosity that is well in excess of the limits of pumpability (LOP), which equates to a consistency in the range of 70 Bc to 100 Bc (Scherer et al., 2010). Note that initial set time of cement slurry can be affected by multiple external factors such as downhole temperature, pressure (Nelson and Guillot, 2006, Taylor, 1997), and the application of shear in mixing (Hodne et al., 2000). The amount of time to the initial set should be longer than the expected pumping time. The API thickening time test used to measure consistency requires shearing the slurry at 150 r/min (API RP 10B-2, 2013). Although the API test can be conducted under simulated downhole temperatures and pressures, the actual temperature (Jones, 1986), pressure and amount of shear applied to the slurry (van Kleef and van Vliet, 1993) in the field might not be in agreement with the simulated ones. The in-situ measurement obtained using the DTSS system determines the initial set point in the field, and thus provides more a reliable estimate of the setting time (or WOC). As shown in Figure 5.1, the temperature change reached a maximum value of 40 °C at 10 hours, which is the end of stage III. The deceleration phase (stage IV) starts at 10 hours and continues until the temperature change reduces to 5 °C at 30 hours. The temperature distribution is relatively uniform along the entire length of the optical fiber in Figure 5.1a, which indicates that the cement slurry was placed without any voids or channels.

Figure 5.2 presents the strain profile during the cement hydration process along the same length of the optical fiber shown in Figure 5.1a. Since it is a measurement of strain applied on the fiber, the results can be interpreted as volumetric changes in cement slurry during the hydration process. For the first 8 hours, the strain increased, reaching a maximum value of 800 με, which indicates to expansion of the cement slurry. This

expansion can be explained by initial swelling of slurry due to domination of repulsive solvation pressures over attractive crystallization forces during this period of cement hydration (Paulini, 1994). The strain values then rapidly reduced in value until 20 hours, after which they decreased slowly, which might indicate shrinkage typical during early-age cement hydration (Bouasker et al., 2008, Bullard et al., 2011).

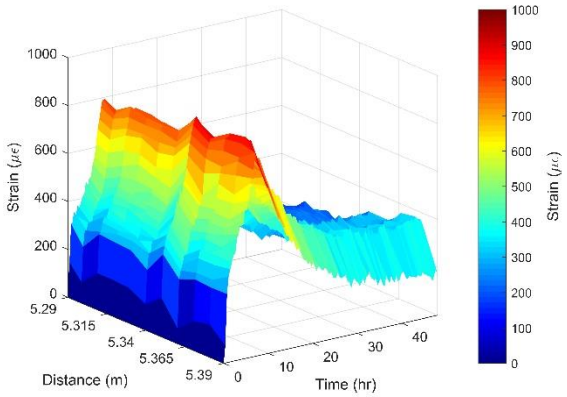

Figure 5.2 – 3D plot showing changes in strain as a function of distance along a section of the cement-embedded fiber optic sensor ('the green cable') over a period of 48 hours, measured during hydration of neat cement slurry at room temperature in an insulated chamber.

5.2 Effect of External Temperature on Cement Hydration

In the field, the temperature profile along the depth of a given oil or gas well varies. The DTSS system is expected to be able to accurately monitor the cement hydration process at elevated temperatures. The 3D temperature profiles shown in Figure 5.3 were obtained at three different external temperatures. Cement reacts with water immediately upon contact and starts generating heat. The first thermocouple reading was at 30 °C and this value was used as the initial temperature of the cement slurry when the test was started.

The temperature values shown in Figure 5.3 are the temperature differences with respect to that initial temperature. It can be seen that as the external temperature was increased from 24 °C (Figure 5.3a) to 49 °C (Figure 5.3b) and finally to 77 °C (Figure 5.3c), the recorded temperature change during hydration also increased and was relatively uniform along the length of the fiber. The average temperature changes along the targeted length of the optical fiber was used to compare the results from the DTSS system with those obtained from the thermocouples (Figure 5.3d) and it can be seen that the results match very well.

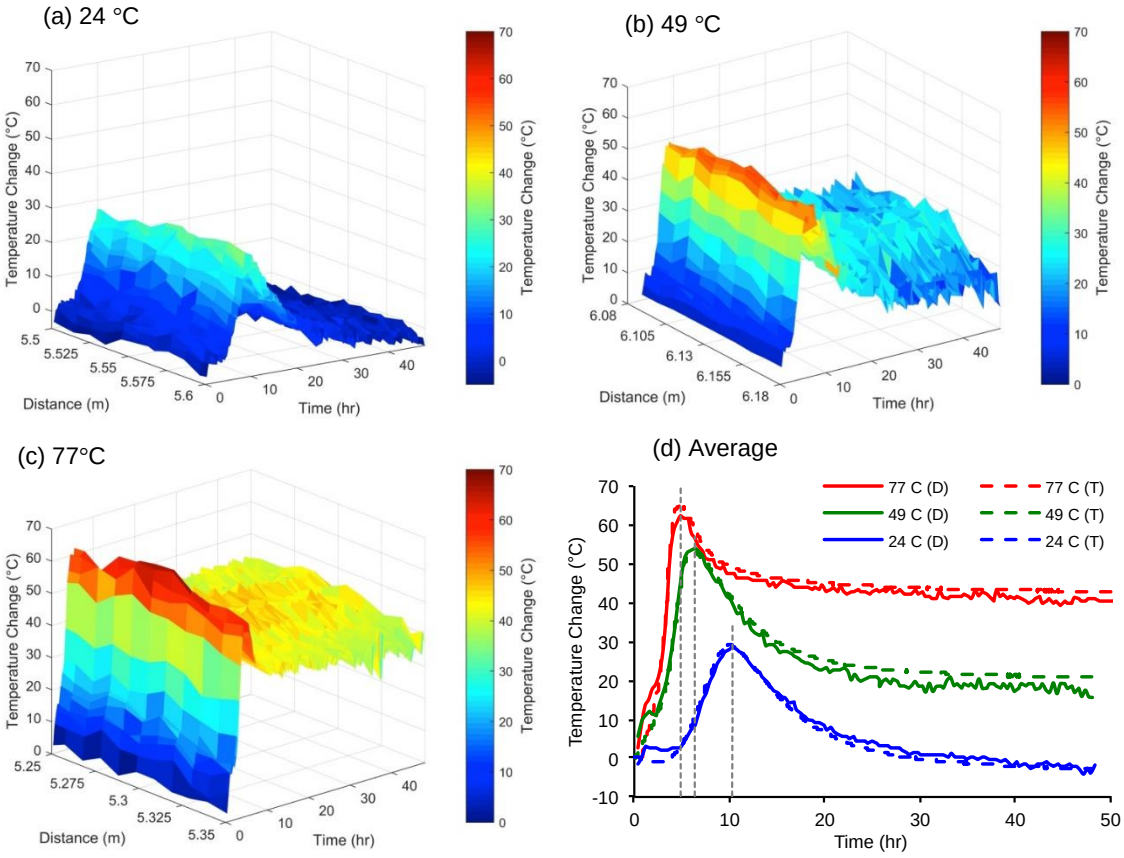

Figure 5.3 – 3D plot showing temperature changes along a section of the fiber embedded in cement over a period of 48 hours at an external temperature of (a) 24 °C, (b) 49 °C and (c) 77 °C. (d) Plot comparing the average data from the DTSS system (D) with the data obtained from thermocouples (T).

For an external temperature of 24 °C, the acceleration phase (stage II) starts at 5 hours and the temperature change reaches a peak value of 29 °C at around 10 hours. For the slurry at 49 °C, the acceleration phase (stage II) starts sooner at 2 hours after pouring the cement slurry and the temperature change reaches its peak of 53 °C around 6.5 hours. For the slurry at 77 °C, the temperature change rises immediately and sharply, reaching its peak value of 63 °C in around 5 hours. As the external temperature increases, the peak height of the change in temperature increases while the width of the curve decreases. The increases in the peak height resulted from the cement slurries being heated up by the surrounding environment. Furthermore, the width of the curves decrease as well as the peaks shift to the left, implying that there is an acceleration in the rate of cement hydration reactions with an increase in temperature. This behavior of course follows the well-known trend of cement hydration acceleration at elevated temperature (Nelson and Guillot, 2006), which is typically modified using suitable accelerators and retarders. Thus, the DTSS system demonstrated its capability to accurately monitor the temperature changes during cement hydration at elevated external temperatures to provide essential information, e.g. about the effectiveness of cement additives such as accelerators and retarders in modifying cement pump and set times.

5.3 Effect of Contamination with Synthetic Based Mud (SBM)

The effect of cement contamination with SBM on heat evolved during hydration can be clearly seen in the 3D plots shown in Figure 5.4. As the contamination level increases from 0% (Figure 5.4a) to 15% SBM by volume (Figure 5.4d), there is a significant decrease in the peak temperature value from approximately 40 °C to 20 °C. Thus, by monitoring the cement hydration process with the DTSS system and analyzing

the temperature profile, SBM contamination can be identified, the amount of SBM in the cement slurry can also be estimated, and the spatial distribution of contamination along the depth of the well can be obtained. Further studies are required to fully understand and quantify the effects of SBM on the hydration reactions.

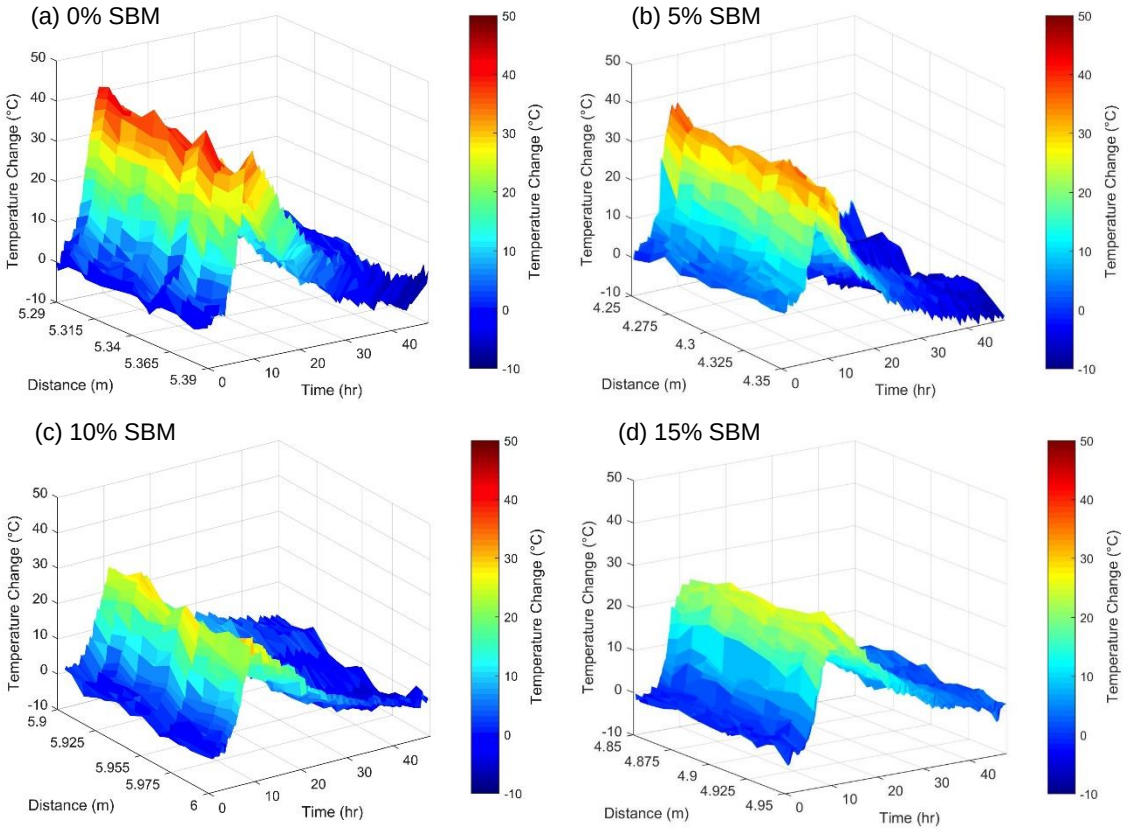

Figure 5.4 – 3D plot showing temperature changes measured over 48 hours during the cement hydration process of (a) neat cement slurry and cement slurry contaminated with (b) 5% SBM (c) 10% SBM and (d) 15% SBM by volume.

Next, experiments were carried out to evaluate the effect of sand replacement on temperature profiles due to a dilution effect (i.e., presence of less cement). The average

temperature change along the length of the fiber for each dosage of SBM is shown in Figure 5.5a. The same volume percentage of cement was substituted with sand (5%, 10%, and 15%) and the corresponding temperature changes are shown in Figure 5.5b. From both figures, it can be seen that there is no significant change in the start or end times for both stage III and stage IV. Since silica sand (particle size > 100 μm) does not interfere with hydration reactions (Wang et al., 2013), the decrease in the peak values observed in Figure 5.5b can be attributed to the dilution effect. For the same volume percentage replacement of SBM, the temperature changes are measurably lower than those of sand, although admittedly by a small amount. By analyzing the curves of temperature changes from the DTSS, the presence of SBM contamination or sand can be distinguished. In actual field applications, it would be safe to assume that any deviation in the measured temperature profile from the expected profile would be due to either mud contamination or absence of cement. Both effects are, of course, a concern for establishing and maintaining zonal isolation.

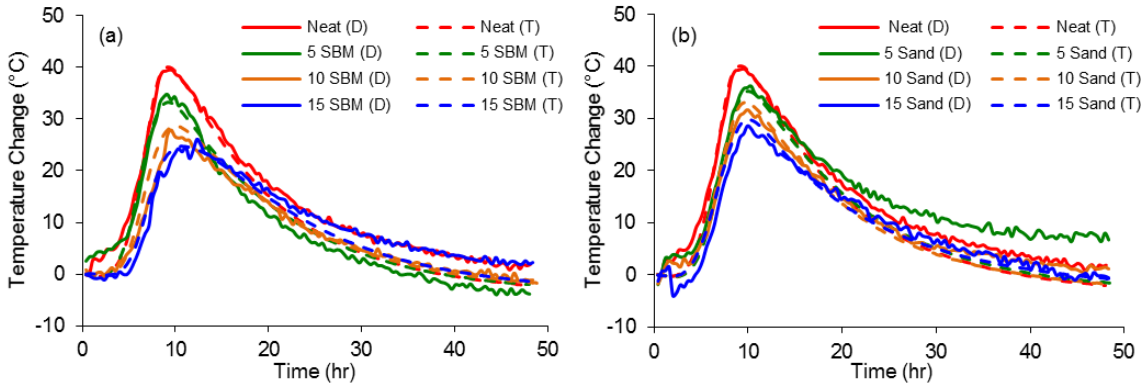

Figure 5.5 – 2D line plot showing average temperature changes for cement slurry at different levels of contamination with (a) SBM (b) Sand. Note: In the legend, D denotes data collected from the DTSS system and T denotes data collected using thermocouples.

Another interesting conclusion can be drawn by comparing the temperature profiles in Figure 5.3d and Figure 5.5. From Figure 5.3d, it can be seen that the external temperature had a significant influence not only on the peak value of temperature change, but also on both start and end times of stages III and IV of the cement hydration process. However, as shown in Figure 5.5, at a given external temperature, contamination with either SBM or sand only affected the peak value but not the time it took to reach it – the amount of heat release appears to be affected by contamination, but the heat release timing is not (at least not in this case).

5.4 Effect of Uncemented Sections (or Voids) and Monitoring the Top of Cement

In cases when the casing is not centralized within a well and/or when borehole caliper is poor, it is possible that cement preferably flows through the wider annular gap while leaving the drilling mud behind in the narrower gap (Nelson and Guillot, 2006). In such cases, the DTSS system can be used to monitor the cement hydration process to clearly differentiate between large uncemented sections versus fully cemented sections. Figure 5.6 presents the result from monitoring cement hydration on a sample with such cemented and uncemented sections. This result immediately points to an important potential use of the DTSS system: the determination of the top of cement (TOC) in real-time without the need for wellbore re-entry required by traditional cement bond logging tools. This is highly relevant information to well construction safety. TOC is a key well construction parameter, and there are often regulatory requirements demanding its determination. Moreover, contamination of cement is one of the main factors that negatively affect zonal isolation. For example, the required isolation between geological strata that prevents both co-

mingling and pressure communication of different formation fluids as well as fluids and associated pressure reaching surface.

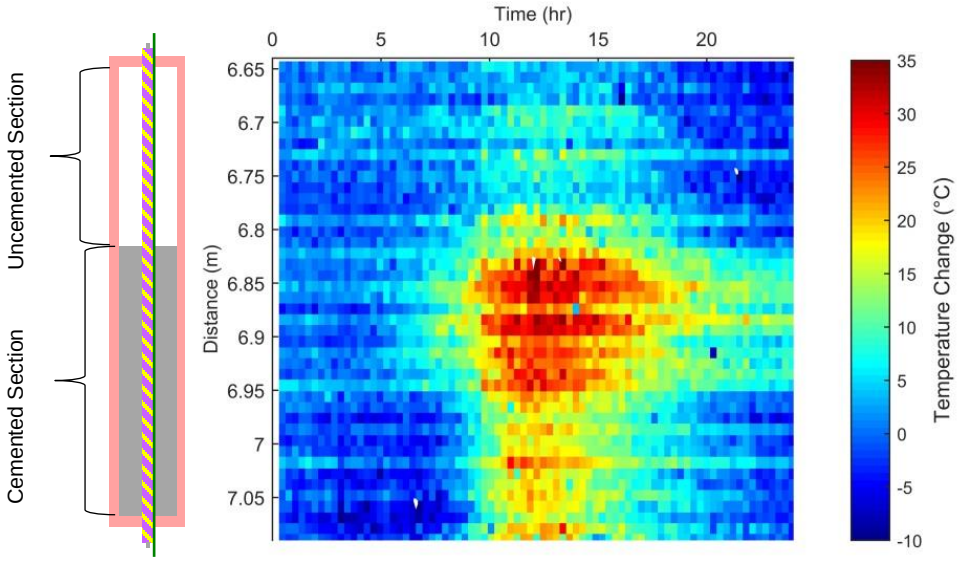

Figure 5.6 – 2D surface plot showing temperature changes in a box, which is half filled with cement slurry. The purple cable described in Section 3.1.1 was used for the monitoring process.

The results of Figure 5.6 indicates that DTSS is well-suited for identifying large uncemented sections (25 cm in this case), but there are scenarios where it is beneficial in the field to have information regarding smaller voids. For such cases, when small variations are anticipated, Rayleigh-based sensing is especially suitable because of its high sensitivity. Two small voids, each 10 cm long, were created as shown in Figure 5.7. Temperature change distribution can then be used to locate sections with and without cement. Although the temperature values obtained by using only the Rayleigh technique are expected to be higher than the actual values (see Figure 5. 1) without separating temperature and strain

measurements, it is more sensitive and provides sufficient information to qualitatively evaluate the state of zonal isolation.

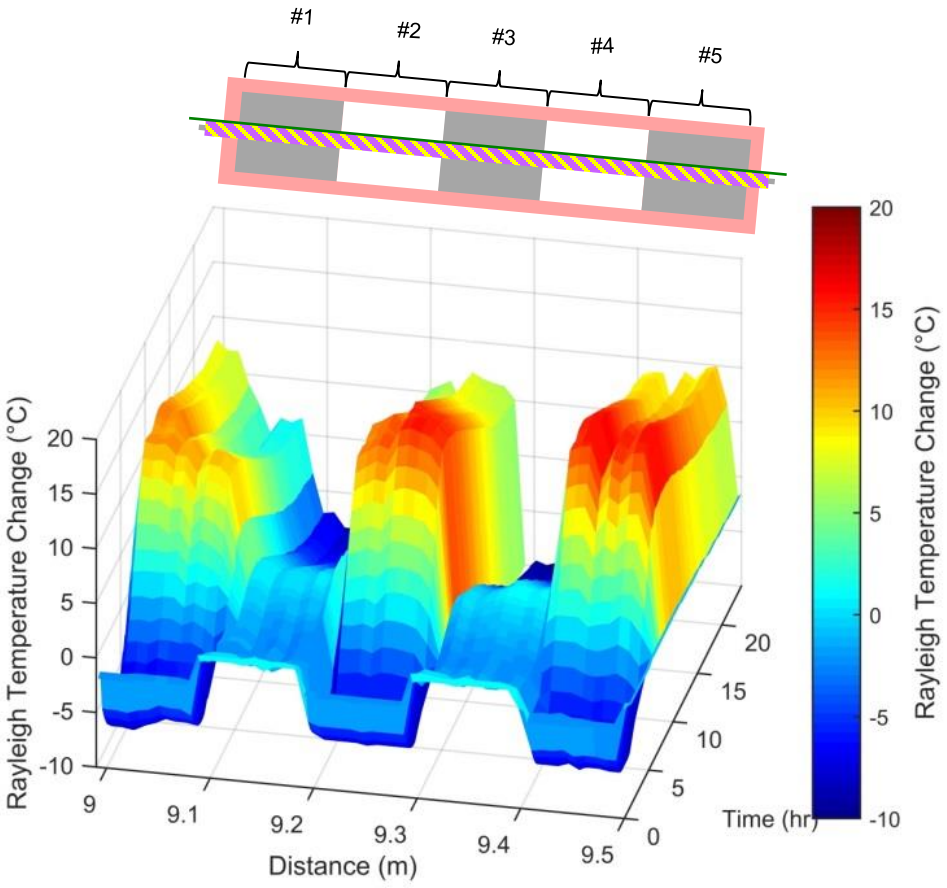

Figure 5.7 – 3D plot showing temperature changes calculated using Rayleigh (incident light) frequency difference. Cement slurry was placed in sections 1, 3 and 5, while the other sections were left empty to simulate void spaces in the cement.

5.5 Increasing Cement Job Monitoring Area using Helical Installation

Cement hydration monitoring using the DTSS system was also demonstrated with helical installation of the fiber optic sensing cable and the experimental setup is described

in Section 3.3.3. As shown in Figure 5.8c, the average temperature changes obtained from the DTSS system match quantitatively with those recorded by a thermocouple, confirming the reliability of the DTSS temperature measurement. Although the changes in temperature are relatively small due to the small quantity of cement slurry used in this test setup, it should be noted that the DTSS system is capable of detecting such small changes. Figure 5.8a shows the temperature profile at section B-B along the height, over a period of 48 hours, which is similar to what can be obtained from straight axial installation as demonstrated in Section 5.1. Figure 5.8b presents a 360-degree image around the rod, which shows the advantage of increasing sensing area using the helical wrapping installation. Such a circumferential annular view increases the accuracy of cement integrity evaluation. For straight axial installation, the DTSS might not be able to detect the presence of channels in the cement annuli if the channels or other defects are not close to the location where the fiber optic cable is installed. This could potentially lead to false-negative results. By using a helical wrapping installation at a relatively low wrapping angle, the sensing area can be significantly increased and optimized to effectively cover a large portion of the annular space, which will improve the quality of zonal isolation monitoring.

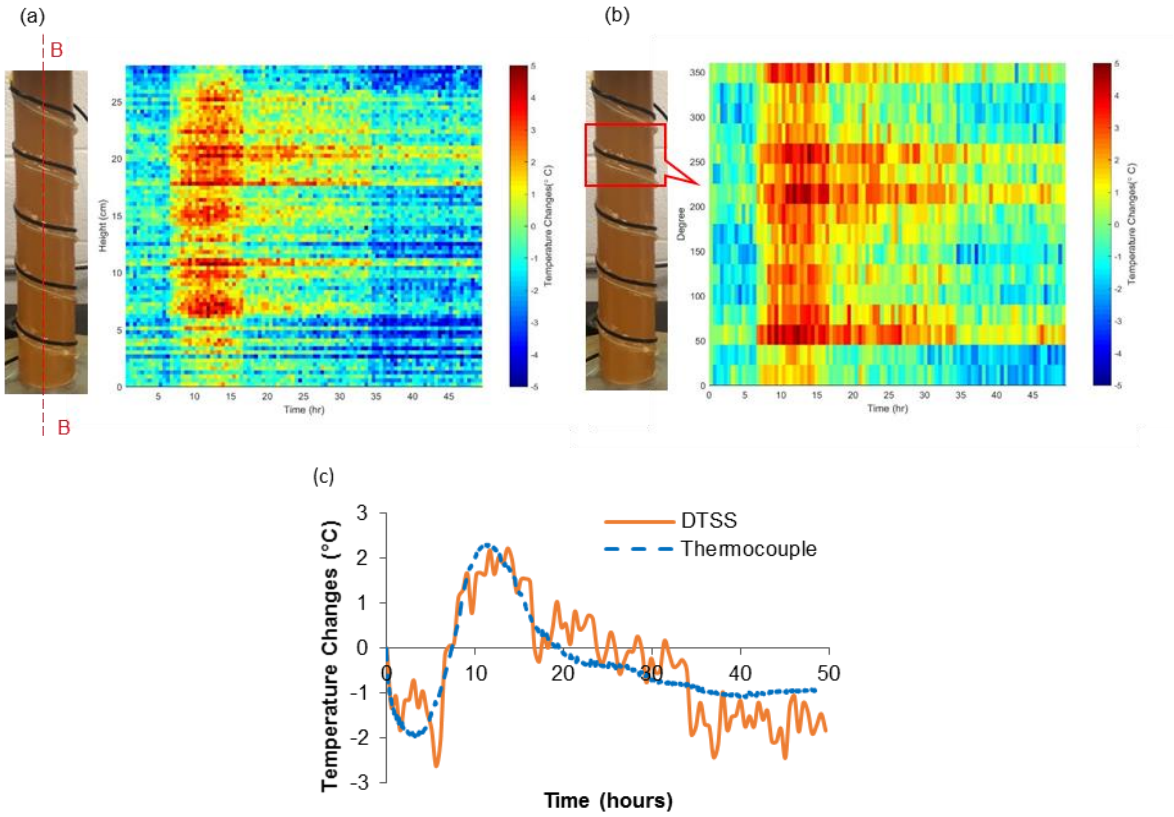

Figure 5.8 – Temperature measurement characterizing exothermic cement hydration (a) at section B-B, and (b) at the first turn of fiber optic cable around the rod; (c) comparison of temperature changes obtained by the DTSS system and a thermocouple, showing good quantitative agreement in spite of very small temperature changes.

Chapter 6: Zonal Isolation Monitoring[3]

This chapter presents the results of multiple experiments described in Section 3.3 to demonstrate the application of the DTSS for zonal isolation monitoring, including fluid invasion detection, casing deformation detection, cement-casing bond evaluation in Sections 6.1 to 6.3. Section 6.1 shows the results that validated the capability of DTSS system to detect the formation fluid migrating from another zone with different temperature, by using the temperature measurement and detection of the presence of unwanted hydrocarbons in the cement annulus using the distributed chemical sensing technique. The results also indicated that the proposed fiber optic sensing cable (the purple cable) has reversibility for multiple-time uses as well as the robustness after exposure to well construction fluids. In Section 6.2, the results and evaluation of the dual-cable design for concurrent detection of casing deformation and hydrocarbon detection are presented. The idea of estimating hydrocarbon exposure time was illustrated based on the experimental results. The discussion includes an evaluation of helical fiber installation and the verification of the measurement accuracy by comparing the DTSS's strain measurement to the values based on the theoretical calculation and the applied loads. Section 6.3 illustrates the results for demonstrating the cement-casing bond evaluation based on the temperature and strain measurement from the DTSS. In addition, section 6.4 contains a discussion on permeability test results (with the test described in Section 3.3.5) to determine the effect of cement-embedded fiber optic cables on the hydraulic properties of the cement sheath in an annulus or plug.

[3] Parts of this chapter was published in: Wu, Q., Nair, S., Shuck, M., et al., 2017. Advanced distributed fiber optic sensors for monitoring real-time cementing operations and long term zonal isolation. J. Pet. Sci. Eng. 158, 479–493. doi:10.1016/j.petrol.2017.08.072. Wu designed and conducted the experiments, analyzed the data and wrote the paper. Other authors advised the research and edited the paper.

6.1 FLUID INVASION DETECTION

This section focuses on the application of the DTSS system in combination of the fiber optic sensing cable and the distributed chemical sensing capability for detection of fluid invasion in the cement annulus or cement plug. The results of invasion fluids, such as elevated-temperature formation fluid (water or brine), and hydrocarbon (kerosene), are presented and illustrated as follows.

6.1.1 Fluid Migration Detection

Results reported in Chapters 4 and 5 already demonstrated the accuracy of temperature measurement using the DTSS system. This section presents the results from the polyurethane rod test described in Section 3.3.3, which shows the capability of the DTSS system to accurately track the presence of fluid (water or brine) using the sensitive temperature measurement. With helical wrapping, the temperature measurement covers the full annulus. Figure 6.1 shows the circumferential images of an annulus, in which the y-axis represents the height of the rod while the x-axis represents the unwrapped circumference of the rod as shown in Figure 3.15b. The increase in heated water level was captured in time from one-quarter of the height to the full level, as shown in Figure 6.1. The results show that the DTSS system is capable of detecting the temperature effects associated with fluid migration in cemented annuli as well as cement plugs. Thus, such information can be applied to detect the loss of zonal isolation when such temperature variations due to fluid invasion is identified.

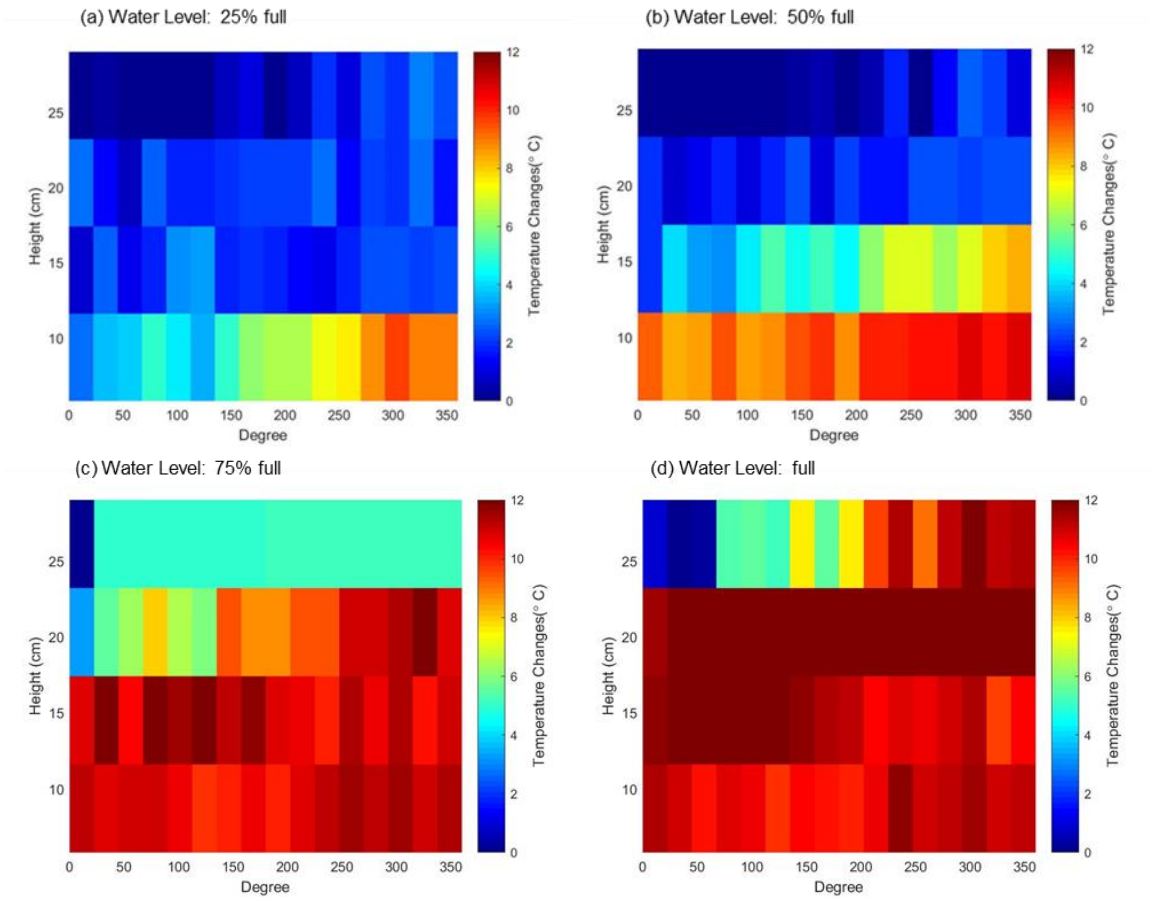

Figure 6.1 – Elevated temperature water level tracking while progressively filling the annulus of the test set-up with elevated temperature water.

6.1.2 Hydrocarbon Detection

Hydrocarbon Detection with Sensing Cable

In Chapter 4, both the purple cable and the black cable described in Section 3.2.1 were found to exhibit a selective sensitivity to tests fluids that the cable might be exposed to during well construction, such as SBM, spacer fluids, mineral oil, brine and hydrocarbons (kerosene), enabled by the strain measurement. This section focuses on the

hydrocarbon detection in the cement annuli using the DTSS and fiber optic sensing cable (the purple cable). The effectiveness of the cable at detecting hydrocarbons even after being exposed to common well construction fluids was also evaluated. Since the experiments were conducted at constant room temperature, all the strain values shown were obtained using the Rayleigh technique. In the first experiment, both the purple cable (p1 cable) without a steel braid (Figure 6.2a) and the modified purple cable (p2 cable) with a steel braid permeable to fluids (Figure 6.2b) were submerged in kerosene for 18 hours. When exposed to kerosene, changes in strain (based on the Rayleigh technique) were plotted in Figure 6.2. It was observed that the presence of kerosene leads to significant swelling of the hydrocarbon sensitive polymer, which yielded elevated strain values that were detected using the DTSS system. It can be seen that the strain distributions along the length of both cables are relatively uniform. For the p1 cable, there was a significant increase in the value of strain during the first 2 hours, reaching a maximum value of 1300 με in 5 hours that was then maintained until the end of the experiment. In contrast, the strain value increased continuously for the p2 cable and reached a maximum value of 2500 με, which is around twice the values obtained with p1 cable. The explanation for the latter behavior is that the steel braid on the p2 cable provides additional confinement to the swelling compared to the p1 cable, resulting in a higher strain value imparted onto the fiber. Note that the steel braid also provides additional protection for the optical fiber and the hydrocarbon sensitive polymer, which is important for application in the complex downhole environment. Thus, the p2 cable demonstrates a proof of concept cable design that can be further developed for application in the field.

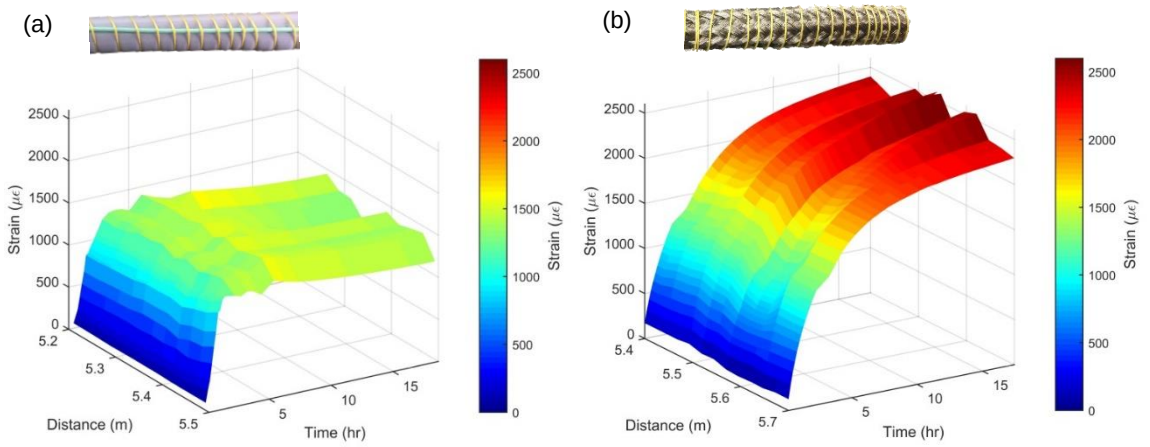

Figure 6.2 – 3D plot showing the strain generated on the optical fiber due to the swelling of the hydrocarbon sensitive polymer in the presence of kerosene over 18 hours. A clear difference can be seen between values obtained from (a) p1 cable without steel braid and (b) p2 cable with steel braid.

After 18 hours of exposure, the p2 cable was removed from kerosene and then exposed to the air. It can be seen in Figure 6.3 that the measured strain decreased exponentially after placing the cable in air at room temperature for another 18 hours. At the end of this experiment, the cable was essentially back to its original size before exposure to kerosene. This is a very important feature of the sensing system, showing that the cable is not just a one-time sensor, but can, in fact, be activated repeatedly and thereby function as a reusable and potentially a lifetime sensor. When such unwanted hydrocarbon presence is detected in the cement annulus, a remedial cementing job can be performed to fix or moderate the problem. In the absence of hydrocarbons, the cable returns back to its original form thereby verifying that the remedial job was successful. It can then continue to be used to monitor the presence of hydrocarbons during the life of the well.

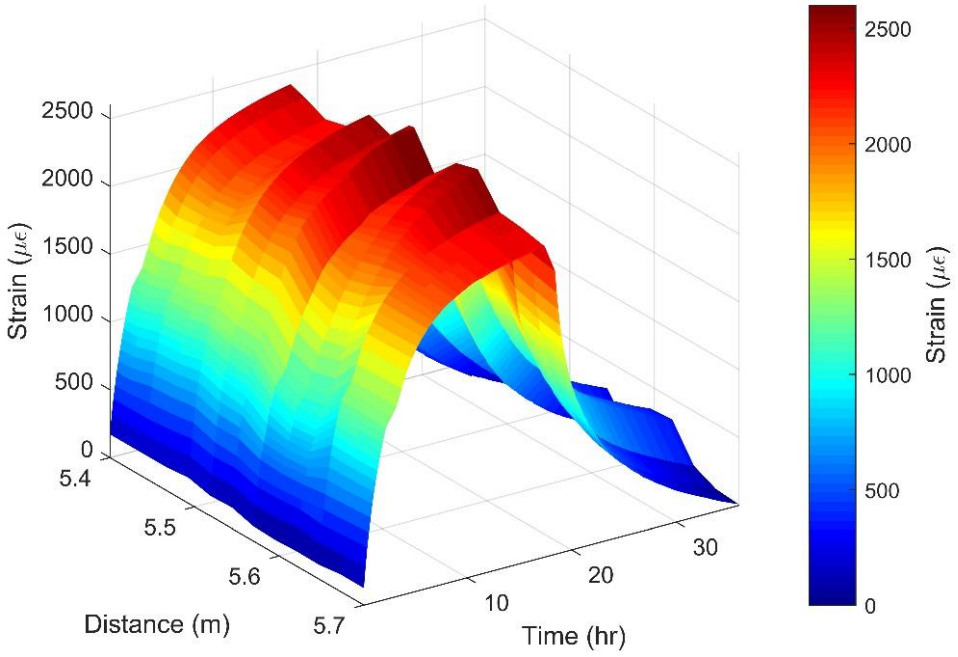

Figure 6.3 – 0-18 hours shows the strain introduced in the p2 cable (with steel braid) due to swelling of the polymer in presence of kerosene and from 18-36 hours shows the reversibility of the swelling with removal of kerosene and exposure to air.

As mentioned in the previous chapters, the fiber optic sensing cable is expected to be installed on and run into the hole concurrently with the casing before a cementing job. Therefore, it will be exposed to well construction fluids such as drilling muds and spacer fluids. To test the sensing capability of the cable after exposure to the well construction fluids, p1 cable was first immersed in SBM for 45 hours, then in a spacer fluid for 70 hours, and finally in kerosene for 24 hours. The results are similar to that of the black cable from Chapter 4 for cement displacement tracking (c.f. Figure 4.11 and Figure 4.12). When submerged in SBM, the cable shows a slight increase in strain up to 200 με and then decreases with time (Figure 6.4). When submerged in spacer fluid, the strain values

decrease to -100 με, which indicates that the spacer fluids might cause a small amount of shrinkage of the hydrocarbon sensitive polymer. After the cable was exposed to the well construction fluids, the cable still responded to the kerosene with the strain increased to a significantly higher value and rose to more than three times that of the value observed in SBM. The long exposure time of the cable to SBM (45 hours) and to spacer fluids (70 hours) was used in the laboratory experiment to evaluate the effect of duration of exposure to well construction fluids. In field application, the actual exposure time of the cables to these various well construction fluids is expected to be much shorter and their influence can be even smaller. This demonstrates that the sensing cable is still highly sensitive to the hydrocarbon (kerosene) after it is exposed to the well construction fluids. It is noted that different types of swellable elastomers are sensitive to different types of hydrocarbons as tested in Section 3.3.6 and Section 4.3. This feature can be exploited to develop "fingerprinting" selectivity that will allow identification of the type and origin of hydrocarbons that present behind casing.

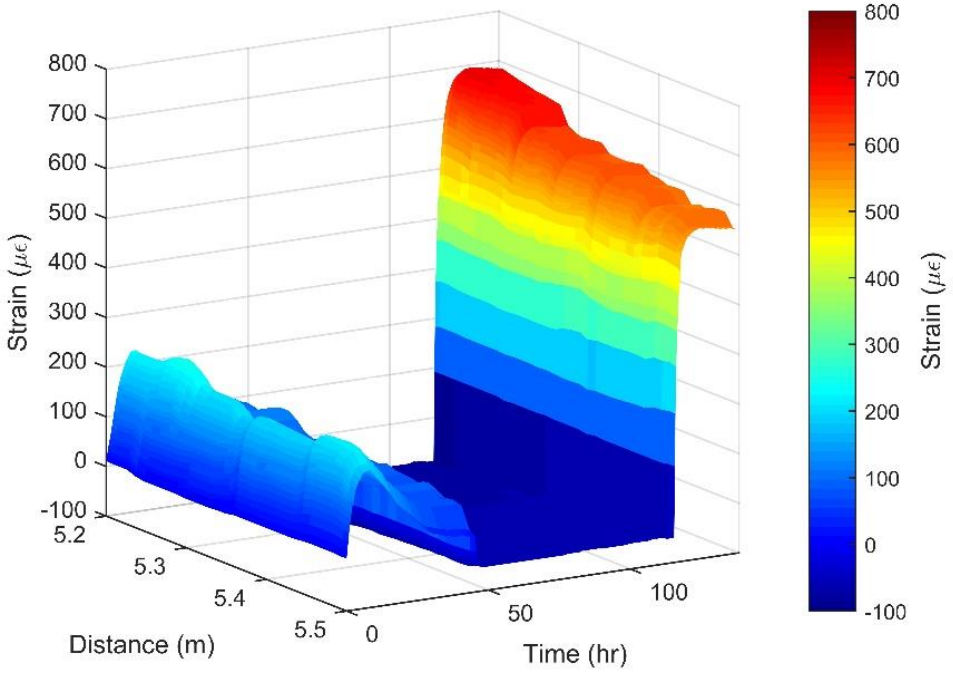

Figure 6.4 – 3D plot showing strain change in the p1 cable (without steel braid). From 0-20 hr: slight increase followed by decrease in strain in presence of SBM; 40-110 hr: no change in strain in the presence of spacer fluid; 110-140 hours: significant increase in strain triggered by the presence of kerosene.

Detecting the Presence of Hydrocarbons in Cemented Annuli

One of the main indications of compromised zonal isolation in an oil and gas well is the presence of fluid communication between different zones. When a cementing job is poorly executed or when cement becomes compromised due to incomplete displacement of drilling mud or other reasons, it is highly possible that there are sections in the annulus that do not have any cement present. In addition, if hydrocarbons are detected above the top of cement (TOC), it is very likely that zonal isolation is compromised. To simulate this situation, half of the length of the sensing cable was cemented and the other half was left

uncemented (c.f. Figure 3.8). When this whole sample was submerged in kerosene, as shown in Figure 6.5, swelling was clearly observed in the uncemented section where an increase in strain up to 900 με was recorded while the strain values in the cemented section were relatively low around 100 με. Thus, the cemented and uncemented sections can be simply differentiated when exposed to kerosene. This result demonstrates that the presence of hydrocarbons above top of cement can be detected using the DTSS system.

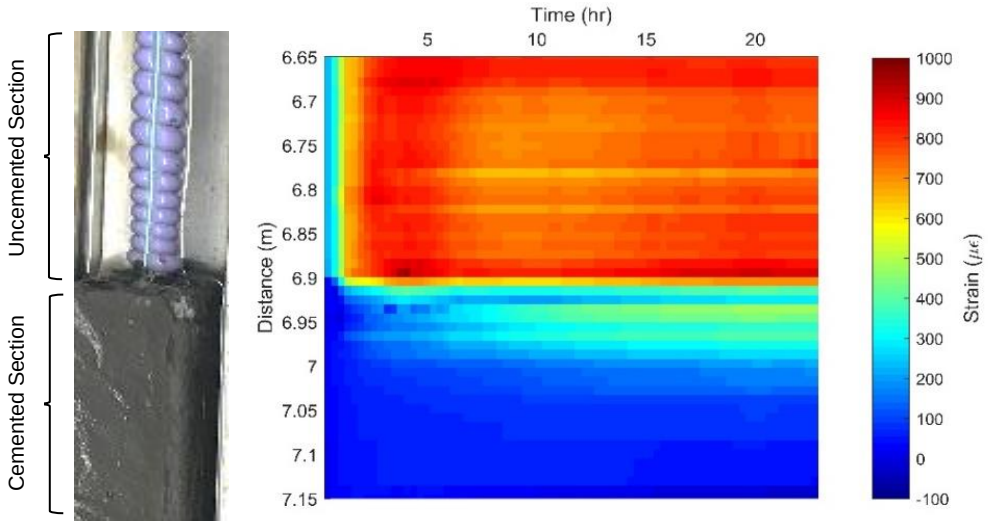

Figure 6.5 – 2D plot showing strain changes in p1 cable in the presence of kerosene. Clearly, the strain change in the uncemented section is significantly higher.

Sections left without cement (i.e. voids) might exist in the annulus due to problems arising during cementing operations such as incomplete displacement of drilling muds. Existing logging tools can detect the absence of cement only when it occurs in a large region, but they may not have the accuracy to detect smaller pockets through which hydrocarbons could potentially migrate. If connected, these small voids and pockets can potentially provide a path for hydrocarbons to migrate in the cement annulus. To simulate

the partial absence of cement in small voids, p1 cable was embedded in cement in sections 1, 3, and 5 and sections 2 and 4 were left uncemented (Figure 6.6). After the cable was submerged in kerosene, visual swelling of the hydrocarbon sensitive polymer was observed in both sections 2 and 4 and there was a corresponding increase in the value of the strain measured in these uncemented sections. Since the length of each section is only 10 cm, the increase in strain is not as high as the previous sample shown in Figure 6.5. However, with an exceptional spatial resolution of 2 cm, it can still be seen that the strain values in uncemented sections 2 and 4 are much higher than that of cemented sections 1, 3, and 5. Thus, five short sections can be clearly differentiated using the DTSS measurement. The location of voids in the cement annulus containing hydrocarbons can, therefore, be identified using the strain distribution profile.

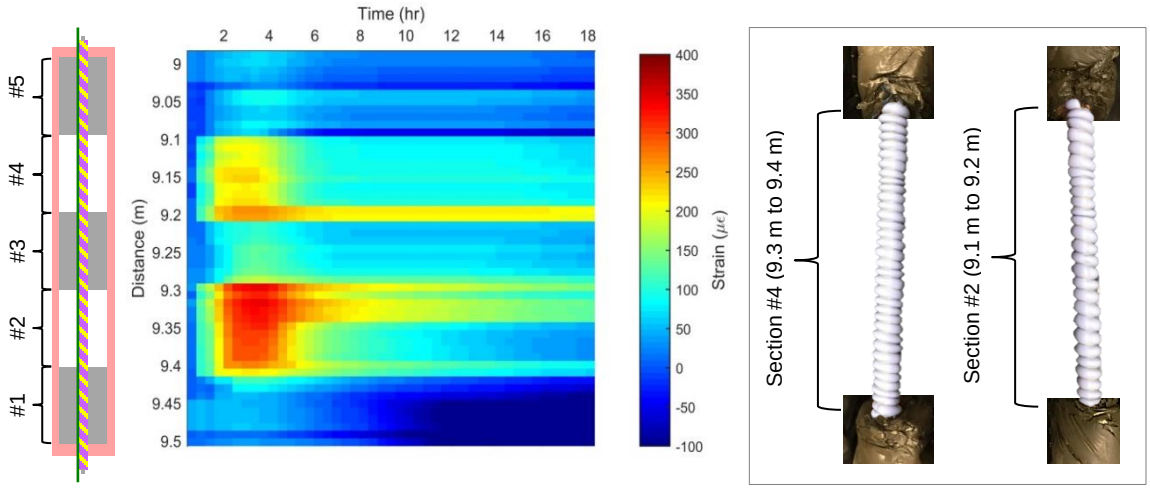

Figure 6.6 – 2D plot showing strain changes in p1 cable in the presence of kerosene. A clear distinction can be observed between the short sections with and without cement.

Poor cementation or changes in the downhole environment (e.g. because of cyclical cement loading and unloading) could also lead to cracking in the cement annulus. Cracks can be connected and enlarged to form channels for upward migration of hydrocarbon to shallower zones (e.g. aquifers) or even to the surface, which compromises zonal isolation. Figure 6.7 shows that when a cement sample with a 0.5 cm wide channel was exposed to kerosene, significant strain changes up to 2000 με were detected by the DTSS system. Along the distance axis, the strain values are not exactly uniform due to the fact that the channel itself is not completely uniform, as shown in Figure 6.7. This non-uniform distribution of strain within the spatial resolution can lead to low correlation and thus it is difficult to obtain the Rayleigh frequency shift (Kishida et al., 2014). Thus, in this case, strain measurement obtained from Brillouin technique was used for analysis.

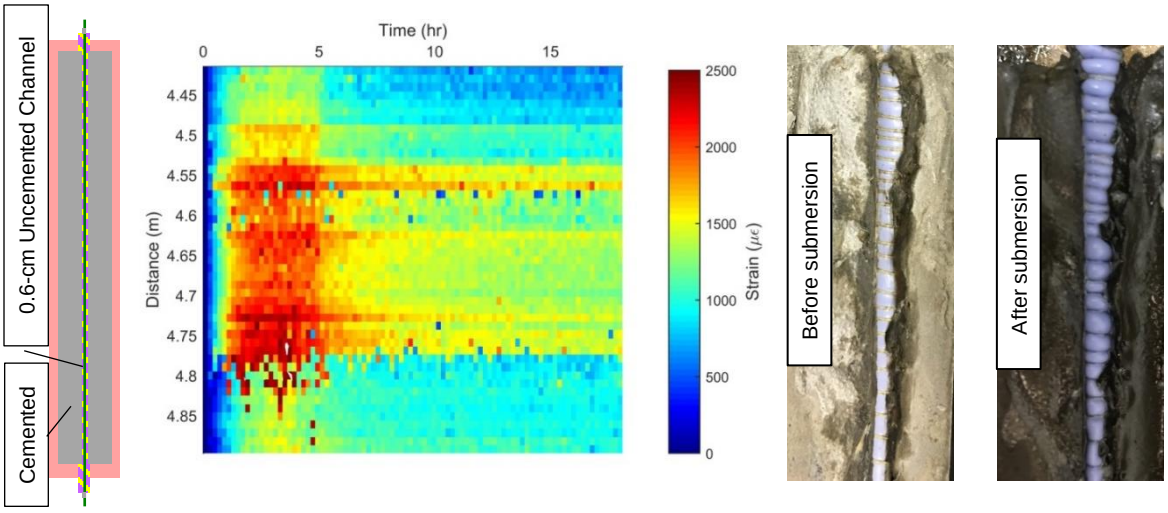

Figure 6.7 – 3D plot showing the change in strain over time for a cement sample with a channel that is exposed to kerosene. The strain values shown were measured using Brillouin frequency shift.

Increasing Hydrocarbon Detection Sensing Area with Helical Installation

The application of hydrocarbon detection using the DTSS and the black cable with sensing polymer was also demonstrated in the polyurethane rod test introduced in Section 3.3.3. Unlike the previous sections using straight axial installation of the purple cable, this test applied the helical installation of the black cable to increase the sensing area for the whole annulus, similar to what was discussed in Section 5.5 for cement hydration monitoring. As shown in Figure 6.8, during the 12-hour monitoring period of the hydrocarbon detection experiment, the strain on the black cable (or 'HC cable') increased over time at the lower section (about 25% of the height of the rod), indicating the presence and the level of kerosene. The distances along the fiber were converted to the height of the rod for better illustration in Figure 6.8. This result demonstrates the capability of using the helical wrapping installation to detect hydrocarbons in the whole annulus when the cement integrity becomes compromised.

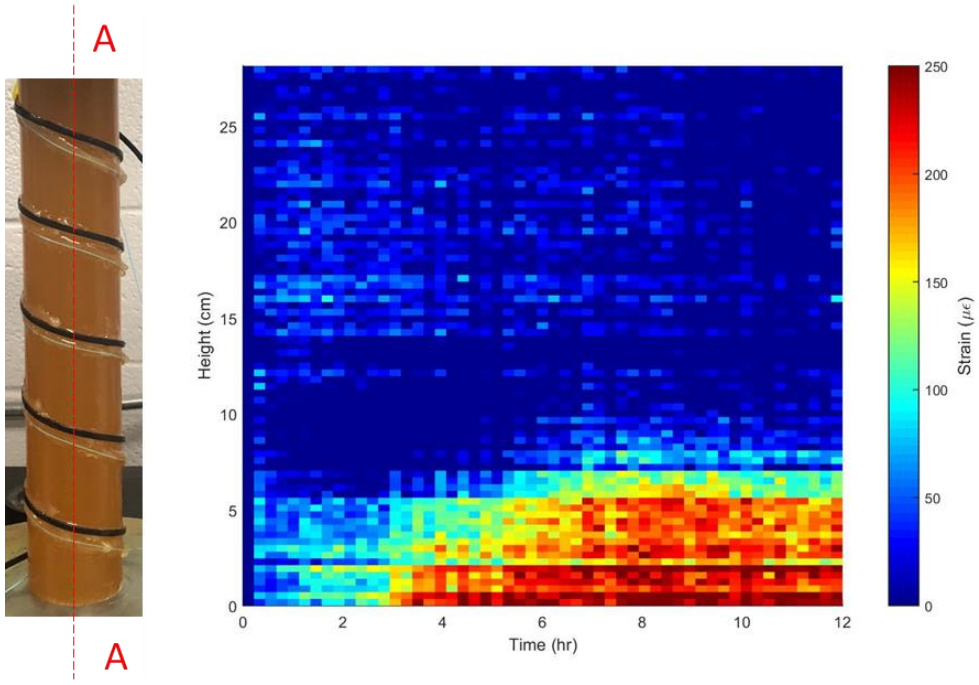

Figure 6.8 – The black cable (HC cable) strain measurement at section A-A during kerosene exposure at 25% of the height of the rod.

In summary, for primary cementing, the proposed system can detect unwanted hydrocarbon migration in cemented annuli and thus monitor the cement integrity in real time. For plug and abandonment, the proposed system can be used as long-term abandonment monitoring, detecting hydrocarbon leaks and loss of zonal isolation due to cement plug failure. This sensing system can provide essential information that is required to identify the need for well intervention and remedial cementing operations.

6.2 Casing Deformation Detection

In addition to using the DTSS system as a cement sensor to monitor the cement annulus, this section presents the laboratory development in improving the system to

integrate the application of casing deformation monitoring using the DTSS system (Wu et al., 2019a). Two fiber optic sensing cable installation options, straight axial installation and helical installation, were both tested and evaluated. The results and discussion are presented as following.

6.2.1 Cantilever Beam Test Results (Straight Axial Installation)

The cantilever beam specimen described in Section 3.3.2 was tested for four different situations and the response was plotted in Figure 6.9. Figure 6.9a represents the initial response of the cables without any strain. In Figure 6.9b (representing casing deformation), only the DEF cable (the green cable introduced in Section 3.2.1) responded to the load with an increase in strain, which matched the strain values calculated using Eqs. 3.1 and 3.2. The HC cable (the black cable introduced in Section 3.2.1) did not detect any strain increase from beam deformation due to its strain-free installation. In Figure 6.9c (representing presence of hydrocarbons), only the HC cable detected a significant strain increase while the DEF cable had minimal strain change in response to the presence of kerosene. In Figure 6.9d (representing combined presence of hydrocarbons and casing deformation), both HC and DEF cable responded with strain increases.

The HC cable can not only detect the presence of hydrocarbon but also monitor the duration of hydrocarbon exposure, as shown in Figure 6.10. There was little strain increase during the first 2 hours of kerosene exposure. Starting from 2 hours onwards, the strain on HC cable increased significantly. After 4 hours, the increase slowed down, reaching the plateau around 1,100 με. The relationship between the increase in strain (ε_{HC} in με) and exposure time ($t_{exposed}$ (hours)) of the HC cable to kerosene was obtained using the least-squared method in regression analysis to find a statistical model with the maximum R

squared value (c.f. Figure 6.11). This result can now be used in reverse: the exposure time of the HC cable to kerosene can be obtained from the strain changes using Eq.6.1. Note that such an equation will vary for different types of sensitive polymer coating on the cable and different kinds of fluids the cable is exposed to. However, the methodology will essentially be the same as demonstrated here:

$$t_{exposed} = -1.422\ln(-0.0001989\varepsilon_{HC} + 0.2094) \quad \text{Eq. 6.1}$$

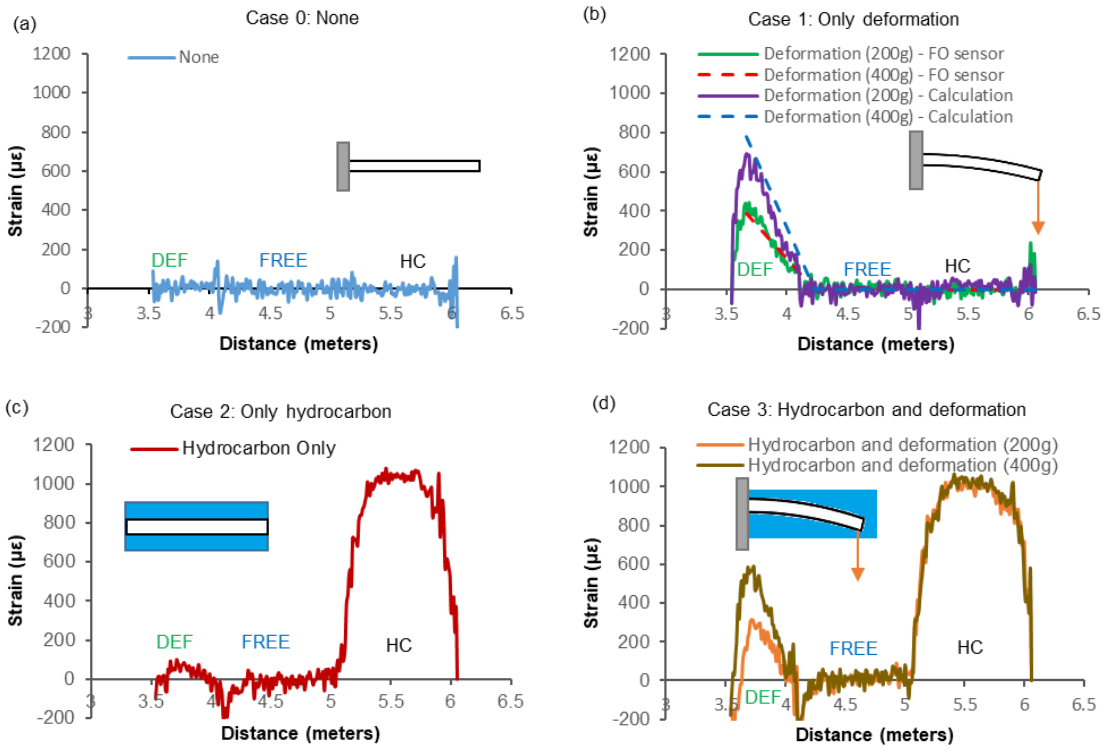

Figure 6.9 – The strain changes for four different scenarios: (a) no strain change; (b) casing deformation only; (c) presence of hydrocarbon only; d) presence of hydrocarbon and casing deformation combined.

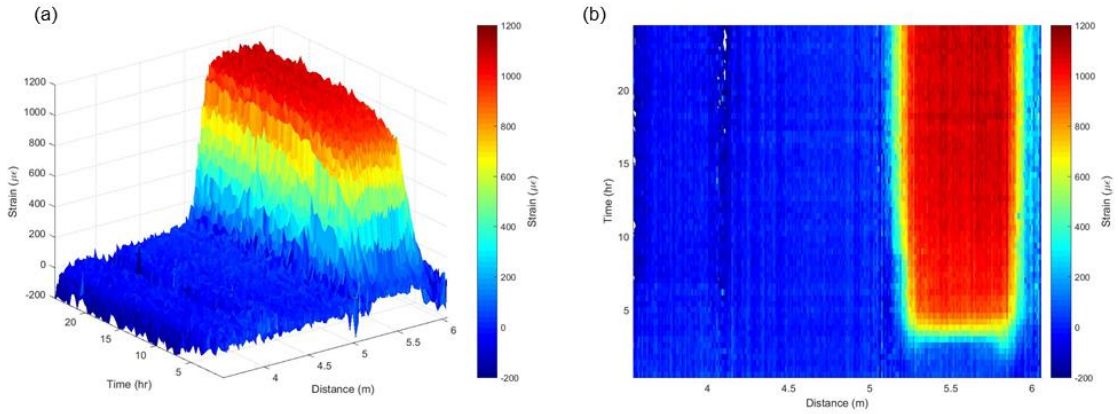

Figure 6.10 – Strain increases on the HC cable ('the black cable') during the exposure to kerosene in (a) 3D view (axes are strain, time and distance along the fiber optic cable), and (b) 2D view (axes are time and distance along the fiber optic cable).

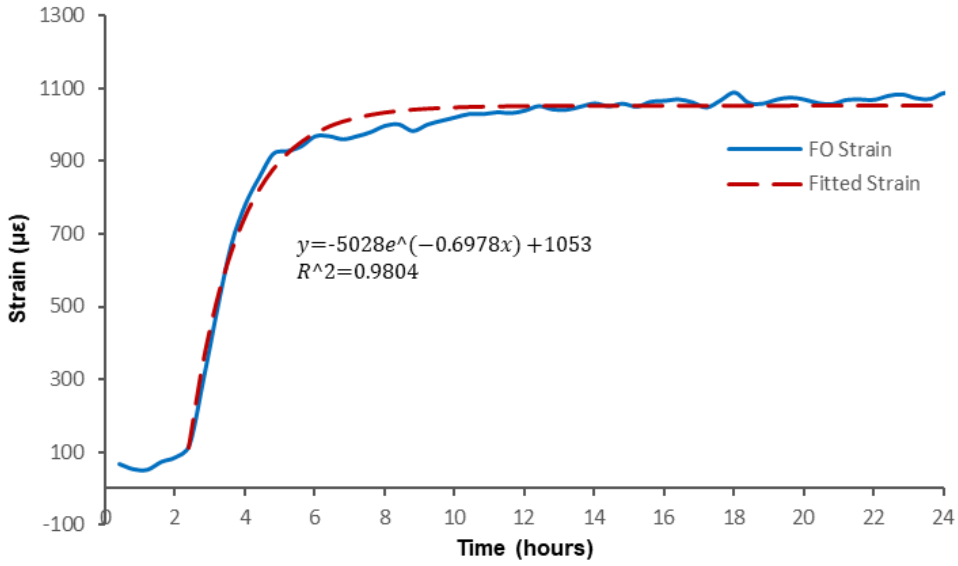

Figure 6.11 – Relationship between the strain values measured on the black cable and the exposure time to kerosene.

In this laboratory demonstration, the beam deformation is relatively small, such that the installation of HC cable can be strain-free. However, in the actual field application, if the casing deformation is expected to be so significant that it can cause bending of HC cable even with the current strain-free installation, modification of the dual-cable design is recommended. In this case, both HC and DEF cables can be fixed to the casing so that they are both sensitive to casing deformation to the same extent. By comparing the strain measurement from the DEF and HC cables, the presence of hydrocarbons can be detected. The amount in which strain changes due to the presence of hydrocarbons can also be determined by subtracting the strain changes obtained on the DEF from those obtained from the HC cable.

6.2.2 Rod Deformation Results (Helical Installation)

The distribution of strain in the DEF cable on the polyurethane rod surface under different loads was measured using the DTSS, and the data are shown in Figure 6.12. Similar to Figure 6.1, the y-axis represents the height of the rod while the x-axis represents the unwrapped circumference of the rod as shown in Figure 3.15b. As the applied load is increased from 89 N (Figure 6.12a) to 223 N (Figure 6.12d), the strain distribution also increases and is relatively uniform along the length of the fiber. The axial strain values of the polyurethane rod under different applied loads were calculated using the three methods discussed in Table 3.4, and the results are plotted in Figure 6.13. The strain values calculated using Eqs. 3.3, 3.4, and 3.5 are close to each other and follow the same trend, as expected. The small variances can be attributed to precision limitations of the load frame, which has a measurement accuracy of 4.45 N (1 lbf). The result demonstrates that the application of the DTSS technique in combination with helical wrapping can be used to

monitor the casing deformation with adequate reliability and accuracy. To increase sensing area and accuracy, the wrapping angle of the DEF cable can be further optimized or multiple DEF cables can be wrapped at different angles to cover even more sensing area. Lower wrapping angle results in more turns of the cable per unit length of the casing string and thus increases the sensing resolution. However, when the wrapping angle decreases to 0°, no axial strain can be detected since the optical fiber is perpendicular to the axis of the applied loads. Different wrapping angles result in variations in sensitivities to different deformation modes, such as axial, bending, and ovalization (Pearce et al., 2009). In field practice, cost performance will need to be taken into consideration when designing the helical wrapping configuration – more wraps increases costs. Thus, the helical wrapping installation design should be optimized depending on the specific application(s).

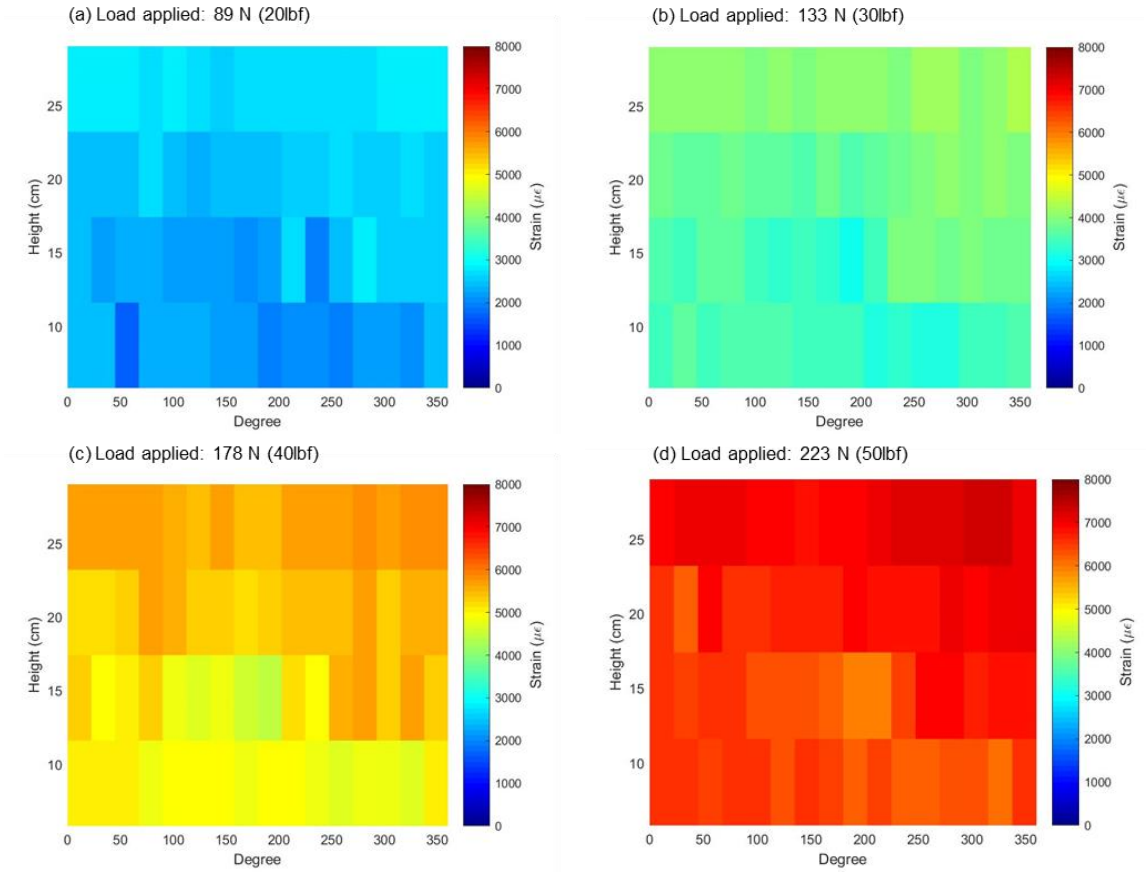

Figure 6.12 – Strain distribution on the polyurethane rod surface measured by the DEF cable (‘the green cable) and the DTSS system under different loads.

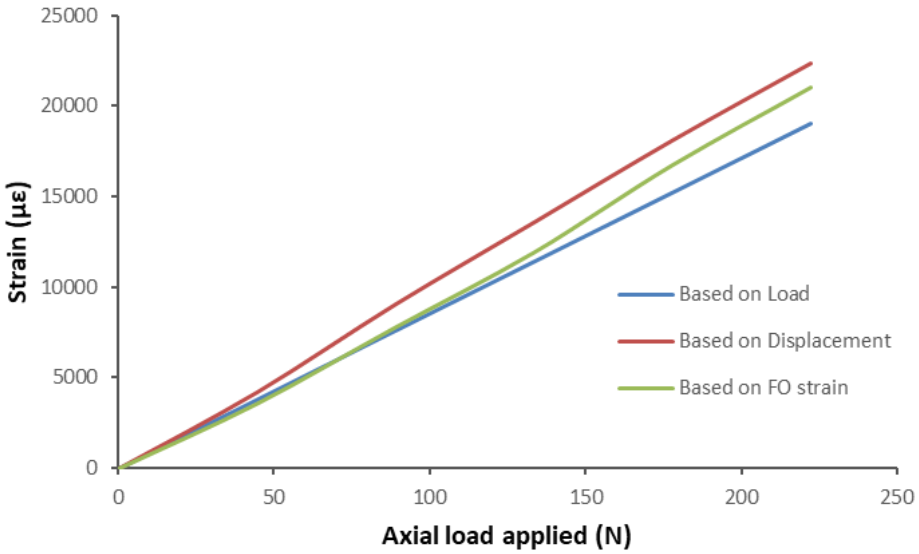

Figure 6.13 – Axial strain on the polyurethane rod obtained from three different methods described in Section 3.3.3 (Eq. 3.3, Eq. 3.4, and Eq. 3.5).

6.3 CASING-CASING BOND MONITORING

In this section, the use of the DTSS system and the fiber optic sensing cable (the green cable) installed helically on the casing to evaluate the cement-casing bond is explained and demonstrated in the laboratory tests as discussed in Section 3.3.4. The evaluation is based on monitoring of the temperature and strain changes. The results from the laboratory tests are presented in the following paragraphs.

6.3.1 Cement-Casing Bond Evaluation Based on Temperature

As illustrated in Chapter 5, when a cement slurry hardens and develops compressive strength, heat is released due to exothermic calcium silicate hydration reactions. This heat release follows a specific pattern that can be used to characterize the quality of the

cementing job. Based on temperature changes recorded using the DTSS system, the previous chapters have already demonstrated the ability to determine wait-on-cement (WOC) time and setting time, to detect the contamination of cement slurry with drilling mud, and to identify the location of top of cement (TOC) and the lack of cement in certain sections such as voids, cracks, and channels (Wu et al., 2016a, Wu et al., 2017b). In this section of the study, the DTSS system was used to measure the temperature and strain changes during cement hydration in the laboratory-scale well model to ensure uniform placement of cement slurry, and thus qualitatively evaluate the cement-casing bond (Wu et al., 2019b). As shown in Figure 6.14a, the temperature change is relatively small due to the small quantity of cement slurry used and the small scale of the well model. However, it still follows the expected pattern and is measurable given the system's high spatial resolution. The helical installation provides a circumferential image, effectively covering of the entire annular space around the casing. A relatively uniform distribution of temperature change along the length of the fiber indicates that there are no voids or significant defects in the cement-casing bond (at the centimeter scale of resolution of the DTSS system). Figure 6.14b confirms the reliability of the measurement obtained from the DTSS system, by showing that the obtained average temperature changes match with those measured using a thermocouple. The two curves shown in Figure 6.14b are not perfectly overlay on each other. This is because the thermocouple was embedded in the middle section of the cement sample and only measured the temperature changes at that specific point while the average temperature changes were calculated based on the entire length of fiber optic cable embedded in the cement sample.

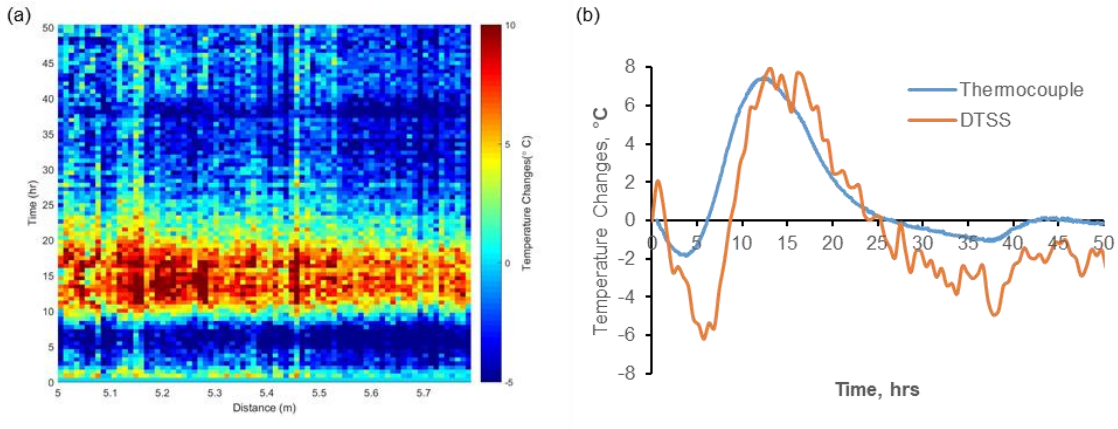

Figure 6.14 – Temperature measurement during cement hydration using the DTSS system: (a) along the distance of the fiber optic sensing cable (‘the green cable) itself; (b) a comparison of the average fiber-optic response and a thermocouple measurement.

6.3.2 Cement-Casing Bond Evaluation Based on Strain

The cement-casing bond test was conducted following the procedure introduced in Section 3.3.4. During the cement-casing bond test, the incremental applied axial load was measured using a load cell as shown in Figure 6.15a. The figure shows that the 4th measurement took place right before debonding between cement and casing occurred. This observation can be used to estimate the approximate shear bond strength when comparing the applied load with the measured strain as shown in Figure 6.15b. The exact value of the applied load when debonding happened was not captured due to the limitations of the load frame under manual control. The shear stress values were calculated using the following equation:

$$\tau = \frac{F}{A} \quad \text{Eq.6.2}$$

where τ is the shear stress, F is the applied shear force and A is the bonding area between the casing and the cement annulus under shear load. The results of shear stress values were

plotted along the y-axis while the strain measured using the fiber optic cable (the green cable described in Section 3.1.1), labeled as 'FO strain', was plotted along the x-axis, as shown in Figure 6.15b. The obtained correlation was almost linear up to the point of debonding. In the field, such stress-strain correlation can be used to estimate the shear stress values at the cement-casing interface from the strain measurement by the DTSS system. If the calculated shear stress is below the expected or pre-determined shear bond strength, the cement-casing bond is not expected to fail; if shear stress values start to approach critical values, however, it may be necessary to consider remedial actions if at all possible. The accuracy of the correlation will improve by increasing the number of measurements and using larger scale models than those used in this study (which serves to demonstrate a proof-of-concept). Further studies are required to explore the factors that affect the correlation between cement bond shear stress and FO strain. Figure 6.16 provides a circumferential image of the strain distribution at the cement-casing bonding location, enabled by the helical installation of fiber optic cable on the casing. The y-axis represents the height of the rod while the x-axis represents the unwrapped circumference of the rod as shown in Figure 3.15b. Such a view on the strain distribution can be used to identify the exact location(s) at which the cement-casing bond is most likely to fail. By obtaining continuous snapshots at various time steps, the changes in strain can be monitored using the DTSS system and bond failures can be identified, and if possible prevented, in real time. Note that the cement-casing bond strength is expected to be much smaller than casing strength, and thus detection of cement-casing bond failure and casing deformation could be differentiated in strain measurement.

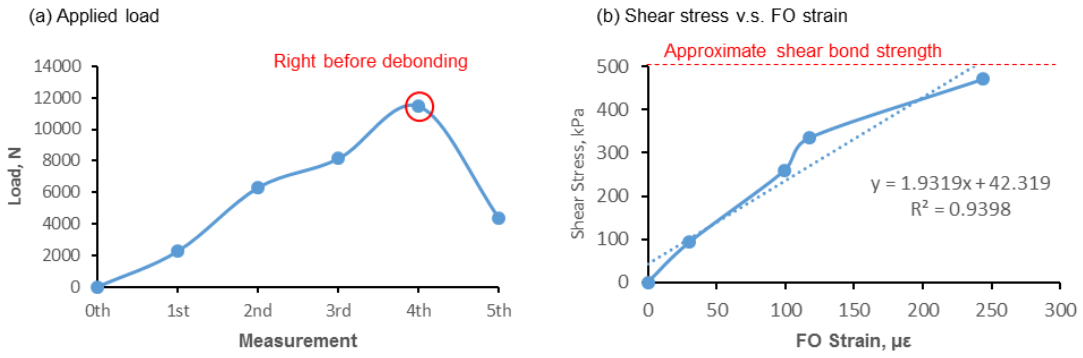

Figure 6.15 – (a) Axial loads recorded in five measurements; (b) calculated shear stress v.s. average FO strain changes at each measurement.

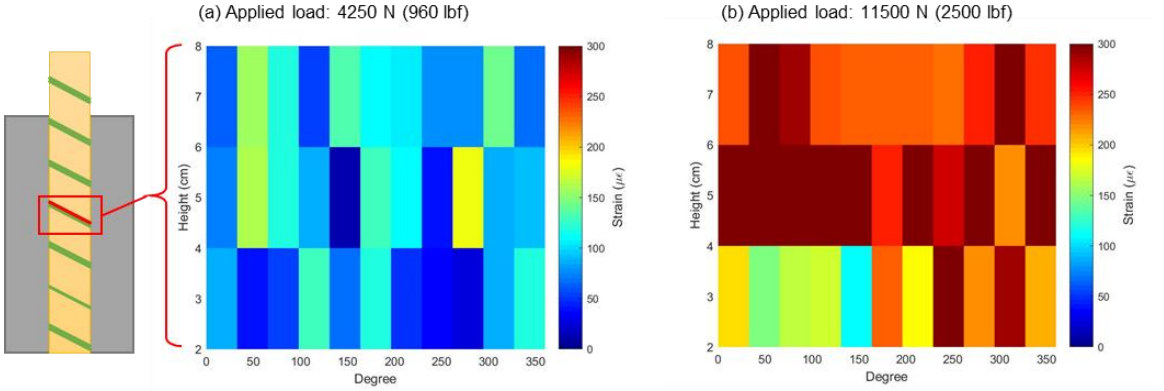

Figure 6.16 – Circumferential view of the selected section under different loads: (a) 4,250 Pa (960 lbf); (b) 11,500 Pa (2,500 lbf).

6.4 Effect of Embedded Fiber Optic Cable on Cement Permeability

Installing the fiber optic sensing cable on the casing enables the application of the DTSS system for cement displacement tracking, cement hydration monitoring, and zonal isolation as discussed in Chapter 4, Chapter 5 and the previous sections of Chapter 6 (Wu et al., 2017a, 2016b). After the cementing operation is completed, the cable(s) is expected to be fully embedded in the hardened cement. In this section, it is investigated whether

embedding the cable itself will have an impact on zonal isolation using the permeability test described in Section 3.3.5. The permeability of the cement can be affected by various factors. Even without any embedded fiber-optic cables, the permeability of cement can vary depending on the type of fluid or gas that is invading the cement annulus. Typical values of permeability for hardened cement are in the order of 1 to 10 µD (Lavrov and Torsæter, 2016). Several studies have reported permeability values that fall within this typical range for water (below 10 µD) and brine (approximately 10 µD) (Bachu and Bennion, 2009; Goode, 1962). There are other factors that can also affect the gas and fluid permeability of the cement annulus. For example, 50% seawater contamination by volume in the cement can lead to an increase of permeability to 50 µD, while the presence of 50% water-based mud (WBM) contamination by volume in the cement can increase gas permeability to 100 µD (Le-Minous et al., 2017). Gelled (not completely hardened) cement can have a gas permeability up to 300 millidarcys (mD), which may potentially lead to gas migration issues (Nelson and Guillot, 2006). Presence of cracks or micro-annuli in the order of 2.5 to 80 µm were found to increase the cement permeability to 0.01-1000 mD (Boukhelifa et al., 2004). An annular gap and/or cracks around 0.01 to 0.3 mm can result in the increase of permeability up to 0.1 to 1 mD (Bachu and Bennion, 2009), which is significantly larger than that of cement with embedded fiber optic cables. It has been reported in the literature that exceeding a cement permeability of 0.1 mD or 100 µD is enough for gas to flow (Goode, 1962; Ozyurtkan et al., 2013). Others consider the threshold value to be at 200 µD (Kutchko et al., 2009).

In this study, cement sample permeability was assessed using nitrogen gas. A summary of the results from the gas permeability test for the three types of cement samples is shown in Figure 6.17. For the plain cement sample without any fibers a permeability value of 2.9 µD was obtained. The permeability of the cement sample with an embedded

mesh cable was 38.1 µD, which is still within the range of typical oil well cement. The permeability of the cement sample with an embedded braid cable was 136.6 µD, which is higher than that observed for the plain sample and the sample with the mesh cable. Note that the acceptability criteria set by the 100 µD value is only slightly exceeded by the cement sample with the braided cable, and that all tested samples meet the 200 µD value criteria, as shown in Figure 6.17. Note that the permeability of cement, with or without fiber-optic cables, is dependent on the age of hardening, a variable that was not fully explored in this investigation.

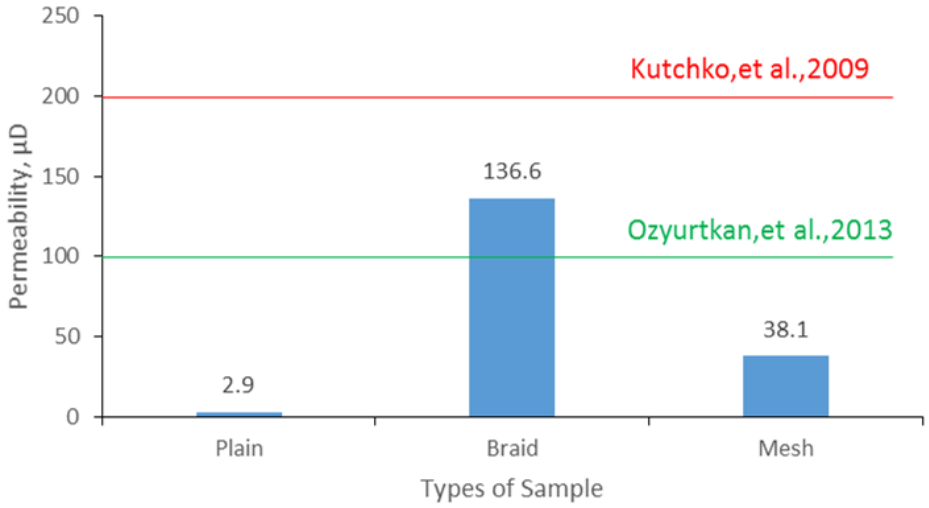

Figure 6.17 – Permeability results for cement samples with and without embedded fibers (protected by steel mesh or braid), with thresholds specified by previous investigations as indicated.

For a specific field case, the leak rate can be calculated to evaluate the effect of a fiber optic cable on the hydraulic properties of cement. According to Darcy's law, leakage

through bulk cement can be calculated using the following equation (Ford et al., 2017; Godoy et al., 2015):

$$Q = (\frac{kA}{\mu L})(\Delta P - \rho g L \cos\theta) \quad \text{Eq. 6.3}$$

where A represents the cross-section of the cement plug or the cemented annulus (m^2), k is the permeability of the cement (m^2), μ is the viscosity of the reservoir fluid (Pa.s), ΔP is the pressure difference between TOC and bottom of cement (Pa), ρ is the density of the reservoir fluid going through the cement (kg/m^3), L is the length of the plug or the annular cement (m), θ is the well inclination at the depth of the plug or annular cement (degrees), and Q is the flow rate (m^3/s). The pressure at TOC can be obtained by calculating the hydrostatic pressure of fluid column (drilling mud) above the cement. The pressure differential, ΔP, is expressed as the difference between the reservoir pressure and the hydrostatic pressure at TOC.

To ensure zonal isolation, most of the current standards require a minimum cement column length for annular spaces or, in case of abandonments, abandonment plugs. For example, API suggests a minimum length of 30 m (100 ft) for cement plugs used for wellbore isolation (API Bulletin E3, 1993). For the case of a 60 m long cemented annulus (Table 6.1), the potential leak rate was calculated using Eq. 6.3, and results are shown in

Table 6.2. By comparing the estimated values and assessing acceptable leakage rates, one can quantitatively evaluate the type of cable that can be used. Such an evaluation process also helps modification and improvement of the installation and design of the fiber optic cable to achieve a better hydraulic seal and bonding with the cement.

Table 6.1 – Information used to estimate gas leakage rate across a hypothetical cemented annulus of 60 m.

Parameters and unites	Values
20” casing ID (m)	0.48
13 3/8” casing OD (m)	0.34
Cross-section area of cement annulus (m^2)	0.090
TOC (m)	1600
Cement annulus length (m)	60
Well inclination (degrees)	0
Reservoir fluid density SG)	0.43
Reservoir pressure (MPa)	18
Reservoir fluid viscosity (μPa.s)	30
Mud density (SG.)	1.1

Table 6.2 – Estimation of leak rate for plain cement and cement with embedded mesh or braid cables.

Type	Permeability (μD)	Estimated leak rate (m^3/yr)
Plain Cement	2.9	0.00226
Cement with Braided Cable	136.6	0.106
Cement with Mesh Cable	38.1	0.0296

Chapter 7: Conclusion and Future Work

This chapter provides a summary of conclusions on this dissertation work and a future outlook. Section 7.1 includes a summary detailing the use of distributed fiber optic sensors for real-time *in situ* monitoring of cement annuli and zonal isolation in an oil and gas well, the laboratory experiments to demonstrate the concepts, as well as discussions based on the results of the experiments. Section 7.2 presents the recommended future work focusing on multiple aspects, such as preparing for actual field installations, optimization and improvement of the polymer-coated fiber optic sensing cable to withstand downhole challenging environments, and potential integration into other currently used fiber optic sensing techniques.

7.1 CONCLUSIONS

The primary focus of this research was development of a sophisticated system integrating: (1) distributed temperature sensing (DTS), (2) distributed strain sensing (DSS), and (3) distributed chemical sensing (DCS) to achieve real-time monitoring of cementing operation, zonal isolation and well integrity. DTS and DSS were achieved by using an advanced distributed temperature and strain sensing (DTSS) system, which offers the capability to separate temperature and strain measurement using one single-mode optical fiber with the hybrid Brillouin-Rayleigh technique. By using a specially designed fiber optic cable coated with a sensitive polymer, distributed chemical sensing capability is added to the DTSS system. Both the tested cables, each with a different type of polymer, were found to have selective sensitivity to hydrocarbons and well construction fluids at different strain levels. The cable is expected to be embedded in the cement annulus of an oil/gas well, either along the casing, within the cement sheath itself, or both. The

measurement of the system can be done *in situ*, continuously and in real-time, without the need for wellbore (re-)entry.

Multiple applications of the system were investigated and are summarized in Table 7.1. These include tracking the cement displacement process, detection of casing deformation, evaluation of cementing job quality, and monitoring the status of zonal isolation and barrier integrity. Zonal isolation / barrier integrity monitoring includes tracking fluid migration from different zones as well as detecting hydrocarbon leakage in cement annuli and across cement plugs used for well abandonments. The demonstration of the concepts and key findings for each application are summarized below.

To demonstrate the novel concept of ***cement displacement tracking***, multiple laboratory experiments were conducted. The proposed fiber optic sensing cables (the purple and black cables) were found to exhibit minor shrinkage in the presence of spacer fluid and are sensitive to synthetic oil and synthetic-based drilling mud, with measurable strains induced in the fiber. This first demonstrates that the proposed cable responds differently to various well construction fluids and thus can be used to track them during the cement displacement process. Two types of experiments were conducted to further illustrate this application. In the first experiment, the black cable was placed sequentially in SBM, spacer fluids, and cement slurry in the same order as these fluids would come in contact with the cable during an actual fluid displacement. Based on temperature and strain measurements, the system was capable of detecting the presence of these well construction fluids and distinguishing the types. In the second experiment, the cable was submerged in a sample box with three separate fluid sections (SBM, spacer fluid, or cement slurry) placed adjacent to each other. The location of each fluid along the length of the fiber was successfully identified. Moreover, the two experiments show that the system has the

capability to identify the top of cement, wait-on-cement time, and to evaluate the quality of cementing job.

The research also focuses on the ***monitoring of cementing hydration*** in order to evaluate the quality of cementing job using the DTSS system. Based on the temperature profiles obtained during cement hydration, the actual setting time and required wait-on-cement time can be determined in real-time and *in situ*. In addition, contamination of the cement slurry by drilling mud can also be detected and the displacement efficiency can be estimated. The system is capable of identifying and locating cemented and uncemented sections. This can be used in an actual field application to determine the top of cement and defects in cement annuli such as channels, cracks and voids. With spatial resolution on the order of centimeters (10^{-2} m), the system is able to detect very small defects in the cemented annuli.

Another application proposed in this research is to monitor the state of zonal isolation by the detection of fluid migration such as the ***unwanted migration of hydrocarbons in cemented annuli***. Extensive testing was conducted with kerosene as a model system for reservoir hydrocarbons using the specially designed fiber optic sensing cables. The changes in strain in the presence of kerosene was an order of magnitude larger than in the presence of synthetic based drilling mud. This shows a clear proof-of-concept for hydrocarbon detection. With the addition of an extra layer of steel braiding, acting both as a constraint and as protection for the optical fiber, the sensitivity and the rigidity of the cable can be increased. A demo cable design (a cable with steel braids) was developed for potential use in the field. The cable can not only detect the presence of hydrocarbons but can also monitor the duration of the hydrocarbon exposure. A correlation between the increase in strain from the exposure to kerosene and the exposure time was obtained. Such correlations can be used in reverse to estimate the exposure time based on the strain

changes in the actual field application. The system is also capable of locating any uncemented sections and/or channels in the cement annuli that are exposed to kerosene. In addition, the temperature measurement obtained from the DTSS system also enables the detection of fluid migration from another zone with a different temperature. For active wells or a new well under construction, it can also be applied for monitoring the state of zonal isolation to identify the invasion of any unwanted hydrocarbons or other fluids due to the presence of channels, cracks or voids in the cement annuli. For abandoned wells, the DTSS system can be used for long-term well abandonment monitoring and used as an early warning system to prevent cement barrier failure and associated hydrocarbon leakage.

The fiber optic sensing cable was found to survive exposure to well construction fluids such as SBM and spacer fluids, and shows "reversibility" (i.e. a return to the initial unexposed state) when exposure to hydrocarbons ceases. The cables were tested in other potential downhole fluids such as brine. Brine did not have any impact on the cables. This is important since there is a large chance for the proposed cable to be exposed to brine in the downhole environment and the cable is only expected to detect well construction fluids and hydrocarbons. This demonstrates that the proposed cables are able to avoid false alarms due to the presence of brine. It has also been shown that the cables are only slightly sensitive to mineral oil so that different types of coating polymers are required in order to detect the presence of oil-based drilling mud.

Moreover, the application of the DTSS system to monitor ***casing deformation*** based on strain measurements was demonstrated in multiple laboratory tests. The DTSS system was used to accurately measure the increase in strain as the applied load increased, which matched well with the calculated and theoretical values. The improved fiber optic cable design using a dual cable configuration allows strain induced by casing deformation and hydrocarbon leakage to be independently resolved by the measurement system. A steel

braid/mesh can be used to provide additional protection for the fiber optic cable in the challenging downhole environment. The system can provide lifetime monitoring of casing deformation caused by subsurface geomechanical changes due to reservoir compaction, surface subsidence, or significant downhole temperature and pressure changes.

The idea of ***cement-casing bond evaluation*** to assess the state of zonal isolation with the DTSS system was also proposed and demonstrated using laboratory tests in this research. Cement-embedded fiber optic sensors captured the increase in strain at the cement-casing interface when the casing (steel pipe) was subjected to increasing axial loads in the cement-casing bond test. A linear correlation between the shear stress of the cement bond and the strain measured on the optical fiber was obtained. It demonstrated the capability of using the strain measurement at the cement-casing interface to estimate the shear stress on the cement bond due to subsurface loads or downhole pressure variations. It also presents a method to analyze the likelihood of cement debonding that can result in a leak path, by comparing the observed strain and associated shear stress values to the pre-determined or known shear bond strength. With the distributed sensing technique, the location of debonding can be identified and the debonding can be evaluated at certain critical locations.

Table 7.1 – A table demonstrating the capabilities of the DTSS system for monitoring zonal isolation.

Application	Demonstrated Capabilities
Cement Displacement Tracking	• Track the location of each fluid during displacement • Identify the presence of each fluid, detect top of cement (TOC) • Evaluate the cement hydration process • Estimate the displacement efficiency
Cement Hydration Monitoring	• Determine the effect of the external temperature on setting time • Locate areas of cement slurry contaminated with SBM • Detect TOC as well as uncemented sections (voids)
Fluid Migration and Unwanted Hydrocarbons Detection	• Detect the presence of unwanted hydrocarbons due to compromised zonal isolation • Locate any uncemented sections and/or channels with the presence of unwanted hydrocarbons • Detect fluid migration from zones with a different temperature • Estimate the cable's exposure time to hydrocarbons by correlating the increase in strain to the exposure time
Casing Deformation Detection	• Detect casing deformation due to geomechanical changes • Differentiate the strain changes in the fiber due to deformation or due to the presence of hydrocarbons with the dual-cable design
Cement-casing Bond Evaluation	• Evaluate the state of the cement bond • Assess the risk of debonding in real-time and *in situ* • Detect the location of debonding • Identify loss of zonal isolation due to cement debonding

In addition to thoroughly researching the potential uses for the DTSS system for monitoring zonal isolation, the research also explored topics related to: 1) the effect of the embedded fiber optic cable on the permeability of cement; 2) the potential polymers for improving the sensing capabilities of the fiber optic cable; 3) fiber optic installation methods (straight axial and helical installation).

The effect of a fiber optic cable embedded in the cement was evaluated using a ***gas permeability*** test. Cement samples with or without embedded fiber optic cables that were protected by either a steel mesh or steel braid showed increases in permeability that were still within acceptable industry norms and acceptance criteria. In general, the presence of fiber optic cables is expected to have minimal effect on the hydraulic sealing integrity provided by the cement.

The study also focuses on potential modifications to the fiber optic sensing cable to better tailor the response time of the cable. Two key aspects that determine the response time are the ***selection of sensitive polymers*** for the cable and the ***packaging mechanism*** to efficiently introduce strain on the cable in presence of well construction fluids. Five different elastomers were tested with kerosene, SBM and spacer fluids to study their sensitivity, each with different response time and magnitude.

To study the fiber optic installation methods, the straight axial installation was tested in the cantilever beam test while the helical installation was tested in the polyurethane rod test. The helical wrapping installation technique was also tested and evaluated in order to increase the sensing area, providing a 360-degree ‘image’ of the cement annulus or the casing, allowing more information to be gathered to evaluate cement and casing integrity compared to a straight axial optical fiber installation.

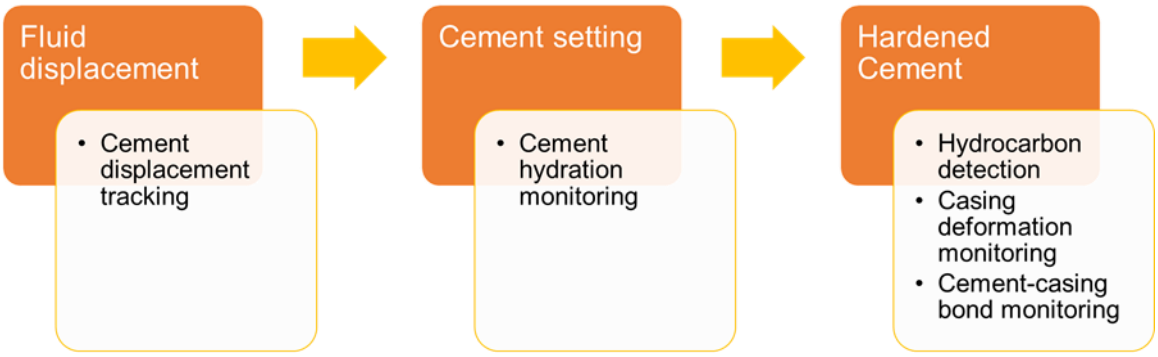

Figure 7.1 – Life-time monitoring of the cement and casing integrity and zonal isolation.

7.2 Future Work

The laboratory demonstrations described here prove the concept and capability of the proposed system for cement displacement during the well construction stage, cement integrity and zonal isolation in hardened cement, and leakage detection of the cement annuli and plugs even after well abandonment. However, the proposed fiber optic sensing system requires further improvement and optimization before being employed in field applications. Future studies will need to focus on its maturation and preparations for field tests, including the aspects given in the following.

The proposed fiber optic sensing cable requires modification and improvement to withstand the downhole challenging environment under high temperature and pressure conditions, while at the meantime maintaining its sensing capability. In this dissertation, several types of sensitive polymers were tested. More types of sensitive polymer can be tested for their sensitivity to downhole fluids as well as their durability in a downhole pressure, temperature and chemical environment. Selective sensitivity of these polymers can be used to tailor the fiber optic sensing cables for sensing different hydrocarbons and well construction fluids, allowing direct hydrocarbon fingerprinting and determination of

the origin of the hydrocarbons behind pipe. The sensitive polymer used in this dissertation showed minimal sensitivity to aqueous fluids such as brine. The exploration of sensitive polymers for aqueous fluids can be conducted to extend the application for detection of brine or water-based drilling mud. The design of the fiber optic sensing cable for chemical sensing can be further improved by investigating different packaging options. The proposed design using steel braids or meshes presents a prototype to reinforce the cable while still allowing the exposure of the sensitive polymer to the environment for detection. The robustness of such a design should be further evaluated and additional reinforcement may be warranted.

In addition, this dissertation compared the straight axial installation and helical installation methods. Other options, such as straight axial installation of multiple fiber optic cable, can be further explored to evaluate their capabilities and limitations. The challenges of actual field installation using these methods should be investigated. The deployment of the proposed fiber optic temperature, strain and chemical sensing system can be extended to temporary methods using wireline and coiled tubing to add flexibility of the proposed system for existing wells.

An added advantage of the DTSS system used in this dissertation is that the very same system can be used for temperature and strain sensing for other well monitoring purposes such as hydrocarbon production monitoring. The proposed fiber optic sensing cables embedded in the cement can be further developed for other downhole purposes (such as DAS and DTS) to maximize its capabilities, and thus reduce the cost for overall downhole sensing with distributed fiber optic sensors. More studies can also focus on modification of the proposed sensing cable to be used with the existing DTS and DAS systems for cement integrity and zonal isolation monitoring.

Appendix

HANDLING FIBER OPTIC SENSING CABLE

In many cases, connections are required for the optical fibers. For example, to simplified the connection to the detection unite (or measurement device), patch cables with connectors that can directly plug into the device as shown in Figure A.1a are usually spliced to fiber optic sensing cable. The male connectors of the patch cable can be cleaned by the CLETOP tape as shown in Figure A.1b and the female connectors on the detection unite can be cleaned with the One-Click cleaner. The fusion splicer as shown in Figure A.2a is often used to connect optical fibers. It generates an electric arc for fusing or welding two fibers together. To prepare the optical fibers for connection, the fiber stripping tool as shown in Figure A.2b was used to remove outer jacket, coatings and cladding, leaving the bare glass core for splicing. The glass cores are cut by the cleaver to achieve the smooth end faces. The cleaning supplies such as the fiber optic cleaning solution (or ethanol) and the Kimwipes as shown in Figure A.1c are used to clean the fiber to avoid any dirt or dusts on the end faces. Both ends of the two optical fibers are placed into the fusion splicer and carefully aligned to avoid significant light loss at the splicing point. After splicing, the splicing sleeve (see Figure A.2b) is moved to cover the splicing point and the bare fiber. The splicing sleeve is heat shrink tube with a steel bar to provide reinforcement at the splicing point for the glass core.

Figure A.1 – (a) The cleaning supplies to remove any dirt or dusts on the fiber end faces; (b) patch cables used to connect the fiber optic sensing cable to the detection unite; (c) a CLETOP tape to clean the male connectors on the patch cables, a One-Click cleaner to clean the female connectors on the detection unite, and a laser pen to check any broken points of the optical fiber (in the orders from left to right).

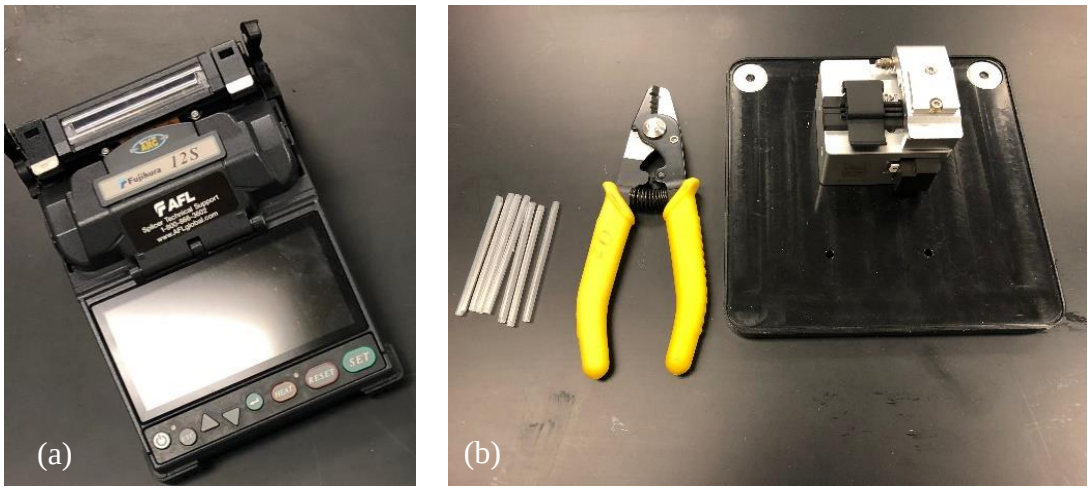

Figure A.2 – (a) A splicing sleeves for protection and reinforcement of connection point (in the orders from left to right), a fiber stripping tool to remove the jacket and cladding on the glass core, a cleaver to cut the smooth end fact for splicing; (b) A fusion splice used to splice two optical fiber together.

The handling procedures to connect the fiber optic cable to the detection unite are summarized as a list as following:

1) Remove outer jacket, coatings, and cladding of the fiber optic sensing cable and the patch cable using the fiber stripping tool
2) Put the splicing sleeve on one optical fiber
3) Cut the end faces of both fiber gas cores using the cleaver
4) Clean the end faces of both optical fibers using the fiber optic cleaning solution or ethanol and the Kimwipes
5) Place each end of the optical fibers in the fusion splicer to align them accurately and then start the splicing and wait for the fusion splicer to complete
6) Place the splicing sleeve carefully on the location where two optical fibers are spliced and then apply heat to shrink the sleeve using the heater of the splicer
7) Connect the patch cable to the laser pen to ensure good connection and no broken points of the optical fibers
8) Clean the male connectors of the patch cable using the CLETOP tape and clean the female connectors of the detection unite with the One-Click cleaner
9) Connect the patch cable to the detection unit

List of Abbreviations

DAS – Distributed Acoustic Sensing

DCS – Distributed Chemical Sensing

DFOS – Distributed fiber optic sensing

DSS – Distributed Strain Sensing

DTS – Distributed Temperature Sensing

DTSS – Distributed temperature and strain sensing

FBG – Fiber Bragg Grating

FO – Fiber optic

LOP – Limits of Pumpability

PPP-BOTDA – Pulse-Pre-Pump Brillouin Optical Time-Domain Analysis

SBM – Synthetic-based Mud

TOC – Top of Cement

TW-COTDR – Tunable Wavelength Coherent Optical Time Domain Reflectometry

WOC – Waiting-on-Cement

List of Key Symbols

C_{11} – Strain coefficient for Brillouin scattering

C_{12} – Temperature coefficient for Brillouin scattering

C_{21} – Strain coefficient for Rayleigh scattering

C_{22} – Temperature coefficient for Rayleigh scattering

E – Modulus of elasticity

I – Moment of inertia

M – Moment

Q – Flow rate

ε_a – Axial strain

ε_f – Strain measured on the optical fiber

ε – Strain

θ – Helical wrapping angle

με – Microstrain

ν – Poison ratio

τ – Shear stress

k – Permeability

μ – Fluid viscosity

List of Publications

1. Wu, Q., Nair, S.D., Shuck, M., et al., 2016a. Advanced Fiber Optic Sensors for Monitoring Poor Zonal Isolation with Hydrocarbon Migration in Cemented Annuli, in: SPE-180329. Presented at the SPE Deepwater Drilling & Completions Conference, Galveston, TX. doi:10.2118/180329-MS
2. Wu, Q., Nair, S.D., Shuck, M., et al., 2016b. Advanced Distributed Fiber Optic Sensors to Monitor Cement Hydration and Detect Annular Hydrocarbon Migration for Enhanced Zonal Isolation, in: SPE-181429. Presented at the SPE Annual Technical Conference and Exhibition, Dubai, UAE. doi:10.2118/181429-MS
3. Wu, Q., Dininger, M., Nair, S., et al., 2017a. Real Time Cement Displacement Tracking using Distributed Fiber Optic Sensors, in: SPE-187409. Presented at the SPE Annual Technical Conference and Exhibition, Society of Petroleum Engineers, San Antonio, Texas, USA. doi:10.2118/187409-MS
4. Wu, Q., Nair, S., Shuck, M., et al., 2017b. Advanced distributed fiber optic sensors for monitoring real-time cementing operations and long term zonal isolation. J. Pet. Sci. Eng. 158, 479–493. doi:10.1016/j.petrol.2017.08.072
5. Wu, Q., Nair, S.D., van Oort, E., et al., 2019a. Concurrent Real-time Distributed Fiber Optic Sensing of Casing Deformation and Cement Integrity Loss, in: SPE-194159. Presented at the SPE/IADC Drilling Conference and Exhibition, Society of Petroleum Engineers, The Hague, The Netherlands.
6. Wu, Q., Nair, S.D., van Oort, E., et al., 2019b. Behavior and Properties of Cement-Embedded Fiber Optic Sensors for Zonal Isolation Monitoring, in: IPTC-19380. Presented at the International Petroleum Technology Conference, Society of Petroleum Engineers, Beijing, China.

Bibliography

Al Hammad, M.A., Altameimi, Y.M., 2002. Cement Matrix Evaluation, in: SPE-77213. Presented at the IADC/SPE Asia Pacific Drilling Technology, Society of Petroleum Engineers, Jakarta, Indonesia. doi:10.2118/77213-MS

Alahbabi, M.N., Cho, Y.T., Newson, T.P., 2005. Simultaneous temperature and strain measurement with combined spontaneous Raman and Brillouin scattering. Opt. Lett. 30, 1276. https://doi.org/10.1364/OL.30.001276.

API BULLETIN E3, 1993. Environmental Guidance Document: Well Abandonment and Inactive Well Practices for U.S. Exploration and Production Operations.

API RP 10B-2, 2013. Recommended Practice for Testing Well Cements.

API RP 40, 1998. Recommended Practices for Core Analysis.

API-10A, 2011. Specification for Cements and Materials for Well Cementing.

ASTM D3699-13be1, 2013. Standard Specification for Kerosene. ASTM International, West Conshohocken, PA. doi:10.1520/D3699-13BE01.

ASTM-C191, 2013. Standard Test Methods for Time of Setting of Hydraulic Cement by Vicat Needle. ASTM International, West Conshohocken, PA. doi:10.1520/C0191.

Aughenbaugh, K., Nair, S.D., Cowan, K., et al., 2014. Contamination of Deepwater Well Cementations by Synthetic-Based Drilling Fluids, in: SPE-170325. Presented at the SPE Deepwater Drilling and Completions Conference, Society of Petroleum Engineers, Galveston, TX. doi:10.2118/170325-MS

Bachu, S., Bennion, D.B., 2009. Experimental assessment of brine and/or CO2 leakage through well cements at reservoir conditions. Int. J. Greenh. Gas Control 4, 494–501. doi:10.1016/j.ijggc.2008.11.002

Baldwin, C.S., 2014. Brief History of Fiber Optic Sensing in the Oil Field Industry, in: SPIE-9098. Presented at the Fiber Optic Sensors and Applications XI, Baltimore, Maryland. doi:10.1117/12.2050550

Bao, X., Chen, L., 2012. Recent Progress in Distributed Fiber Optics. Sensors 12, 8601–8639. doi:10.3390/s120708601.

Bao, X., Webb, D.J., Jackson, D.A., 1994. Combined distributed temperature and strain sensor based on Brillouin loss in an optical fiber. Opt. Lett. 19, 141–143. doi:10.1364/OL.19.000141

Batcheller, G.W., 2013. Cement Evaluation Challenges in Horizontal Wells-Guidelines for Providing Meaningful Data, in: SPE-164513. Presented at the SPE Production

and Operations Symposium, Oklahoma City, Oklahoma. doi:10.2118/164513-MS.

Bentz D.P., Ferraris C.F., Rheology and setting of high volume fly ash mixtures, Cem. Concr. Compos, 32, 2010, 265-270, doi:10.1016/j.cemconcomp.2010.01.008

Bittleston, S., Guillot, D., 1991. Mud removal: research improves traditional cementing guidelines. Oilfield Rev. 3, 44–54.

Boone, K., Ridge, A., Crickmore, R., et al., 2014. Detecting Leaks in Abandoned Gas Wells with Fibre-Optic Distributed Acoustic Sensing. International Petroleum Technology Conference. doi:10.2523/17530-MS

Bostick, F.X.I., 2003. Commercialization of Fiber Optic Sensors for Reservoir Monitoring. Presented at the Offshore Technology Conference, Offshore Technology Conference, Houston, Texas. doi:10.4043/15320-MS

Bouasker, M., Mounanga, P., Turcry, P., Loukili, A., Khelidj, A., 2008. Chemical Shrinkage of Cement Pastes and Mortars at Very Early Age: Effect of Limestone Filler and Granular Inclusions. Cem. Concr. Compos. 30, 13–22. doi:10.1016/j.cemconcomp.2007.06.004.

Boukhelifa, L., Moroni, N., James, S.G., et al., 2004. Evaluation of Cement Systems for Oil and Gas Well Zonal Isolation in a Full-Scale Annular Geometry. Presented at the IADC/SPE Drilling Conference, Society of Petroleum Engineers. doi:10.2118/87195-MS

Brown, G., Carvalho, V., Wray, A., et al., 2004. Monitoring Alternating CO2 and Water Injection and Its Effect on Production in a Carbonate Reservoir Using Permanent Fiber-Optic Distributed Temperature Systems, in: SPE-90248-MS. Presented at the SPE Annual Technical Conference and Exhibition, Society of Petroleum Engineers, SPE, p. 7. doi:10.2118/90248-MS

Brown, G.A., Pinzon, I.D., Davies, J.E., et al., 2007. Monitoring Production from Gravel-Packed Sand-Screen Completions on BP's Azeri Field Wells Using Permanently Installed Distributed Temperature Sensors, in: SPE-110064-MS. Presented at the SPE Annual Technical Conference and Exhibition, Society of Petroleum Engineers, SPE, p. 16. doi:10.2118/110064-MS

Bruno, M.S., 2001. Geomechanical Analysis and Decision Analysis for Mitigating Compaction Related Casing Damage. Presented at the SPE Annual Technical Conference and Exhibition, Society of Petroleum Engineers. doi:10.2118/71695-MS

Buerck, J.M., Vogel, B.H., Roth, S., et al., 2004. Distributed Fiber Optical HC Leakage and pH Sensing Techniques for Implementation into Smart Structures, in: SPIE-5384. Presented at the Smart Structures and Materials 2004: Smart Sensor Technology and Measurement Systems, San Diego, CA. doi:10.1117/12.538240

Bullard, J.W., Jennings, H.M., Livingston, R.A., Nonat, A., Scherer, G.W., Schweitzer, J.S., Scrivener, K.L., Thomas, J.J., 2011. Mechanisms of cement hydration. Cem. Concr. Res. 41, 1208–1223. doi:10.1016/j.cemconres.2010.09.011.

Carpenter, C., 2016. Distributed Acoustic Sensing for Downhole Production and Injection Profiling. J. Pet. Technol. 68, 78–79. doi:10.2118/0316-0078-JPT

Carrillo, A., Gonzalez, E., Rosas, A., et al., 2002. New Distributed Optical Sensor for Detection and Localization of Liquid Leaks: Part I. Experimental Studies. Sens. Actuators Phys. 99, 229–235. doi:10.1016/S0924-4247(02)00002-X

Carter, K.M., van Oort, E., Barendrecht, A., 2014. Improved Regulatory Oversight using Real-Time Data Monitoring Technologies in the Wake of Macondo, in: SPE-170323. Presented at the SPE Deepwater Drilling and Completions Conference, Galveston, TX. doi:10.2118/170323-MS

Cernocky, E.P., Scholibo, F.C., 1995. Approach to Casing Design for Service in Compacting Reservoirs. Presented at the SPE Annual Technical Conference and Exhibition, Society of Petroleum Engineers. doi:10.2118/30522-MS

Chen, Z., Chaudhary, S., Shine, J., 2014. Intermixing of Cementing Fluids: Understanding Mud Displacement and Cement Placement. Presented at the IADC/SPE Drilling Conference and Exhibition, Society of Petroleum Engineers. doi:10.2118/167922-MS

Childers, B.A., Rambow, F.H.K., Dria, D.E., et al., 2007. Downhole fiber optic real-time casing monitor, in: SPIE 6527. Presented at the Industrial and Commercial Applications of Smart Structures Technologies. doi:10.1117/12.715289

Clanton, R.W., Haney, J.A., Pruett, R., et al., 2006. Real-Time Monitoring of Acid Stimulation Utilizing a Fiber-Optic DTS System, in: SPE-100617-MS. Presented at the SPE Western Regional/AAPG Pacific Section/GSA Cordilleran Section Joint Meeting, Society of Petroleum Engineers, SPE, p. 10. doi:10.2118/100617-MS

Crisp, J., 2005. Int • Delepine-Lesoille, S., Guzik, A., Bertrand, J., et al., 2013. Validation of TW-COTDR Method for 25km Distributed Optical Fiber Sensing, in: SPIE-8794. Presented at the Fifth European Workshop on Optical Fibre Sensors, Krakow, Poland. doi:10.1117/12.2025802

Cunningham, E.B., 2000. Applications for RAB Large Borehole Caliper in Deepwater Cementing. Presented at the Offshore Technology Conference, Offshore Technology Conference. doi:10.4043/11883-MS

Degenhardt, R., 2011. EPA Investigates Fracking Impacts. EHS J. URL http://ehsjournal.org/http:/ehsjournal.org/rachel-degenhardt/epa-investigates-fracking-impacts-hydraulic-fracturing/2011.

Denney, D., 2012. Distributed Acoustic Sensing for Hydraulic- Fracturing Monitoring and Diagnostics. J. Pet. Technol. 64, 68–74. doi:10.2118/0312-0068-JPT

Diarra, R., Carrasquilla, J., Gonzalez, Y., et al., 2014. Cement Evaluation Using Slickline Distributed Temperature Measurements, in: AADE-14-FTCE-41. Presented at the AADE Fluids Technical Conference and Exhibition, American Association of Drilling Engineers, Houston, TX.

Earles, D.M., Gill, C.C., Stoesz, C.W., et al., 2011. Fiber Optic Installation at the Sand Face Enables Real-Time Flow Monitoring and Compaction mitigation in Openhole Applications. Presented at the OTC Brasil, Offshore Technology Conference, Rio de Janeiro, Brazi. doi:10.4043/22681-MS

Earles, D.M., Stoesz, C.W., Surveyor, N.D., et al., 2011. Fiber Optic Strain Sensing at the Sand Face Enables Real-Time Flow Monitoring and Compaction Mitigation in Openhole Applications. Presented at the SPE Annual Technical Conference and Exhibition, Society of Petroleum Engineers. doi:10.2118/147439-MS

Enayatpour, S., van Oort, E., 2017. Advanced Modeling of Cement Displacement Complexities. Presented at the SPE/IADC Drilling Conference and Exhibition, Society of Petroleum Engineers. doi:10.2118/184702-MS

Evans, G.W., Carter, L.G., 1962. Bounding Studies of Cementing Compositions to Pipe and Formations. Presented at the Drilling and Production Practice, American Petroleum Institute.

Fang, Z., Chin, K., Qu, R., et al., 2012. Fundamentals of Optical Fiber Sensors. Wiley.roduction to Fiber Optics. Elsevier.

Ford, E.P., Moeinikia, F., Lohne, H.P., et al., 2017. Leakage Calculator for Plugged and Abandoned Wells. Presented at the SPE Bergen One Day Seminar, Society of Petroleum Engineers. doi:10.2118/185890-MS

Fredrich, J.T., Arguello, J.G., Deitrick, G.L., et al., 2000. Geomechanical Modeling of Reservoir Compaction, Surface Subsidence, and Casing Damage at the Belridge Diatomite Field. SPE Reserv. Eval. Eng. 3, 348–359. doi:10.2118/65354-PA

Fredrick, J.T., Deitrick, G.L., Arguello, J.G., et al., 1998. Reservoir Compaction, Surface Subsidence, and Casing Damage: A Geomechanics Approach to Mitigation and Reservoir Management. Presented at the SPE/ISRM Rock Mechanics in Petroleum Engineering, Society of Petroleum Engineers. doi:10.2118/47284-MS

Froggatt, M., Moore, J., 1998. High-spatial-resolution Distributed Strain Measurement in Optical Fiber with Rayleigh Scatter. Appl. Opt. 37, 1735–1740. doi:10.1364/AO.37.001735.

Fryer, V.I., Dong, S., Otsubo, Y., et al., 2005. Monitoring of Real-Time Temperature Profiles Across Multizone Reservoirs during Production and Shut in Periods Using Permanent Fiber-Optic Distributed Temperature Systems, in: SPE-92962-

MS. Presented at the SPE Asia Pacific Oil and Gas Conference and Exhibition, Society of Petroleum Engineers, SPE, p. 6. doi:10.2118/92962-MS

Godoy, R., Fontan, M., Capra, B., et al., 2015. Well Integrity Support by Extended Cement Evaluation - Numerical Modeling of Primary Cement Jobs. Presented at the Abu Dhabi International Petroleum Exhibition and Conference, Society of Petroleum Engineers. doi:10.2118/177612-MS

Goode, J.M., 1962. Gas and Water Permeability Data for Some Common Oilwell Cements. J. Pet. Technol. 14, 851–854. doi:10.2118/288-PA

Hartog, A.H., 2017. An Introduction to Distributed Optical Fibre Sensors. CRC Press.

Hodne, H., Saasen, A., O'Hagan, A.B., Wick, S.O., 2000. Effects of time and shear energy on the rheological behaviour of oilwell cement slurries. Cem. Concr. Res. 30, 1759–1766. doi:10.1016/S0008-8846(00)00416-6.

Horiguchi, T., Kurashima, T., Koyamada, Y., 1994. 1 m Spatial Resolution Measurement of Distributed Brillouin Frequency Shift in Single-mode Fibers. Presented at the Symposium on Optical Fiber Measurements, NIST, Boulder, Colorado, pp. 73–76.

Horiguchi, T., Kurashima, T., Tateda, M., 1989a. Tensile strain dependence of Brillouin frequency shift in silica optical fibers. IEEE Photonics Technology Letters 1, 107-108. doi:10.1109/68.34756

Horiguchi, T., Tateda, M., 1989b. BOTDA-Nondestructive Measurement of Single-mode Optical Fiber Attenuation Characteristics using Brillouin Interaction: Theory. J. Light. Technol. 7, 1170–1176. doi:10.1109/50.32378.

Huckabee, P.T., 2009. Optic Fiber Distributed Temperature for Fracture Stimulation Diagnostics and Well Performance Evaluation, in: SPE-118831-MS. Presented at the SPE Hydraulic Fracturing Technology Conference, Society of Petroleum Engineers, SPE, p. 21. doi:10.2118/118831-MS

Huerta, N.J., Checkai, D., Bryant, S.L., 2009. Utilizing Sustained Casing Pressure Analog to Provide Parameters to Study CO2 Leakage Rates Along a Wellbore. Presented at the SPE International Conference on CO2 Capture, Storage, and Utilization, Society of Petroleum Engineers. doi:10.2118/126700-MS

In 't Panhuis, P., den Boer, H., Van Der Horst, J., et al., 2014. Flow Monitoring and Production Profiling using DAS, in: SPE-170917. Presented at the SPE Annual Technical Conference and Exhibition, Society of Petroleum Engineers. doi:10.2118/170917-MS

Jadhav, R., Palla, V.G.R., Datta, A., et al., 2017. Effect of Casing Coating Materials on Shear-Bond Strength. Presented at the SPE/IATMI Asia Pacific Oil & Gas Conference and Exhibition, Society of Petroleum Engineers. doi:10.2118/186441-MS

Johannessen, K., Drakeley, B.K., Farhadiroushan, M., 2012. Distributed Acoustic Sensing - A New Way of Listening to Your Well/Reservoir, in: SPE-149602-MS. Presented at the SPE Intelligent Energy International, Society of Petroleum Engineers, SPE, p. 9. doi:10.2118/149602-MS

Jones, R.R., 1986. A Novel Economical Approach for Accurate Real-Time Measurement of Wellbore Temperatures. Presented at the SPE Annual Technical Conference and Exhibition, Society of Petroleum Engineers. doi:10.2118/15577-MS.

Juarez, J.C., Maier, E.W., Choi, K.N., et al., 2005. Distributed fiber-optic intrusion sensor system. J. Light. Technol. 23, 2081–2087.

Julian, J.Y., 2007. Downhole Leak Determination Using Fiber-Optic Distributed-Temperature Surveys at Prudhoe Bay, Alaska, in: SPE-107070-MS. Presented at the SPE Annual Technical Conference and Exhibition, Society of Petroleum Engineers, SPE, p. 17. doi:10.2118/107070-MS

Jutten, J.J., Hayman, A.J., 1993. Microannulus Effect on Cementation Logs: Experiments and Case Histories, in: SPE-25377. Presented at the SPE Asia Pacific Oil and Gas Conference, Society of Petroleum Engineers, Singapore. doi:10.2118/25377-MS.

Kamal, S.Z., 2014. Fiber Optic Sensing: Evolution to Value, in: SPE-167907. Presented at the SPE Intelligent Energy Conference & Exhibition, Society of Petroleum Engineers, Utrecht, The Netherlands. doi:10.2118/167907-MS.

Kersey, A.D., Dandridge, A., 1990. Applications of fiber-optic sensors. IEEE Trans. Compon. Hybrids Manuf. Technol. 13, 137–143. doi:10.1109/33.52861

Khalifeh, M., Hodne, H., Saasen, A., et al., 2018. Bond Strength Between Different Casing Materials and Cement. Presented at the SPE Norway One Day Seminar, Society of Petroleum Engineers. doi:10.2118/191322-MS

Kishida, K., Li, C.-H., Nishiguchi, K., 2005. Pulse pre-pump method for cm-order spatial resolution of BOTDA, in: SPIE 5855. Presented at the 17th International Conference on Optical Fibre Sensors, 559–562 doi:10.1117/12.624259

Kishida, K., Li, C.H., Nishiguchi, K., et al., 2012. Hybrid Brillouin-Rayleigh Distributed Sensing System, in: SPIE 8421. Presented at the 22nd International Conference on Optical Fiber Sensors, Beijing, China. doi:10.1117/12.975668

Kishida, K., Yamauchi, Y., Guzik, A., 2014. Study of Optical Fibers Strain-Temperature Sensitivities Using Hybrid Brillouin-Rayleigh System. Photonic Sens. 4, 1–11. doi:10.1007/s13320-013-0136-1.

Koelman, J.V.V., Lopez, J.L., Potters, H., 2012. Optical Fibers: The Neurons For Future Intelligent Wells, in: SPE-150203. Presented at the SPE Intelligent Energy International, Society of Petroleum Engineers. doi:10.2118/150203-MS

Kolchanov, P., Perroni, D., Medvedev, A., et al., 2018. Effective Zonal Isolation in Horizontal Wells: Mitigating Negative Impact of Mud Channels. Presented at the

SPE Annual Technical Conference and Exhibition, Society of Petroleum Engineers. doi:10.2118/191561-MS

Krietsch, H., Gischig, V., Jalali, M.R., et al., 2018. A Comparison of FBG- and Brillouin-Strain Sensing in the Framework of a Decameter-Scale Hydraulic Stimulation Experiment. Presented at the 52nd U.S. Rock Mechanics/Geomechanics Symposium, American Rock Mechanics Association.

Kurashima, T., Horiguchi, T., Tateda, M., Thermal effects on the Brillouin frequency shift in jacketed optical silica fibers. Applied Optics 29, 1990, 2219-2222 doi:10.1364/AO.29.002219

Kutchko, B.G., Strazisar, B.R., Huerta, N., et al., 2009. CO2 Reaction with Hydrated Class H Well Cement under Geologic Sequestration Conditions: Effects of Flyash Admixtures. doi:10.1021/es803007e.

Kwon, I.-B., Kim, C.-Y., Cho, S.-B., Lee, J.-J., 2003. Temperature Compensation of a Strain Sensing Signal from a Fiber Optic Brillouin Optical Time Domain Analysis Sensor. J. Opt. Soc. Korea 7, 106–112.

Lavrov, A., Torsæter, M., 2016. Physics and Mechanics of Primary Well Cementing, SpringerBriefs in Petroleum Geoscience & Engineering. Springer International Publishing.

Lee, C.C., Chiang, P.W., Chi, S., 2001. Utilization of a dispersion-shifted fiber for simultaneous measurement of distributed strain and temperature through Brillouin frequency shift. IEEE Photonics Technol. Lett. 13, 1094–1096. doi:10.1109/68.950746.

Lee, W.T., Dorge, W.D., 1983. Cementing-Simultaneous Rotation-Reciprocating Technique (ROTO-TEK System), in: SPE-11419. Presented at the IADC/SPE Drilling Conference, New Orleans, Louisiana. doi:10.2118/11419-MS.

Le-Minous, J.C., Mutti, D., Bouvet, A., et al., 2017. Permeability Study of API Class G and B Cements Considering Seawater and WBM Contamination. Presented at the SPE/IADC Drilling Conference and Exhibition, Society of Petroleum Engineers. doi:10.2118/184613-MS

Li, X., Parker, T., Farhadiroushan, M., et al., 2004. Evaluating a Concept of Using Distributed Optical Fiber Temperature and Strain Sensor for Continuous Monitoring of Casing and Completion Mechanical Deformation in Intelligent Wells, in: OTC-16285. Presented at the Offshore Technology Conference, Offshore Technology Conference, Houston, Texas. doi:10.4043/16285-MS

Liehr, S., Münzenberger, S., Krebber, K., 2018. Wavelength-scanning coherent OTDR for dynamic high strain resolution sensing. Opt. Express 26, 10573–10588. doi:10.1364/OE.26.010573

Liu, X., Ramos, M.J., Nair, S.D., et al., 2017. True Self-Healing Geopolymer Cements for Improved Zonal Isolation and Well Abandonment. Presented at the SPE/IADC Drilling Conference and Exhibition, Society of Petroleum Engineers. doi:10.2118/184675-MS

Lockyear, C.F., Ryan, D.F., Gunningham, M.M., 1990. Cement Channeling: How To Predict and Prevent. SPE Drill. Eng. 5, 201–208. doi:10.2118/19865-PA.

López, R.M., Spirin, V.V., Miridonov, S.V., et al., 2002. Fiber Optic Distributed Sensor for Hydrocarbon Leak Localization Based on Transmission/Reflection Measurement. Opt. Laser Technol. 34, 465–469. doi:10.1016/S0030-3992(02)00043-9

MacLean, A., Moran, C., Johnstone, W., et al., 2003. Detection of Hydrocarbon Fuel Spills using a Distributed Fibre Optic Sensor. Sens. Actuators Phys. 109, 60–67. doi:10.1016/j.sna.2003.09.007

MacPhail, W.F.P., Lisoway, B., Banks, K., 2012. Fiber Optic Distributed Acoustic Sensing of Multiple Fractures in a Horizontal Well, in: SPE-152422-MS. Presented at the SPE Hydraulic Fracturing Technology Conference, Society of Petroleum Engineers, SPE, p. 18. doi:10.2118/152422-MS

Malekzadeh, M., Gul, M., Kwon, I.-B., et al., 2014. An integrated approach for structural health monitoring using an in-house built fiber optic system and non-parametric data analysis. Smart Structures and Systems 14, 917–942. doi:10.12989/sss.2014.14.5.917

Mateeva, A., Mestayer, J., Cox, B., et al., 2012. Advances in Distributed Acoustic Sensing (DAS) for VSP. Presented at the 2012 SEG Annual Meeting, Society of Exploration Geophysicists.

Mathur, K.S., 2018. Fundamentals of Fiber Optics Communications. Zorba Books.

McLean, R.H., Manry, C.W., Whitaker, W.W., 1967. Displacement Mechanics in Primary Cementing. J. Pet. Technol. 19, 251–260. doi:10.2118/1488-PA.

Miah, K., Potter, D.K., 2017. A Review of Hybrid Fiber-Optic Distributed Simultaneous Vibration and Temperature Sensing Technology and Its Geophysical Applications. Sensors 17. doi:10.3390/s17112511

Miranda, C.R., Carvalho, K.T., Vargas, A.A., et al., 2007. Minimizing Fluid Contamination During Oilwell Cementing Operations. Presented at the Offshore Mediterranean Conference and Exhibition, Offshore Mediterranean Conference.

Mishra, A., Al Gabani, S.H., Jumaa Al Hosany, A., 2017. Pipeline Leakage Detection Using Fiber Optics Distributed Temperature Sensing DTS, in: SPE-18840. Presented at the Abu Dhabi International Petroleum Exhibition & Conference, Society of Petroleum Engineers, Abu Dhabi, UAE. doi:10.2118/188407-MS

Mizuno, Y., Hayashi, N., Tanaka, H., et al., 2015. Brillouin scattering in multi-core optical fibers for sensing applications. Sci. Rep. 5, 11388. doi:10.1038/srep11388

Molenaar, M., Fidan, E., Hill, D., 2012. Real-Time Downhole Monitoring Of Hydraulic Fracturing Treatments Using Fibre Optic Distributed Temperature And Acoustic Sensing, in: SPE-152981. Presented at the SPE/EAGE European Unconventional Resources Conference and Exhibition, Society of Petroleum Engineers, Vienna, Austria. doi:10.2118/152981-MS

Molenaar, M.M., Hill, D., Webster, P., et al., 2012. First Downhole Application of Distributed Acoustic Sensing for Hydraulic-Fracturing Monitoring and Diagnostics. SPE Drill. Complet. 27, 32–38. doi:10.2118/140561-PA

Morikawa, S., Camerini, C.S., Braga, A.M.B., et al., 2010. Real time continuous structural integrity monitoring of flexible risers with optical fiber sensors. Presented at the Offshore Technology Conference, Offshore Technology Conference, Houston, Texas, USA. doi:10.4043/20863-MS

Moroni, N., Ravi, K., Hemphill, T., et al., 2009. Pipe Rotation Improves Hole Cleaning and Cement-Slurry Placement: Mathematical Modeling and Field Validation. Presented at the Offshore Europe, Society of Petroleum Engineers. doi:10.2118/124726-MS

Mueller, D.T., 2012. Deepwater Cementing Standards: Applicability and Regulatory Impact of Best Practices, in: OTC-23664. Presented at the SPE Offshore Technology Conference, Houston, TX. doi:10.4043/23664-MS

Mullens, S., Lees, G., Duvivier, G., 2010. Fiber-Optic Distributed Vibration Sensing Provides Technique for Detecting Sand Production, in: OTC-20429-MS. Presented at the Offshore Technology Conference, Offshore Technology Conference, OTC, p. 11. doi:10.4043/20429-MS

Nair, S.D., Wu, Q., Cowan, M., van Oort, E., 2015. Cement Displacement and Pressure Control Using Magneto-Rheological Fluids, in: SPE-173124. Presented at the SPE/IADC Drilling Conference and Exhibition, London, UK. doi:10.2118/173124-MS.

Nelson, E.B., Guillot, D., 2006. Well Cementing. Schlumberger.

Neubrex Co., Ltd., 2007. FutureNeuro - Strain Sensing (surface and embeddding installation). URL http://www.neubrex.com/htm/products/pro-fiber_7.htm.

Nie, X., Yang, Y., Cui, Y., et al., 2018. Long-Term Monitoring System of Submarine Pipeline Vibration Based on Fiber Grating Sensor Technology. Presented at the The 28th International Ocean and Polar Engineering Conference, International Society of Offshore and Polar Engineers.

Ozyurtkan, M.H., Altun, G., Mihcakan, I.M., et al., 2013. An Experimental Study on Mitigation of Oil Well Cement Gas Permeability. Presented at the International

Petroleum Technology Conference, International Petroleum Technology Conference. doi:10.2523/IPTC-16577-MS

Parcevaux, P.A., Sault, P.H., 1984. Cement Shrinkage and Elasticity: A New Approach for a Good Zonal Isolation. Presented at the SPE Annual Technical Conference and Exhibition, Society of Petroleum Engineers. doi:10.2118/13176-MS

Parker, T.R., Farhadiroushan, M., Feced, R., Handerek, V.A., Rogers, A.J., 1998. Simultaneous distributed measurement of strain and temperature from noise-initiated Brillouin scattering in optical fibers. IEEE J. Quantum Electron. 34, 645–659. doi:10.1109/3.663443.

Paulini, P., 1994. A Through Solution Model for Volume Changes of Cement Hydration. Cem. Concr. Res. 24, 488–496. https://doi.org/10.1016/0008-8846(94)90137-6.

Pearce, J., Legrand, P., Dominique, T., et al., 2009a. Real-Time Compaction Monitoring With Fiber-Optic Distributed Strain Sensing (Dss), in: SPWLA-2009-85310. Presented at the SPWLA 50th Annual Logging Symposium, Society of Petrophysicists and Well-Log Analysts, The Woodlands, Texas.

Pearce, J., Rambow, F.H.K., Shroyer, W.W., et al., 2009b. High Resolution, Real Time Casing Strain Imaging for Reservoir and Well Integrity Monitoring: Demonstration of Monitoring Capability in a Field Installation, in: SPE-124932. Presented at the SPE Annual Technical Conference and Exhibition, Society of Petroleum Engineers, New Orleans, Louisiana. doi:10.2118/124932-MS

Plank, J., Tiemeyer, C., Buelichen, D., et al., 2014. A Study of Cement/Mudcake/Formation Interfaces and Their Impact on the Sealing Quality of Oilwell Cement. Presented at the IADC/SPE Asia Pacific Drilling Technology Conference, Society of Petroleum Engineers. doi:10.2118/170452-MS

Potyrailo, R.A., Hieftje, G.M., 1998. Distributed Fiber-Optic Chemical Sensor with Chemically Modified Plastic Cladding. Appl. Spectrosc. 52, 1092–1095.

Rahman, M., Zannitto, P.J., Reed, D.A., et al., 2011. Application of Fiber-Optic Distributed Temperature Sensing Technology for Monitoring Injection Profile in Belridge Field, Diatomite Reservoir, in: SPE-144116-MS. Presented at the SPE Digital Energy Conference and Exhibition, Society of Petroleum Engineers, SPE, p. 13. doi:10.2118/144116-MS

Rajan, G., Prusty, B.G., 2016. Structural Health Monitoring of Composite Structures Using Fiber Optic Methods. CRC Press.

Rambow, F.H.K., Dria, D.E., Childers, B.A., et al., 2010. Real-Time Fiber-Optic Casing Imager. SPE J. 15, 1089–1097. doi:10.2118/109941-PA

Rassenfoss, S., 2012. Fiber Optic Sensing - Learning How It Really Feels Downhole. J. Pet. Technol. 64, 36–43. doi:10.2118/0312-0036-JPT

Ren, L., Li, H.-N., Zhou, J., et al., 2005. Development of Health Monitoring System For Ocean Offshore Platform With Fiber Bragg Grating Sensors, in: ISOPE-I-05-415. Presented at the The Fifteenth International Offshore and Polar Engineering Conference, International Society of Offshore and Polar Engineers.

Sabins, F.L., Tinsley, J.M., Sutton, D.L., 1982. Transition Time of Cement Slurries Between the Fluid and Set States. Soc. Pet. Eng. J. 22, 875–882. doi:10.2118/9285-PA.

Sanchez, A., Brown, G.A., Carvalho, V.L.S., et al., 2005. Slickline With Fiber-Optic Distributed Temperature Monitoring for Water-Injection and Gas Lift Systems Optimization in Mexico, in: SPE-94989-MS. Presented at the SPE Latin American and Caribbean Petroleum Engineering Conference, Society of Petroleum Engineers, SPE, p. 10. doi:10.2118/94989-MS

Sathyamoorthy, M., 1997. Nonlinear Analysis of Structures. CRC Press.

Scherer, G.W., Funkhouser, G.P., Peethamparan, S., 2010. Effect of pressure on early hydration of class H and white cement. Cem. Concr. Res. 40, 845–850. doi:10.1016/j.cemconres.2010.01.013.

Shatalin, S.V., Treschikov, V.N., Rogers, A.J., 1998. Interferometric optical time-domain reflectometry for distributed optical-fiber sensing. Appl. Opt. 37, 5600–5604. doi:10.1364/AO.37.005600

Siebenaler, S., Krishnan, V.R., Lumens, P., et al., 2015. Evaluation of Distributed Acoustic Sensing Leak Detection Technology for Offshore Pipelines. Presented at the The Twenty-fifth International Ocean and Polar Engineering Conference, International Society of Offshore and Polar Engineers, Kona, Hawaii, USA.

Sierra, J.R., Kaura, J.D., Gualtieri, D., et al., 2008. DTS Monitoring of Hydraulic Fracturing: Experiences and Lessons Learned. Society of Petroleum Engineers. doi:10.2118/116182-MS

Sinchenko, E.I., Gibbs, W.E.K., Stoddart, P.R., 2008. Fluorescence-based distributed chemical sensing for structural health monitoring. p. 72681K–72681K–10. doi:10.1117/12.814703

Skorpa, R., Vrålstad, T., 2016. Visualization and Quantification of Fluid Flow through Degraded Cement Sheaths. Presented at the SPE Bergen One Day Seminar, Society of Petroleum Engineers. doi:10.2118/180019-MS

Soga, K., Mohamad, H., Bennett, P., 2008. Distributed Fiber Optics Strain Measurements for Monitoring Geotechnical Structures. Int. Conf. Case Hist. Geotech. Eng.

Sookprasong, P.A., Hurt, R.S., Gill, C.C., 2014. Downhole Monitoring of Multicluster, Multistage Horizontal Well Fracturing with Fiber Optic Distributed Acoustic Sensing (DAS) and Distributed Temperature Sensing (DTS). Presented at the

International Petroleum Technology Conference, International Petroleum Technology Conference. doi:10.2523/IPTC-17972-MS

Talabani, S., Chukwu, G.A., Hatzignatiou, D.G., 1993. Gas Channeling and Micro-Fractures in Cemented Annulus. Presented at the SPE Western Regional Meeting, SPE. doi:10.2118/26068-MS.

Taylor, H.F.W., 1997. Cement chemistry, 2nd ed. ed. T. Telford, London.

Thiercelin, M.J., Dargaud, B., Baret, J.F., Rodriquez, W.J., 1998. Cement Design Based on Cement Mechanical Response. SPE Drill. Complet. 13, 266–273. doi:10.2118/52890-PA.

Thodi, P., Paulin, M., Forster, L., et al., 2014. Arctic Pipeline Leak Detection using Fiber Optic Cable Distributed Sensing Systems. Presented at the OTC Arctic Technology Conference, Offshore Technology Conference, Houston, Texas. doi:10.4043/24589-MS

Udd, E., Spillman, W.B., 2011. Fiber Optic Sensors: An Introduction for Engineers and Scientists. John Wiley & Sons.

Ugueto, G.A., Ehiwario, M., Grae, A., et al., 2014. Application of Integrated Advanced Diagnostics and Modeling To Improve Hydraulic Fracture Stimulation Analysis and Optimization. Presented at the SPE Hydraulic Fracturing Technology Conference, Society of Petroleum Engineers, The Woodlands, Texas, USA. doi:10.2118/168603-MS

van der Horst, J., 2015. Recent Advances in Fiber Optic Technology for In-Well Production and Injection Profiling. Presented at the International Petroleum Technology Conference, International Petroleum Technology Conference. doi:10.2523/IPTC-18563-MS

van der Horst, J., Den Boer, H., In ’t Panhuis, P., et al., 2014. Fibre Optic Sensing For Improved Wellbore Production Surveillance, in: IPTC-17528-MS. Presented at the International Petroleum Technology Conference, International Petroleum Technology Conference, IPTC, p. 7. doi:10.2523/IPTC-17528-MS

van Kleef, R.P. a. R., van Vliet, J.P.M., 1993. Improving the Reliability of Cement-Setting-Time Tests by Taking Into Account the Influence of Shear. SPE Drill. Complet. 8, 51–56. doi:0.2118/20926-PA.

Vignes, B., Aadnøy, B.S., 2010. Well-Integrity Issues Offshore Norway. SPE Prod. Oper. 25, 145–150. doi:10.2118/112535-PA

Walker, I., Carr, D., 2003. Fibre Optic Leak Detection, in: OTC-15360. Presented at the Offshore Technology Conference, Offshore Technology Conference, Houston, Texas. doi:10.4043/15360-MS

Wang, Y., Ye, G., van Breugel, K., Microstructure of Cement Paste Blended with Micronized Sand (MS), in: Freitas, V.P. de de, Delgado, J.M.P.Q. (Eds.),

Durability of Building Materials and Components, Building Pathology and Rehabilitation 3, 2013, 61–84, Springer Berlin Heidelberg doi:10.1007/978-3-642-37475-3_3

Weaver, M.A., Kragas, T.K., Burman, J., et al., 2005. Installation and Application of Permanent Downhole Optical Pressure/Temperature Gauges and Distributed Temperature Sensing in Producing Deepwater Wells at Marco Polo, in: SPE-95798-MS. Presented at the SPE Annual Technical Conference and Exhibition, Society of Petroleum Engineers, SPE, p. 10. doi:10.2118/95798-MS

Webster, P., Wall, J., Perkins, C., et al., 2013. Micro-Seismic Detection Using Distributed Acoustic Sensing, in: SEG-2013-0182. Presented at the 2013 SEG Annual Meeting, Society of Exploration Geophysicists.

Weng, Y., Ip, E., Pan, Z., et al., 2015. Single-end simultaneous temperature and strain sensing techniques based on Brillouin optical time domain reflectometry in few-mode fibers. Opt. Express 23, 9024–9039. doi:10.1364/OE.23.009024

Wilson, D.C., Eustes, A.W., Fleckenstein, W.W., 2018. Lab Testing Cement-Steel Bonding at Shallow Temperature and Pressure Conditions. Presented at the SPE Western Regional Meeting, Society of Petroleum Engineers. doi:10.2118/190031-MS

Wu, Q., Nair, S.D., Shuck, M., et al., 2016a. Advanced Fiber Optic Sensors for Monitoring Poor Zonal Isolation with Hydrocarbon Migration in Cemented Annuli, in: SPE-180329. Presented at the SPE Deepwater Drilling & Completions Conference, Galveston, TX. doi:10.2118/180329-MS

Wu, Q., Nair, S.D., Shuck, M., et al., 2016b. Advanced Distributed Fiber Optic Sensors to Monitor Cement Hydration and Detect Annular Hydrocarbon Migration for Enhanced Zonal Isolation, in: SPE-181429. Presented at the SPE Annual Technical Conference and Exhibition, Dubai, UAE. doi:10.2118/181429-MS

Wu, Q., Dininger, M., Nair, S., et al., 2017a. Real Time Cement Displacement Tracking using Distributed Fiber Optic Sensors, in: SPE-187409. Presented at the SPE Annual Technical Conference and Exhibition, Society of Petroleum Engineers. doi:10.2118/187409-MS

Wu, Q., Nair, S., Shuck, M., et al., 2017b. Advanced distributed fiber optic sensors for monitoring real-time cementing operations and long term zonal isolation. J. Pet. Sci. Eng. 158, 479–493. doi:10.1016/j.petrol.2017.08.072

Wu, Q., Nair, S.D., van Oort, E., et al., 2019a. Concurrent Real-time Distributed Fiber Optic Sensing of Casing Deformation and Cement Integrity Loss, in: SPE-194159. Presented at the SPE/IADC Drilling Conference and Exhibition, Society of Petroleum Engineers, The Hauge, Netherlands.

Wu, Q., Nair, S.D., van Oort, E., et al., 2019b. Behavior and Properties of Cement-Embedded Fiber Optic Sensors for Zonal Isolation Monitoring, in: IPTC-19380.

Presented at the International Petroleum Technology Conference, Society of Petroleum Engineers, Beijing, China.

Xu, Y., Ren, M., Lu, Y., et al., 2016. Multi-parameter sensor based on stimulated Brillouin scattering in inverse-parabolic graded-index fiber. Opt. Lett. 41, 1138–1141. doi:10.1364/OL.41.001138

Xue, Z., Hashimoto, T., 2016. Geomechanical Monitoring of Caprock and Wellbore Integrity using Fiber Optic Cable: Strain Measurement from the Fluid injection and Extraction Field Tests. Presented at the 13th International Conference on Greenhouse Gas Control Technologies, GHGT-13, Lausanne, Switzerland.

Xue, Z., Park, H., Kiyama, T., Hashimoto, T., Nishizawa, O., Kogure, T., 2014. Effects of hydrostatic pressure on strain measurement with distributed optical fiber sensing system. Energy Procedia, 12th International Conference on Greenhouse Gas Control Technologies, GHGT-12 63, 4003–4009. doi:10.1016/j.egypro.2014.11.430.

Yahei, K., Mutsumi, I., Kazuo, H., Koyamada, Y., Imahama, M., Hogari, K., 2007. Practical method for measuring distributed strain and temperature with very high measurand resolution based on Rayleigh backscatter traces at multiple laser frequencies. IEICE Tech. Rep. Optical Fiber Technology. 107(191), 83–88.

Zhang, H., Wu, Z., 2012. Performance Evaluation of PPP-BOTDA-Based Distributed Optical Fiber Sensors. Int. J. Distrib. Sens. Netw. doi:10.1155/2012/414692

Zhang, J., Weissinger, E.A., Peethamparan, S., Scherer, G.W., 2010. Early hydration and setting of oil well cement. Cem. Concr. Res. 40, 1023–1033. doi:10.1016/j.cemconres.2010.03.014.

Zhao, Z., Dang, Y., Tang, M., et al., 2017. Spatial-division multiplexed Brillouin distributed sensing based on a heterogeneous multicore fiber. Opt. Lett. 42, 171–174. doi:10.1364/OL.42.000171

Zou, W., He, Z., Hotate, K., 2009. Complete discrimination of strain and temperature using Brillouin frequency shift and birefringence in a polarization-maintaining fiber. Opt. Express 17, 1248. doi:10.1364/OE.17.001248.

Vita

Qian Wu is a graduate student majoring in Civil Engineering at the University of Texas at Austin. She completed her master's program in 2015 and then continued to pursue a PhD degree. She received her two B.S. degrees in Civil Engineering from both New York University and South China University of Technologies in a four-year dual degree program. Her research interests include fiber optic sensing, oil and gas well cementing, structural health monitoring, magnetorheological fluids, drilling and completion, well abandonment as well as statistical learning and analysis. Qian is an active member of American Concrete Institute (ACI) and Society Engineering of Petroleum (SPE). Qian completes her PhD study in 2019, starting a new journey in her life.

Permanent email: qianwu@utexas.edu

This dissertation was typed by Qian Wu.